Numerical Simulations of Stent-Based Local Drug Delivery

2D geometric investigations and the evaluation of 3D stent designs on the basis of local delivery effectiveness

Neil Bulman-Fleming, McGill University, Montreal

August 26, 2003

A thesis submitted to McGill University in partial fulfillment of the requirements of the degree of
Masters of Engineering

To Stanley and Isabelle Bulman-Fleming, my dear grandparents.

Acknowledgements

I would like to acknowledge the support that NSERC has provided throughout my degree. This funding was made possible by Rosaire Mongrain, whom I thank for his help and guidance during my time at McGill. I solemnly thank my brother Andy, who will be rewarded for his Herculean efforts proofreading and editing this work in the great hereafter. Thanks to Jennifer Bisson, who usually stands by me during the majority of difficult times, and to my parents Barbara and Sydney who always offer sound academic advice. I would also like to thank Nasrollah, Nima, José, Lokesh, and David for their friendship, and my colleagues Tin, Isam, Youssef, Adrian, Jean and Ramses for their constant encouragement.

Abstract

Drug-eluting coronary stents have been identified as a promising means of treating in-stent restenosis. Animal models used to investigate these devices can deliver results for restenosis rates, but cannot provide accurate dose delivery information which would be very useful for refining stent geometries and apposition techniques to optimize dose delivery. In this study, a two-dimensional numerical model is constructed to explore geometrical situations of interest following stent implantation. Metallic stents with a polymer coating and biodegradable solid polymeric stents represent two different vehicles for local delivery. A comparison between these stent types is carried out through the variation of geometric parameters of interest. An investigation of solid polymeric stent struts in a curved vessel is then done through a comparison of dose delivery characteristics on inner and outer walls. Dose delivery success is measured using three quantities: the dose homogeneity in a defined therapeutic region, the percentage of mass remaining in that therapeutic region after a defined therapeutic duration, and the amount of contact between the stent and the vascular wall. The appropriateness of a quasi-stationary hypothesis is then justified in two dimensions through analysis of flow and diffusion parameters. This simplification is applied to stent geometries in three dimensions and a single local delivery effectiveness score based on the three dose delivery parameters is calculated. This tool for evaluating stent designs on the basis of local delivery effectiveness provides a starting point for similar, more sophisticated methods that could eventually be applied to a larger sample of existing stent geometries. Ultimately, the output of such a tool could be used to optimize drug-eluting stent designs.

Résumé

Les stents coronairiens qui délivrent des médicaments sont maintenant établi en tant que traitement de la resténose. Les modèles animaux peuvent être utilisés pour l'investigation de ces prothèses endovasculaires et permettent d'obtenir de l'information concernant l'incidence de la resténose. Cependant, ils ne peuvent fournir des valeurs de concentration de façon suffisamment précise afin d'améliorer le design du stent ainsi que son apposition. Dans ce travail, un modèle numérique bidimensionel est construit pour investiguer les différentes designs de stents déployés. Puisque le développement des stents polymériques complètement biodégradables sont en développement pour libérer localement des médicaments, une comparaison entre ce type de stents et l'approche traditionnelle d'un stent métallique en desous d'une surface polymèrique est effectuée. Une investigation concernant les stents polymèriques dans un segment artériel courbé est aussi effectuée à l'aide d'une comparaison des caractéristiques de livraison de dose entre les murs intérieur et extérieur. Le succès de la libération locale de médicaments est évalué l'aide des trois quantités suivante: l'homogénéité de la dose dans une région d'intérêt, le pourcentage de médicament qui demeure dans la région d'intérêt après la période de thérapie, ainsi que le degré de contact entre le mur artériel et le stent. La validité d'une hypothèse assumant un écoulement quasi stationaire a été évaluée à l'aide des paramètres de succès de livraison locale tel que mentionnés au paravant. Cette simplification est appliquée à quelques géométries de stents en trois dimensions. Cette méthode simplifiée d'évaluation de designs de stent peut être adaptée à divers designs de stents. L'information résultante des paramètres de succès de livraison locale permet de guider les concepteurs de stent afin d'en optimiser leurs designs.

Contents

List of Tables

List of Figures

Chapter 1

Introduction

1.1 Overview

Atherosclerosis is a disease that blocks arteries through the deposition of fatty and calcific materials against the innermost tissue layer of arteries, the endothelium. It commonly affects the coronary arteries which deliver blood to the heart. The accumulation of these deposits leads to the formation of plaque, also called coronary lesions, that occlude the coronary arteries and lead to angina (chest pain) and in more severe cases the formation of blood clots (thrombus) which can lead to blockage of the artery, and ultimately heart attack. In cases where arteries are sufficiently occluded to cause chronic low oxygen levels and poor waste clearance (myocardial ischemia), surgical intervention is necessary. Coronary artery bypass grafts (CABG), first performed in the 1960s, were the first surgical interventions commonly used to treat atherosclerosis. They involve the grafting of healthy sections of vein from elsewhere in the body to bypass occluded coronary arteries. Percutaneous transluminal coronary angioplasty (PTCA), a procedure developed in the 1970s involving the mechanical widening of occluded arteries using an inflatable balloon fixed to a catheter, has been introduced as an alternative to coronary bypass operations in many cases of atherosclerosis because of its minimal invasiveness. This procedure alone was moderately successful, but in a significant number of cases the diseased artery was seen to reocclude within six months after initial treatment.

The development of coronary stents, small metallic scaffolding devices, during the 1980s helped to reduce the likelihood of restenosis following angioplasty. These devices were either implanted following PTCA or placed directly over the balloon on the catheter and implanted during initial balloon expansion. In spite of noted improvements using stents, reocclusion was still found to occur in a high proportion of cases. In-stent restenosis is thought to be caused by tissue inflammation due to trauma associated with balloon expansion and an immune system reaction to the implanted device. These factors lead to neointimal hyperplasia, the proliferation of smooth muscle cells on the innermost surface of the artery, which cover the stent and reocclude the vessel. Coating stents with biologically neutral materials and reducing the total surface contact area of the implant were seen to stall but not prevent neointimal hyperplasia. Ongoing investigations concerning new solutions to the problem of in-stent restenosis involve eliminating the proliferative ability of neointimal cells through the use of systemic drug delivery, local drug delivery, brachytherapy and nucleic-acid based treatments. Perhaps the most promising of these treatments is local drug delivery from drug-eluting stents. This treatment involves the loading of an anti-proliferative drug in a polymer which is then used to coat the stent. In order to achieve maximum therapeutic success, the anti-proliferative agent must reach sufficiently high dose concentrations in all of the tissue susceptible to restenosis, and maintain this concentration over the entire desired therapeutic duration called the therapeutic window.

There are several means of evaluating the behaviour of drug-eluting stents, including clinical investigations in animal and human subjects and verification through numerical modelling of the system. Clinical studies have shown variable results with drug-eluting stent therapy, and concentrate on measuring the physical and temporal characteristics of restenosis rather than examining the pharmacokinetics of the loaded drug. The design cycle of stents and drug loading is then essentially a black box approach; starting with an initial geometry and drug concentration, the resulting effects on restenosis are observed. In order to clarify this situation, some method of either accurately measuring the dose distribution in time through clinical investigations or implementing a suitable three-dimensional numerical model must be done. In the ideal case, high quality clinical results would be used to verify a complete three-dimensional numerical model. High-resolution three-dimensional concentration measurements are extremely difficult to achieve, so a more basic approach is taken. Current clinical results of pharmacokinetic investigations offer information on radial concentration distributions and diffusivities of various compounds in different directions in the arterial wall. These values, along with indirect comparisons with restenosis results, provide the main source of validation for numerical drug-eluting stent models.

Numerical tissue transport models fall into two broad categories: porous models and advection-diffusion models. Porous models approximate tissue transport using macroscopic molecular transport equations based on observed tissue characteristics. Advection-diffusion models combine trans-intimal pressure gradients and tissue-dependent diffusivities to approximate tissue transport. Considering the difficulty in characterizing the tissue consistently, and the simple fact that tissue composition, shape, and uniformity between subjects is extremely variable, the appropriateness of these models is not assured. Models do however show good basic agreement. The exact spatial distribution and overall concentration levels generally agree to within one order of magnitude, and so distilling the basic principles of both models into a single, purely diffusive model would preserve these lower-order features.

In this study, a basic tissue transport model is developed incorporating an effective diffusivity in a purely diffusive arterial wall medium capable of reproducing the general dose distribution characteristics of more complex numerical models. The model is then applied to approximations of realistic post-implantation scenarios. The first part of the study investigates the effects of inter-strut spacing, blood flow velocity, and vessel curvature on dose characteristics in two dimensions. The second part of the study extends the two-dimensional model to three dimensions, and the effects of three-dimensional geometric features on dose distribution are determined. The results from both parts are then discussed in the context of possible improvements to dose delivery characteristics of drug-eluting stents through changes to current stent designs and implantation procedures.

1.2 Literature Review

This section will outline the development of in-stent restenosis treatment, beginning with a more general look at atherosclerosis treatment and leading up to the numerical modelling and clinical investigations of drug-eluting stents. The review of previous works will begin with PTCA treatment and coronary artery stenting. A detailed review of in-stent restenosis treatments will follow, focusing on investigations of atherectomy, brachytherapy, stent coating, local drug delivery and the recent possibility of nucleic acid-based therapies. The survey of literature will conclude with results from clinical drug-eluting stent investigations, general arterial tissue transport studies, and previous numerical pharmacokinetic simulations.

1.2.1 Atherosclerosis Treatments

The degree of severity and likelihood of future complications determines the course of treatment for atherosclerosis. The wide scope of these factors explains the necessity for a large number of therapies. Cases where multiple blockages are accompanied by other indicators of imminent plaque rupture and infarction are treated using CABG. In less complicated cases involving partial occlusion and more stable plaques, less invasive catheter-based treatments are implemented. Owing to the stark procedural differences between CABG and catheter-based therapies, the latter will be the focus of the review and CABG details will not be covered.

Angioplasty

PTCA was introduced in 1977, and quickly became the standard treatment for non-occlusive atherosclerosis due to its minimal invasiveness and high success rates [1]. A registry established by the National Heart, Lung, and Blood Institute (NHLBI) showed that greater experience on the part of doctors performing PTCA reduces complications and improves outcome [1]. Restenosis, defined by Holmes, Vlietstra, Hugh *et al* as "an increase of at least 30% from the immediate post-PTCA stenosis to the follow-up stenosis or a loss of at least 50% of the gain achieved at PTCA" [2], was seen to occur in 33.6% of the patients from the same NHLBI registry. Restenosis manifests itself as the proliferation of smooth muscle cells in the intima, referred to as neointimal hyperplasia [3,4], and typically occurs within three months following PTCA after which point its development is infrequent [5,6]. Diabetes and unstable angina, indicative of an unstable underlying lesion, have been identified as predictors of restenosis following PTCA; however, the exact trigger for neointimal hyperplasia has not been identified [7]. Finally, the overall usefulness of PTCA is limited by significant rates of restenosis, and in order for the underlying procedure to remain beneficial, these rates must be reduced significantly.

Coronary Artery Stenting

Coronary stents were developed in an attempt to prevent acute closure and restenosis of coronary arteries following PTCA. Canine trials meant to determine the safety of and tissue reaction to stents were performed in 1987, and showed favourable outcomes [8,9]. These early trials also showed evidence of "rapid endothelialization" of the stents and neointimal proliferation which would later become known as in-stent restenosis, and acute thrombosis. Following approval of the use of stents in humans a number of post implantation studies were performed to determine the characteristics of in-stent restenosis [10, 11]. Results showed that restenosis occurred in 14% of patients undergoing an interventional procedure for the first time, and 39% of those having already undergone some form of intervention. Further experiments have established that the use of coronary stents does improve restenosis outcomes compared with normal PTCA, however the incidence of minor complications is slightly greater [12, 13, 14]. Differences between the composition of stenotic tissues in the two treatments have also been noted, with smooth muscle cells dominating in-stent restenosis. This result suggests that different treatments for restenosis following PTCA and stenting are necessary [15]. Longer lesions, smaller initial lumen diameter, genetic predisposition, female gender, lack of normal media tissue and high stent-to-lesion length ratio have all been identified as predictors of in-stent restenosis [16, 17, 18]. Stent design, surface material and degree of arterial remodelling, which is defined as the change in artery shape resulting from balloon expansion, have also been shown to affect restenosis rates, with stent design experiments showing that strut configuration correlates with neointimal hyperplasia, and surface material with thrombosis [19, 20]. So despite an overall improvement in clinical outcome with the use of coronary stents the problem of restenosis remains, with reported restenosis occurrence in 10% to 50% of all stent recipients within six months of implantation [16, 21].

1.2.2 In-stent Restenosis Therapies

This section will summarize the various treatments that have been developed to control in-stent restenosis. The majority of these methods are under continued development, and in some cases combinations of these therapies are being tested as possible solutions. First attempts using systemically administered drugs produced negative results not seen in animal trials; this was attributed to the fact that dosages were reduced to limit possible side-effects [22].

Atherectomy and Excimer Laser Angioplasty

A very direct method of treating in-stent restenosis is to physically remove the stenotic tissue directly. There are few common methods for ablating stenotic tissues: rotational atherectomy and excimer laser angioplasty. They are usually followed by PTCA. Rotational atherectomy involves removing atherosclerotic tissue by applying a rotating metallic burr, often with an abrasive coating such as diamond powder, to the affected area. Burrs typically rotate at about 150 000 RPM. Early results of human trials showed a marked reduction in restenosis [23,24], however subsequent trials such as the Angioplasty Versus Rotational Atherectomy for Treatment of Diffuse In-Stent Restenosis Trial (ARTIST) claim that PTCA alone produces superior results [25]. Excimer Laser Angioplasty (ELA) uses ultraviolet laser light transmitted through fibre-optic cable to vaporize stenotic tissue. This technique has been shown to produce results similar to rotational atherectomy [26,27], with slight reductions in restenosis rates. Based on these mixed clinical results, neither rotational atherectomy or ELA have proven to be the ideal treatment method for in-stent restenosis.

Stent Coatings

Coating the metallic surface of stents to improve biocompatibility has been attempted with a number of different compounds. It is thought that reducing platelet adhesion to stent struts may in some way affect the immune response which might control the rate of neointimal hyperplasia. Polymer coatings, both biodegradable and non-biodegradable, have been shown to elicit severe inflammation in surrounding tissues while reducing platelet adhesion [28], and coating stainless steel stents with titanium oxides has been shown to reduce neointimal proliferation [29]. There has been no coating identified which offers a simple solution to the problem of restenosis, however secondary forms of treatment involving the introduction of bioreactive agents onto stent coatings show a great deal of promise [30].

Brachytherapy and Gene-Based Treatments

Exposing tissue to beta and gamma radiation has been shown to inhibit the reproductive ability of cells. Radiation therapy using either catheter- or stent-based radiation dose delivery methods has lately been examined as an alternative for the treatment of restenosis, and in the year 2000 devices of this nature received FDA approval in the United States [31]. As was the case for early atherectomy and excimer laser studies, the first results for radiation therapy were very promising [32, 33]. More recent studies conclude that although these devices reduce the occurrence of in-stent restenosis, incidence of myocardial infarction increases [31], and edge effects [34] and late in-stent restenosis [35, 36] can occur up to one year after implantation. For stent-based radiation therapies, difficulties in achieving an even radiation dosage was identified as one cause of the treatment's inconsistency. This inconsistency is an inherent result of highly elevated doses immediately surrounding stent struts. Presently, these problems make radiation therapy impractical as an everyday, stand-alone solution to the problem.

Another potential means of controlling cell proliferation in the neointima is offered by gene-based therapies. Gene therapies have generated a great deal of interest because they offer targeted delivery with few side-effects and an ability to prevent rather than treat restenosis. In addition, they are suitable for essentially all patients [37]. Cell proliferation-inhibiting gene therapies include the use of adenoviruses, ribozymes and antisense oligonucleotides as vectors to deliver therapies which affect appropriate genes [38, 39, 40]. As with the other therapies surveyed, these methods meet with some success, but suffer serious drawbacks such as inflammation in surrounding tissues, transient expression of the active gene and geographic inconsistency in gene expression [41]. In addition, these methods are intended as preventative therapies, and their implementation on arteries which would not restenose would negatively affect vascular function [42]. These factors render the use of gene therapy for in-stent restenosis premature.

Drug-Eluting Stents

Drug-eluting stents deliver drugs either directly from a drug layer or from a matrix material, such as a polymer, coating the stent struts. Loading drugs in this way reduces systemic exposure and would ideally target the desired tissue, however suitable retention and elution characteristics must be achieved in order to provide appropriate dose delivery. Clinical studies have used several drugs such as the thrombolytic agents heparin and forskolin, group IIa/IIIb platelet blockers c7E3-Fab and AZ1, cell reproduction inhibitor paclitaxel and immunosuppressants such as sirolimus and other corticosteroids [22]. Owing to the very wide range of possible drug choices and matrix loading materials available, and the promising preliminary clinical results with some of these compounds, drug-eluting stents in some form appear to be the most promising method for treatment of in-stent restenosis. The next section is devoted to a detailed discussion of clinical trials and numerical models of drug-eluting stents.

1.2.3 Pharmacokinetics of Drug-Eluting Stents

In order for the pharmacokinetic results of drug-eluting stent numerical simulations to be meaningful and instructive, they must be carefully verified through comparisons to *in vivo* drug delivery models. The ideal relationship between these two aspects of research would allow the numerical models, after careful verification, to act as predictive tools in determining local dose characteristics. Success in this area would greatly reduce the size and number of animal experiments. In addition, it would allow stent designers to optimize strut designs for ideal dose characteristics, and could lead to improvements in deployment techniques in actual surgical procedures based on other geometric considerations. The progress in both of these areas, as well as their overlap, will now be discussed.

Laboratory Studies of Drug-Eluting Stents

The study of mass transport characteristics in coronary arteries began as an attempt to explain the formation of atherosclerotic plaques on vessel walls. An attempt was made to correlate the transport of lipids, oxygen, calcium, water and other compounds with plaque formation [43, 44]. After some success with stent-based local drug delivery following kidney surgery, the concept was adapted to coronary arteries in the early and mid 1990s with stent coatings containing forskolin, heparin, AZ1, corticosteroids and other compounds. Animal trials with forskolin-loaded stents conducted by Lambert, Dev *et al* in 1994 showed favourable biological effects after stent implantation. After one day, 5% of the drug remained in the polymer coating and overall high dose retention rates were observed in arterial media compared with blood and other tissues [45].

A study by Lovich and Edelman in 1995 describing the perivascular and endovascular delivery of heparin *in vitro* reported rapid transport of heparin into arterial media, with diffusion-dominated transport in uninjured tissue and more pronounced convective contributions in cases following endothelial injury. This study also provided diffusivity measurements for heparin through various arterial tissues, which are a useful starting point for simple numerical models [46].

Corticosteroid investigations with methylprednisolone and dexamethasone were carried out to investigate the effects of immunosuppressant agents on in-stent restenosis. The study involving methylprednisolone showed promising results, with 4% of the drug remaining after 24 hours and increased lumen diameter in drug-loaded versus control stents [47]. The animal model dexamethasone investigation established that a high molecular weight polymer coating produced much less inflammation than coating with equivalent low molecular weight polymers, and showed elevated corticosteroid concentrations up to 28 days following implantation, but no reduction in neointimal hyperplasia was noted [48]. These first experiments together proved that local delivery was a promising potential treatment, but sustained delivery and positive outcomes had not been achieved.

The generation of investigations that followed focused on characterizing the mechanisms of mass transport *in vivo*, and on the evaluation of paclitaxel as a potentially suitable compound in the prevention of neointimal hyperplasia. Edelman and Lovich compared a rudimentary one-dimensional numerical model to *in vivo* results of heparin transport in rat arteries, and successfully characterized radial concentrations as well as overall drug mass in time. The ultimate conclusion of this study is aptly explained by its title: "Tissue concentration of heparin, not administered dose, correlates with the biological response of injured arteries *in vivo*" [49].

General pharmacokinetic behaviour following balloon inflation and stent deployment was characterized by Baumbach, Herdeg *et al*, comparing heparin and paclitaxel. The report showed that increased balloon deployment pressure increased drug uptake (probably due to greater trauma to the neointimal layer which acts as a diffusive barrier, and a higher degree of strut embedment), that paclitaxel was retained in higher quantities than heparin, and that stent deployment had little effect on overall outcomes [50]. Other paclitaxel studies characterized the effects of protein binding on pharmacokinetic behaviour [51] and transmural mass transport *ex vivo* [52], and moderately successful animal studies with paclitaxel-coated stents [53, 54] further established the drug as a potential solution to the problem of in-stent restenosis. Overall, animal models studying antithrombotic agents were not very impressive, but were found to produce sufficiently good results to justify the step to human trials [55], whereas compounds which control the neointimal layer's reproductive ability showed very promising results even prior to human testing [56, 57].

Human trials on drug-eluting stents, beginning in the mid-1990s, have produced very interesting results. Heparin has been shown to have little or no effect on complication rates, stent thrombosis or rates of in-stent restenosis [58, 59], confirming what earlier pharmacokinetic investigations had predicted: A rapid emptying of heparin into the bloodstream and little prolonged efficacy due to heparin's hydrophilic nature. Human trials with sirolimus-coated stents have shown success in controlling neointimal hyperplasia [60, 61], and a wide range of preliminary human studies using paclitaxel-coated stents have produced very successful results thus far [62, 63, 64, 65]. Randomized blind clinical trials for drug-eluting stents are currently underway.

From this summary of human and animal studies involving drug-eluting coronary stents, it can be seen that the bulk of information gathered concerns restenosis rates, complication rates, and other outcome-based conclusions. The actual pharmacokinetic information is restricted to rates of mass loss in the stent coating, and more infrequently some rudimentary radial concentration distribution results. As Lovich and Edelman showed, it is drug concentration that correlates to restenosis rates, so in order to improve success rates through optimized stent and coating designs a more accurate method for dose delivery measurement must be established. Tomographic techniques are in development, however resolution and accuracy of dose measurement would limit their usefulness in drug-eluting stent applications [66]. Due in part to the difficulty of accomplishing this goal, numerical methods have been developed to provide an alternative to experimental pharmacokinetic measurements of this nature.

Numerical Models of Drug-Eluting Stents

Quantitative modelling of vascular macromolecular transport matured in the 1970s with work by Colton, Smith, Truskey and Bratzler. Numerical mass transport models in the arterial wall were originally intended to shed light on the formation of atherosclerosis through lipid transport and uptake in the vascular wall, and oxygen transport which is crucial to the normal function of the arterial tissues. These models rely on an augmented form of the advection-diffusion equation describing flow through interstitial fluid, which includes rates of transformation and reaction and cell permeation terms. Two concentrations, freely diffusible solute and intracellular solute, are modelled in the following mass balance equation:

$$\frac{\partial}{\partial x}\left(D\frac{\partial C_f}{\partial x}\right)-\frac{V}{\epsilon}\frac{\partial C_f}{\partial x}-P\left(C_f-C_i\right)-r_1=\frac{\partial C_f}{\partial t} \tag{1.1}$$

where D is the effective diffusivity in the interstitium, V is the filtration velocity, ϵ is the tissue porosity, P is the cell wall permeability coefficient, r_1 is the binding rate and subscripts f and i represent free and intracellular concentrations C. This primary governing equation and others form a system of equations solved with Laplace transforms, and through modulation of transport constants the authors were able to achieve good agreement with experimental LDL uptake data [67].

The overall success of this model in predicting mass transport phenomena allowed for further refinements by other groups. In 1987, Saidel, Morris and Chisolm developed analytical solutions to the one-dimensional advection-diffusion equation similar to Equation 1.1 with an added first-order reaction constant k_i, given by

$$\frac{\partial C_i}{\partial t}+v_i\frac{\partial C_i}{\partial z}=D_i\frac{\partial^2 C_i}{\partial z^2}-k_iC_i \tag{1.2}$$

where C_i is the concentration, v_i the velocity in the z-direction, and D_i the diffusivity. The degree of complexity was increased by adding time-varying boundary conditions meant to ease comparison with experimental results using radio labelling techniques, however no such study followed [68]. In some cases the mathematical representation of physical systems in these first models was limited by the need for analytical solutions, leading to the development of numerical methods for solving arterial mass transport problems.

Weinbaum and others added several degrees of complexity to the advection-diffusion model through consideration of filtration, transverse convection and four distinct transport regions. Here a velocity field based on results from filtration considerations described by Darcy's Law in two dimensions, seen in Equation 1.3, are passed to advection-diffusion equations in each of four regions: intima, subendothelial intima, internal elastic lamina (IEL) and media. In this equation κ is the hydraulic resistivity, μ is the viscosity, P is the pressure and R is the radius of the conduit.

$$V_s = \frac{\kappa}{\mu}\left(-\frac{dP}{dR}\right) \tag{1.3}$$

Solutions were found using finite-difference techniques. The results from this model helped to explain experimental results concerning transport in the three intimal layers, and provided the basis for further refinement of tissue transport models [69].

Consideration of the effects of macroscopic blood flow on tissue transport were numerically modelled by Rappitsch and Perktold in 1995. Many of the fundamental principles described in that paper are central to the work presented here, most notably the coupling of the Navier-Stokes and advection-diffusion equations to describe mass transport into the arterial wall. The effects of flow constriction and shear-dependent wall permeability conditions on steady-state radial concentration profiles were determined, leading to the conclusion that flow profiles are very important in determining mass transport behaviour [70]. This conclusion seems intuitively correct, however the presence of recirculation regions in the flow seem unrealistic in large arteries; the pulsatility of the flow would wash out stagnant fluid and reduce these effects.

In a later work by Perktold and Karner, a model closely resembling Weinbaum's was adopted and solutions were obtained using the finite element method (FEM). This model incorporates Darcy's Law to describe transport across the endothelium and IEL, and the advection-diffusion-reaction equation in the intima and media (Equation 1.2). These regions were coupled using the Kedem-Katchalsky equations describing solute and volume flux across porous barriers, given in Equations 1.4 and 1.5, where J_v and J_s are volume and solute fluxes, P is the wall layer permeability coefficient, L_p is the hydraulic conductivity, σ_d and σ_f are osmotic and solvent drag reflection coefficients,

Δp and $\Delta\Pi$ are transmural and osmotic pressure differentials, Δc_w is the concentration differential and $\bar{c}_w$ is the mean concentration in the wall layer:

$$J_v = L_p(\Delta p - \sigma_d \Delta\Pi) \tag{1.4}$$

$$J_s = P\Delta c_w + J_v(1 - \sigma_f)\bar{c}_w \tag{1.5}$$

The purpose of the study was to determine the effects of endothelial injury and increased blood pressure on mass transport by varying the endothelial permeability and transmural pressure gradients [71]. It was found that increasing permeability increased concentrations in the wall tissues, that increasing blood pressure decreased intimal concentration and increased medial concentration in the case of normal permeabilities, and that elevated concentrations in both regions resulted from higher permeabilities.

Another approach which focussed on purely diffusive drug release from complex geometries was attempted by Zhou and Wu in 1997 [72, 73]. In this study FEM is used to explore purely diffusive mass transport described by Fick's Law. Various cylindrical transport models were investigated, but owing to the lack of convective coupling and correspondence to real biological systems these results provided only limited new information.

Two reports by Tarbell and associates in 1994 and 1997 further developed the two-dimensional multi-layered porous model. The first investigated the effects of using a deformable porous media on macromolecular transport, and the second modeled the media as a series of cylinders surrounded by a flow region, and applied FEM to interstitial flow past the cylinders. The first study was very similar to the work of Weinbaum, but introduced variable porosity through a spatially varying hydraulic permeability κ [74]. The result of the second paper which is important to this work is the conclusion that applying an effective diffusivity in one-dimensional simulations adequately predicts the results from more complex two-dimensional models, which will be explained shortly [75].

The majority of numerical simulations developed up to this point have been independent of parallel experimental trials. In order for numerical results to be meaningful, such trials must be carried out at some point during the life of a numerical model. The current leader in conducting such parallel studies is Elazer Edelman, who has already been cited a great deal in this review of the literature for his involvement in purely experimental studies. A study with Lovich in 1995 was conducted to determine the pharmacokinetics of heparin into *ex vivo* rat aortas from both endovascular and perivascular aspects. The numerical component of this study focused on the change in hydraulic resistivity and Peclet number (Pe), which is an indicator of relative convective and diffusive transport contributions, with medial thickness [46]. A more complete numerical model was constructed with Lovich in 1996 based on Fick's Law, but including binding terms in order to account for heparin uptake and release within the vascular wall, described by the equation

$$\frac{\partial C_i}{\partial t} = D\frac{\partial^2 C_i}{\partial x^2} - k_{\text{on}} C_i B_f + k_{\text{off}} C_i \tag{1.6}$$

where k_{on} and k_{off} are binding rate constants and B_f is the molar density of free binding sites. One-dimensional models with multilayered tissues were designed to describe heparin uptake from endovascular hydrogel and heparin in solution. Comparison with experimental results allowed differentiation between permanently bound drug and reversibly bound drug, important because the permanently bound drug has no therapeutic effect [76].

In works published in the last two years with Hwang and Wu, Edelman has developed an advection-diffusion based model which includes a wall flux boundary condition in two dimensions. This paper is especially notable because it models drug delivery from stent struts, where other models have dealt only with the general pharmacokinetics of local delivery. Diffusivities are made directionally dependent with transverse diffusion coefficients an order of magnitude higher than values in the radial direction, a feature based on previous experimental work carried out with Hwang [77]. The resulting model is applied with hydrophilic and hydrophobic diffusion and flux characteristics, and for homogeneous and nonhomogeneous strut distributions in a transverse arterial section. Simulations were run until steady-state concentrations ($\Delta C_i < 0.05\%$) were achieved. Dose homogeneity was evaluated using the coefficient of variation, which is a normalized variance, and final overall dose was measured. Results showed that hydrophilic drugs lead to more homogeneous results, with maximal homogeneity occurring in the Pe$\simeq$10 range, and that hydrophobic drugs demonstrate mass retention an order of magnitude higher than that of hydrophilic drugs [78]. This investigation is of central importance because it considers the effects of geometrical factors and identifies key tools in quantifying dose homogeneities that are built on in the present work.

To this point only 1D, 2D and quasi-3D models have been discussed. Three-dimensional works in hemodynamics [79, 80], and for stent design optimization [81] have been undertaken but have little connection to controlled local delivery models as their primary concern is characterizing rates and areas of shear stresses. Qiu and Tarbell investigated Oxygen mass transfer for in a pulsatile, compliant curved artery model, however the arterial wall was not actually included in the solution domain. Instead the results were based on wall flux predictions rather than diffusive or porous transport models in the arterial tissue, and the bulk of the conclusions resulted from the curvature of the artery [45]. These 3D results are useful in establishing certain discretization and solution techniques which will be applicable in a general sense to the model developed here.

1.2.4 Conclusions

Interventional treatment of atherosclerosis has improved significantly with the advent of non-invasive catheter-based therapies. Although coronary stents are a great improvement in terms of post-procedural complications and restenosis rates, in-stent restenosis limits their overall effectiveness. The numerous potential treatments are able to reduce the restenosis rates to about 10% within six months after intervention, but there is strong evidence to indicate that this can improve further. Drug-eluting stents offer very promising results, but experimental results typically concentrate on restenosis rates rather than dose delivery characteristics. Numerical models, verified by parallel experimental trials, will be essential tools in determining first-order pharmacokinetics of drug-eluting stents, and will ultimately replace expensive, wasteful and controversial animal testing as a means of evaluating new stent designs and pharmacological approaches.

Up to this point, numerical models have increased their degree of complexity in order to more accurately describe mass transfer in the arterial tissues. Without very high resolution drug concentration measurements available experimentally, these models are difficult to validate. This difficulty justifies a movement towards implementing simplified mass transfer models that consider realistic drug delivery scenarios such as pathological artery and real stent geometries. Although providing less detailed pharmacokinetic information, these models provide the necessary first-order information for optimizing stent designs and implantation procedures with the goal of improving overall dose delivery characteristics.

1.3 Objectives of Current Study

The objectives of the first part of this study are to develop a 2D diffusive arterial tissue model without porous wall conditions using coupled advection-diffusion and Navier-Stokes governing equations. Using FEM, this model is applied to various realistic post-implantation geometric scenarios. A comparison of solid polymeric stents and coated metal stents is carried out, and the effects of varying inter-strut spacing, strut apposition, and vessel curvature are determined. The role of blood flow on mass transport in the vascular wall is also characterized for the purpose of justifying the appropriateness of a quasi-stationary flow hypothesis.

Qualitative verification of the model is performed through comparison to previous works, and evaluation of dose characteristics is achieved using three dimensionless parameters; the dose homogeneity index (DHI), the final mass percentage (FMP) and the area contact index (ACI). The use of these quantities places importance on relative dose characteristics rather than absolute drug concentrations.

The second part of this investigation extends the basic two-dimensional model to three dimensions, and examines the results obtained with real 3D stent geometries. Although limited studies of mass transport in 3D have been attempted, this will be, to the best of our knowledge, the first of such investigations dealing specifically with drug-eluting stents. As with the 2D model, results are evaluated with 3D analogs of FMP, DHI and ACI.

The results of the 2D simulations are considered in the context of improving current stent design parameters and stent deployment techniques. The primary role of the three-dimensional study is to show that implementing 3D dose-delivery models is possible using currently available software, and to develop a method for evaluating actual stent designs based on their local drug delivery effectiveness.

Chapter 2

Two-Dimensional Model Development

2.1 Overview

This section will outline the development and implementation of a 2D numerical model used to characterize local delivery from drug-eluting stents. Previous studies discussed in Chapter 1 will be referred to in this section, with emphasis on elements common to the model developed here. The geometry, material properties and boundary conditions are presented, followed by the underlying theory of FEM that applies to the model, including mesh generation in 2D and a brief description of the solver used. The methods of data analysis specific to dose evaluation will be described, followed by an explanation of model verification including grid and time-step independence, and comparison to experimental dose delivery results.

2.2 Mass Transport

Mass transport in the 2D model occurs in three distinct regions: the vascular wall, the vessel lumen (blood), and the drug-eluting polymer. First we consider mass transport in the lumen, starting with Navier-Stokes equation which governs flow, given by:

$$\rho\left(\frac{\partial \mathbf{u}}{\partial t} + \mathbf{u}\cdot\nabla\mathbf{u}\right) = -\nabla p + \mu\nabla^2\mathbf{u} + \rho f \tag{2.1}$$

where ρ is the density, here held constant, $\mathbf{u}$ is the velocity, p the pressure, μ the viscosity and f a body force term. The lumen transports mass according to the advection-diffusion equation:

$$\rho\left(\frac{\partial c}{\partial t} + \mathbf{u}\cdot\nabla c\right) = \rho\nabla\cdot(D\nabla c) + q_c + R \tag{2.2}$$

where c is the concentration, D the diffusivity in cm/s^2, q_c is a general source term and R is a production rate term. Here q_c and R are taken to be zero, and D is constant, so this expression simplifies to:

$$\frac{\partial c}{\partial t} + \mathbf{u}\cdot\nabla c = D\nabla^2 c \tag{2.3}$$

The flow is also considered incompressible, giving rise to a third governing equation in the lumen:

$$\nabla\cdot\mathbf{u} = 0 \tag{2.4}$$

In the two solid regions, the vascular wall and the polymer, (2.3) further simplifies to

$$\frac{\partial c}{\partial t} = D\nabla^2 c \tag{2.5}$$

owing to the lack of flow in these regions. This equation is a form of Fick's Law:

$$\mathbf{J} = -D\nabla c \tag{2.6}$$

where $\mathbf{J}$ is the mass flux. The results from a transient simulation based on these equations are concentration fields at time intervals $\triangle t$ in two dimensions. The simulations are run for a total of 6×10^5 seconds (6.94 days, or approximately one week). This period of time is selected based on an observed therapeutic window during which the prescribed dose must be maintained to have the desired therapeutic effect.

2.3 Geometry

The basic geometry used in these simulations is shown in Figure 2.1. Blood flows in the z-direction, and the model is symmetric about the z-axis. Five struts were found to be adequate in showing mass and homogeneity properties in the vascular wall. Inter-strut spacing and strut dimensions are based on an average of values from actual stents. The struts in their basic configuration are taken to be half-embedded which is a realistic physiologic post-deployment scenario. Physiologic dimensions are modelled after typical values for coronary arteries, with a lumen diameter of 3 mm and vascular wall thickness of 0.4 mm. No distinction is made between intimal, medial and adventitial tissues, however the vasa vasorum, located at the outer extreme of the vascular wall, is assigned a distinct boundary condition. For comparison, the therapeutic region is taken to be a region 200 μm measured radially from the lumen/vascular wall interface, and extending 200 μm beyond the extreme struts. Dose delivery analysis is limited to this therapeutic region unless otherwise noted. A description of the variation of geometric parameters follows.

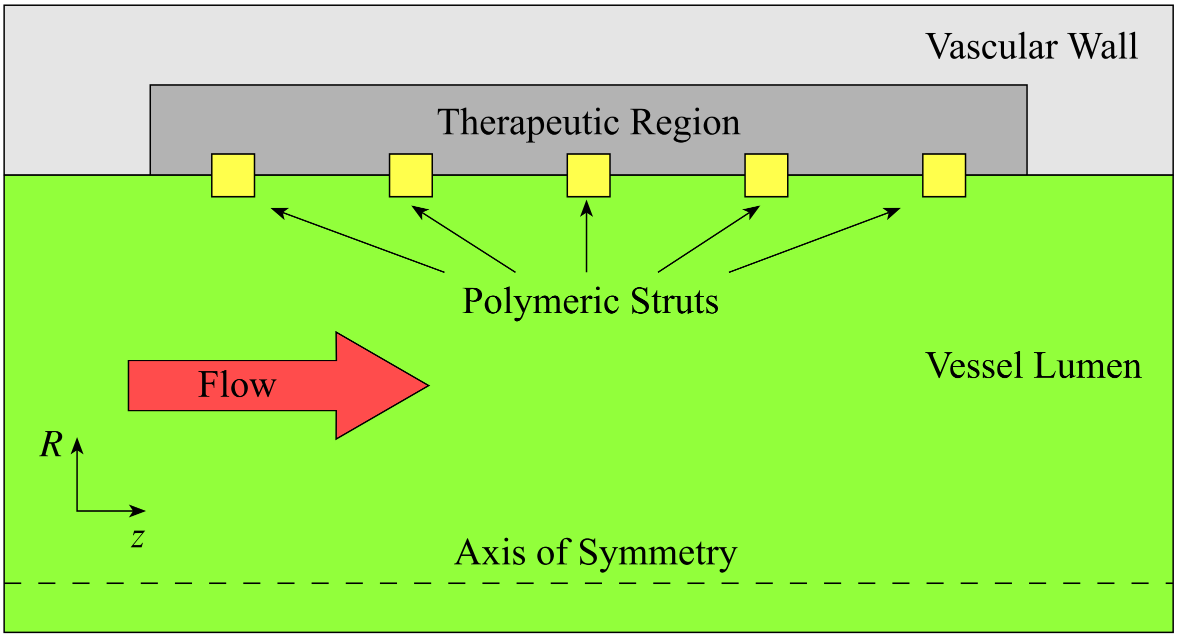

Figure 2.1: Basic two-dimensional geometry with solid polymeric struts.

2.3.1 Coated Metallic vs Solid Polymeric Stents

Owing to the recent development of solid polymeric stents which may be capable of eluting drugs, a comparison between a metallic stent with a 10 μm polymeric coating and such a solid polymeric stent is carried out. These stent configurations are shown in Figure 2.2. The overall dimensions of the metal/polymer coated stent and the solid polymer stent are equal, with a strut thickness and height of 80 μm. The goal of comparing these configurations is to evaluate their dose delivery characteristics and to determine whether one design is significantly better in this regard. Parallel simulations for solid and coated stents are carried out for apposition and inter-strut spacing studies, as described below.

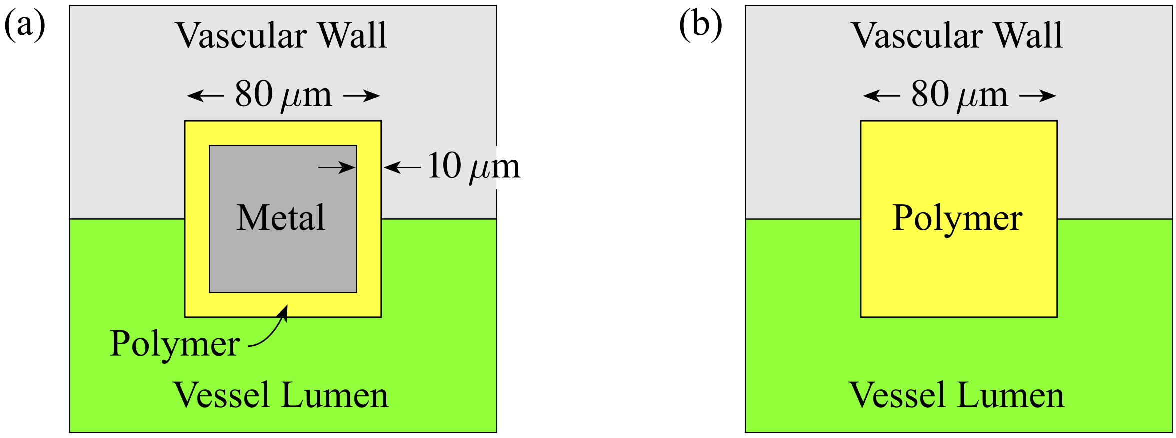

Figure 2.2: Schematics of coated (a) and solid polymeric stent struts (b).

2.3.2 Inter-Strut Spacing

Inter-strut spacing (labelled ISS in Figure 2.3) is varied from 500 to 2000 μm, and dose delivery characteristics for both solid and coated struts are carried out.

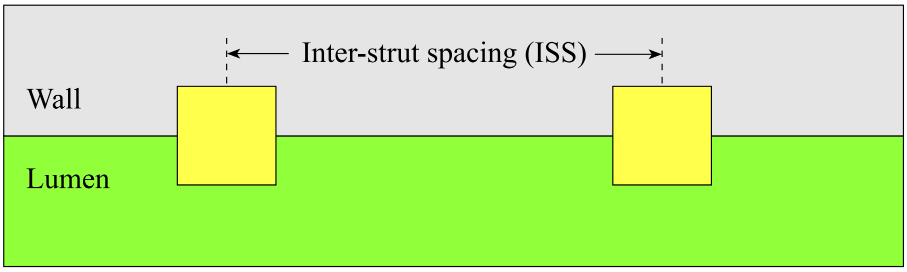

Figure 2.3: Inter-strut spacing dimension.

2.3.3 Apposition

The degree of embedment, or apposition, of struts has been seen to vary significantly, and to correlate with restenosis after stent deployment. Here three apposition scenarios are investigated: fully embedded struts, halfway embedded struts, and contacting struts, shown in Figure 2.4. These three apposition situations are compared for coated and solid struts.

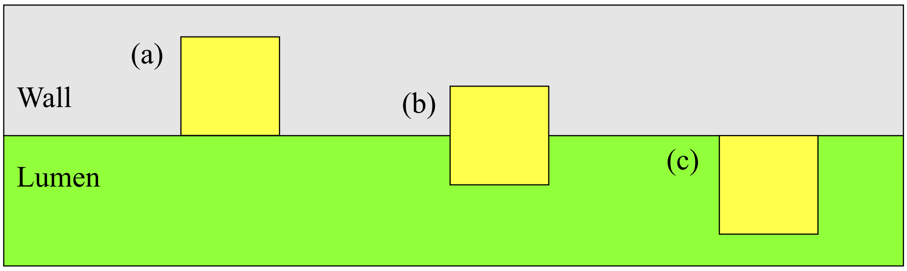

Figure 2.4: Three strut apposition scenarios: fully embedded (a), halfway embedded (b) and contacting (c).

2.3.4 Vessel Curvature

The curvature of coronary arteries has been seen to correlate with restenosis rates in experimental drug-eluting stent studies. In order to supply possible insight into the role of pharmacokinetics on these findings, a series of 2D curved artery simulations are developed based on the geometry shown in Figure 2.5. In this figure, R is the radius of curvature measured to the midline of the lumen, and d is the vessel diameter taken to be 3 mm. The ratio R/d is varied from 10, corresponding to a radius of curvature $R = 3$ cm, to infinity, representing a straight artery. Five stent struts on the inside and outside walls are placed at constant-angle intervals corresponding to a vessel midline length of 1500 μm. This midline inter-strut spacing value is held constant for varying values of R/d. The therapeutic region is equivalent to that presented for straight arteries, extending 200 μm into the vascular wall and extending 200 μm beyond extreme struts. These simulations are run for solid polymeric struts only, and compare dose delivery characteristics in the inside and outside walls.

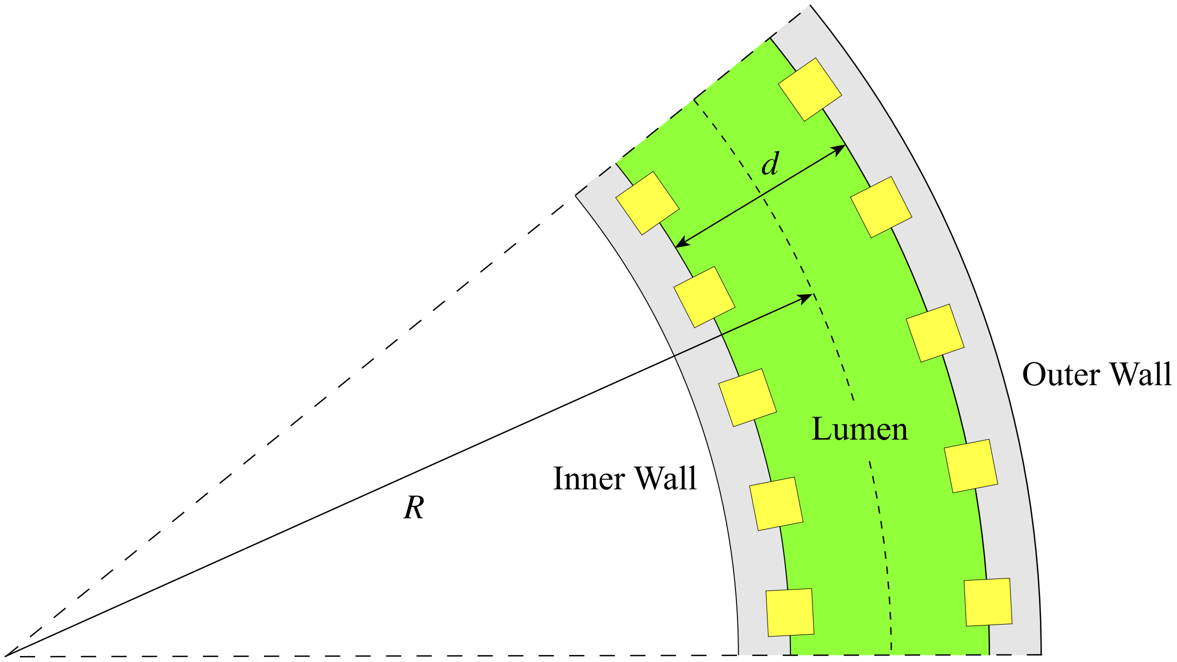

Figure 2.5: Vessel curvature schematic with vessel diameter d and radius of curvature R.

2.4 Material Properties of Blood

Material properties for blood, with the exception of its diffusivity, are based on values implemented in other numerical models and from empirical blood data. The non-

Newtonian, shear-thinning properties of blood are ignored here and a constant viscosity is adopted based on low shear and shear rate conditions. The density is fixed at $\rho = 1.051$ g/cm^3 and the viscosity at $\mu = 3.5$ cP. For ease of comparison with other works, and to adopt the most general representation of flow fields, these values are incorporated into the Reynolds number and are not referred to after this point. The Reynolds number is given by the expression:

$$\mathrm{Re} = \frac{\rho u_0 L}{\mu} \tag{2.7}$$

where u_0 is a characteristic velocity and L is a characteristic length. For the majority of the 2D simulations presented in this study, the Reynolds number is set to 100, which corresponds to a mean flow velocity of 11.1 cm/s and flow rate of 0.05 L/min. in the vessel lumen. The role of flow is characterized in Chapter 4 for Reynolds numbers spanning the physiologic range in coronary arteries.

2.5 Boundary and Initial Conditions

2.5.1 Velocity Boundary Conditions

Velocity boundary conditions are set up in the following way. The inlet velocity is taken to be fully developed Poiseuille flow with a mean flow velocity of 11.1 cm/s (Re=100, $q = 0.05$ L/min. $d_{\text{vessel}} = 3$ mm). Note that this is steady (non-pulsatile) flow, so there is no representation of the beating of the heart in these simulations. Table 2.1 shows complete u_r and u_z boundary conditions for 2D simulations.

2.5.2 Concentration Boundary and Initial Conditions

Two zero-concentration boundaries are set in the problem. The first is at the vasa vasorum, meant to account for the dilution of accumulated dose by the vasa vasorum capillaries, and the second is at the vessel inlet to reflect the very large volume of blood

Boundary Entity	u_r (cm/s)	u_z (cm/s)
Inlet	0	$22.20 - 986.71r^2$
Outlet	Free	Free
Symmetry line	0	Free
Vascular wall and stent	0	0

Table 2.1: Velocity boundary conditions for basic 2D simulations.

compared to the total drug mass loaded on the stent. These conditions are adopted from the work of Sara Julien [82]. The remaining concentration condition is the initial condition in the polymer, set to $c = 1.0$. This value of unity is adopted so that all concentration values after time $t = 0$ are automatically normalized, so with knowledge of a desired therapeutic dose concentration C_{ther}, one could determine a theoretical initial dose based on a normalized final average concentration $\overline{c}_{\text{final}}$ in the following way. Express $\overline{c}_{\text{final}}$, the normalized final average concentration, as:

$$\overline{c}_{\text{final}} = \frac{C_{\text{final}}}{C_{\text{initial}}} \tag{2.8}$$

Setting the desired therapeutic dose concentration equal to the final dose concentration, $C_{\text{ther}} = C_{\text{final}}$, substituting into Equation 2.8, and solving for C_{initial} yields:

$$C_{\text{initial}} = \frac{C_{\text{ther}}}{\overline{c}_{\text{final}}} \tag{2.9}$$

This demonstrates a simplistic means of determining an appropriate initial dose based on normalized final dose concentration data.

2.6 Similar Models

Systemic delivery models [69] and local "bathing" models [76] that concentrate on transmural mass transport and one-dimensional radial concentration results do make use of advection-diffusion and Fick's Law equations, but also incorporate binding site mechanics and porous transport considerations, making useful comparison difficult. The works of Wu and Zhou [72, 73] focus on diffusion from a drug-eluting solid of various geometries and boundary conditions in 2D. These works involve diffusion from tablet-like geometries into solutions, and examine drug concentrations in the solution over time without particular attention to the drug distribution outside of the tablet itself. Owing to the geometric differences between this model and the model developed here, the only useful comparison is a qualitative comparison of remaining dose in the polymer entity with that remaining in the tablet.

Comparable models have been presented by Rappitsch and Perktold in 1996 [70], Hwang, Wu, and Edelman in 2001 and 2002 [78, 77], and the masters thesis of Sara Julien [82]. Rappitsch and Pertold present a 2D model employing Navier-Stokes and advection-diffusion equations in the vessel lumen, and examine the effects of disturbing blood flow on drug concentration in the vessel lumen. That model is focussed on the coronary arteries and employs steady flow at the vessel inlet with Reynolds number $\mathrm{Re} \approx 450$ and Peclet number $\mathrm{Pe} \approx 10^6$. Recirculation and shear stress at the vascular wall interface are shown to affect concentration levels at the wall and in recirculation zones, however no other vascular wall dose information is explored. As a result the most important comparisons occur for the flow field and blood diffusion characteristics used.

The models described above use similar governing equations, but do not focus on drug-eluting stent simulations which share geometric features with the current model. Hwang and Edelman [78] look at cylindrical cross-sections and resulting steady-state doses from stents having constant concentrations. This model investigates possible differences in dose delivery between hydrophobic (paclitaxel) and hydrophilic (heparin) drugs, as well as the effects of randomly placed stent struts using Monte Carlo simulations. A zero-concentration boundary condition is applied at the vessel interface meaning that flow is not modelled in the lumen itself, however a radial velocity field is applied in the vascular wall. The means of evaluation and analysis of dose delivery are also very useful to the present study. Here the coefficient of variation is employed as a means of evaluating dose homogeneity, and final mean concentration gives an estimate of the remaining mass. Both of these parameters are central to the present work, but are adapted for axisymmetric geometries in 2D and full 3D results. Mass and homogeneity results from this work of Hwang and Edelman are also used as an additional means of verifying the appropriateness of diffusion coefficient values in three regions.

The direct predecessor of the present study is the work of Sara Julien, *Étude Numérique de la Diffusion et la Convection du* ^{45}*Ca-DTPA Émis par un Stent pour le Contrôle de la Resténose*, carried out at the University of Montreal as her Master's thesis, completed in 2000. The basic dimensions for the current work were adapted from this study, as well as adventitial boundary conditions and inlet concentration boundary conditions. The analysis of results in 2D focus on the effects of varying Peclet number (through variation of diffusion coefficients) and examining concentrations at constant radius in the vascular wall. The major differences between the present work and Julien's work are the analysis techniques in 2D, and an interest in varying geometric parameters rather than material constants. Constant radius concentration analysis in Julien's work is replaced in the present work by a holistic evaluation of dose delivery in the therapeutic region. In spite of these differences, Julien's thesis has provided many important building blocks for the numerical simulations outlined here.

2.7 Model Implementation

This section will describe the adaptation of the general model already outlined into actual FEM simulations. In 2D, both the meshing and solving aspects of the simulations were carried out using software packages from Fluent Inc. The geometry creation, meshing and exporting using GAMBIT will be outlined, followed by a description of the implementation of the solver FIDAP. Since FIDAP is an off-the-shelf FEM implementation, a brief discussion of how the package works is also presented for the sake of completeness.

2.7.1 Geometry Meshing

All 2D geometries are created and meshed using GAMBIT. Four continuum entities are specified to represent the solid polymer, solid therapeutic region (within the vascular wall), solid vascular wall outside the therapeutic region, and liquid lumen. `PLOT` type boundary regions are specified for the vessel inlet, vessel outlet, line of symmetry, vascular wall/lumen interface (including the wetted surface of the stent struts) and vasa vasorum. The stent struts are meshed with structured quadrilateral elements. A boundary layer is created on the outer layer of the struts in order to make the transition from small to large elements more compact and geometrically regular. Typical meshes for coated and solid struts appear in Figure 2.6. Within the therapeutic region unstructured quadrilateral elements are used to fill the solution domain. An area mirroring the therapeutic region is meshed in the vessel lumen to capture flow and mass transfer characteristics near the intima. The remaining regions in the vessel lumen and outer vascular wall are meshed using structured quadrilateral elements. This general scheme is applied to models for all of the 2D geometries presented here, with curved

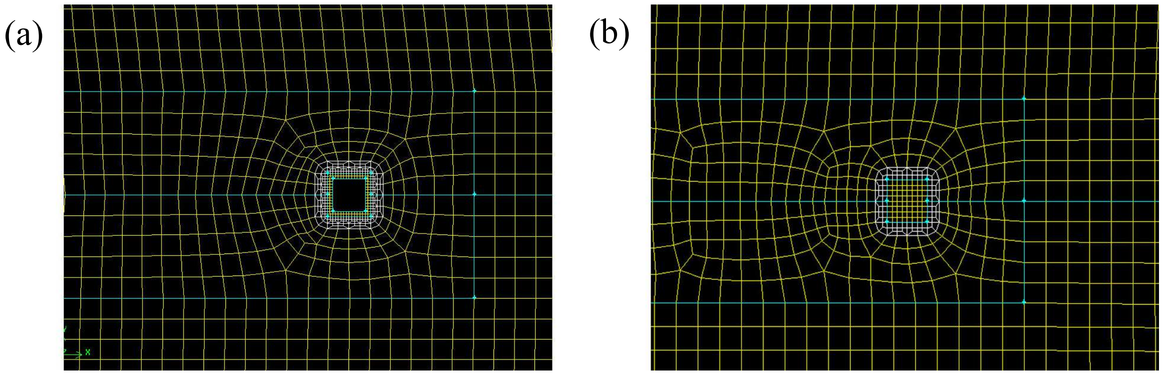

Figure 2.6: Meshes for coated (a) and solid (b) stent struts.

vessel geometry meshes being equivalent to a mapping of straight-vessel geometry onto a curved solution domain.

Each mesh is written to a specialized FIDAP mesh input `.FDNEUT` file. A `.FIPREP` file containing boundary and continuum entity information is created by GAMBIT along with the `.FDNEUT` files. These files are modified from their original output form to reflect the boundary conditions, material properties, time-stepping algorithms and solution parameters particular to each simulation. Upon completion of this process, the `.FIPREP` files are ready to be used by FIDAP to construct a solution database.

2.7.2 FIDAP Implementation

The finite element method was developed in order to allow numerical solution of systems of differential equations for which no analytical solution can be found. The method involves the division of a solution domain into elements and assigning nodes to these elements. The behaviour of solution parameters at each node are then determined by a simplified system of equations based on the governing equations. By measuring the residue following the simultaneous solution of a large number of linear equations, the desired solution accuracy is obtained. FIDAP is a commercial FEM code that functions on these basic principles. The inclusion of common physical and chemical governing equations make it applicable to a large number of problems including those considered here.

Depending on the size and complexity of the problem, different methods of solution can be selected in FIDAP. These 2D simulations are relatively small and simple, and are solved using a successive substitution (or fixed-point) method with four-node quadrilateral elements and a backward-Euler time-stepping algorithm. 48 fixed time steps of 0.125×10^5 s are implemented up to the final time of 6×10^5 s. Convergence criteria based on both the normalized solution vector and residual vector at successive iterations were set to 10^{-3}.

Although the Navier-Stokes and advection-diffusion equations have been described as coupled up to this point, the constant flow field can be applied as a continuum entity boundary condition applied at each node in the vessel lumen. This method greatly reduces solution times because the need to solve flow field equations at each time-step is removed. In FIDAP this is classified as an advection-diffusion type problem, and is carried out in the following way:

1. The flow field is solved independently of the mass-transport equations.
2. The simulation is stopped and the problem definition is changed.
3. The simulation is restarted, and the flow field is read into the solution database.
4. The species equation is solved independently of the momentum equation.

A sample `.FIPREP` file appears in Appendix A-1 for both the flow field and species equation parts of the total solution. Batches of simulations were controlled from the FIDAP command line interface using MS/DOS batch files. The output from these simulations appears as five-column arrays containing node number, position and concentration information in tab-separated text files.

2.8 Data Analysis Methods

The key factors in evaluating dose delivery characteristics in 2D are dose homogeneity and final mass in the therapeutic region. Two numerical indices are developed to quantify these factors; the Dose Homogeneity Index (DHI) and the Final Mass Percentage (FMP). These numbers are independent of the magnitude of the dose concentration and the volume of polymer available for mass loading, and so provide a standardized method of evaluating dose delivery for different stent designs and geometries. A third factor, the Area Contact Index (ACI), is also used and is an indicator of tissue injury in the stented region. These numerical indices will now be described.

2.8.1 Dose Homogeneity Index

Formulation of the DHI

Achieving a homogeneous dose distribution in the therapeutic region is important for two reasons. Firstly, the lowest concentrations in the therapeutic region determine the initial mass loading, meaning that the highest concentrations may approach the toxic threshold if the dose is sufficiently inhomogeneous. Secondly, a wide variation in concentration in the therapeutic region could easily lead to variable restenosis rates as a result of unequal dose delivery. For these reasons, the measure of homogeneity within the therapeutic region is crucial in attaining a meaningful evaluation of a stent's dose delivery characteristics.

The DHI is based on the coefficient of variation (CV) of the concentration at each node in the therapeutic region. A similar method has been used by Hwang and Edelman [78], however their analysis measures the CV throughout the vascular wall and is not restricted to a particular region of interest.

The CV is the standard deviation of a sample normalized by its mean. The DHI is this quantity evaluated within the therapeutic region:

$$\mathrm{DHI} = \mathrm{CV}|_{\text{therapeutic region}} = \frac{\sigma_c}{\bar{c}} \tag{2.10}$$

In order to ensure that this quantity is a meaningful measure of homogeneity, it is important that the values in the sample being compared are identical in nature. In particular, the element area (or volume in 3D) must be equal for all sample points to avoid smoothing effects. In the present work a MATLAB script is used to isolate the concentrations within the therapeutic region and force them into a regular, equal element area mesh. The mesh is constructed using the `meshgrid` function, and a concentration field based on FIDAP output is forced to this mesh using the `griddata` function with cubic interpolation (see Appendix A-2). In order to account for stent embedment, zero-concentration points are added to the FIDAP output to prevent in-accurate interpolations in those areas. Once the concentration data have been cast in this form calculating the DHI is trivial.

Interpreting the DHI

In order to properly interpret the DHI it is necessary to understand the CV. It is often presented as a percentage, and indicates the portion of a sample's mean over which the sample itself varies. In basic terms, the lower the DHI the more homogeneous the dose. The minimum possible value of DHI is zero, corresponding to a standard deviation of zero, which would indicate an equal concentration at every field point. Table 2.2 outlines the interpretations of DHI over the range encountered in this work. The majority of DHIs seen in the results section lie between 0.5 and 1.5, which spans "good" to "poor" values in the dose homogeneity spectrum. The special case where the concentration is zero everywhere, resulting in a DHI of zero, should also be noted. The adaptation of the DHI to 3D analyses appears in Chapter 5.

DHI	CV	Interpretation
0.0	0%	Equal concentration at every point.
1.0	100%	Concentration varies over the magnitude of its mean.
2.0	200%	Concentration varies over twice the magnitude of its mean.

Table 2.2: Interpretations of DHI values and corresponding CVs.

2.8.2 Final Mass Percentage

The drug mass in the therapeutic region measured after deployment is an important indication of dose delivery success for the following reason: If the ratio of mass in the therapeutic region to initial mass is high, then the difference between them is low, meaning that the drug-eluting stent was successful in transmitting dose to the therapeutic region with minimal waste. This point can also be illustrated by considering a scenario where the remaining mass is very low; in such a case, the initial mass loading would have to be commensurably higher, bringing early concentrations closer to a potential toxic threshold. It is also important to note the connection between the DHI and the FMP. Unless the DHI is below an acceptable limit, the FMP is not a useful dose delivery indicator because the dose will be highly localized. This would again pose possible toxicity problems based on preceding arguments. So it is important to achieve some degree of balance between the DHI and FMP.

The development of the FMP specific to these simulations is as follows, with the initial normalized concentration set to $c_{\text{intial}} = 1.0$ in the polymer, and equal volume (actually area in 2D) element sizes in the therapeutic region:

$$\begin{aligned} \text{FMP} &= \frac{\text{mass remaining in therapeutic region at } t_{\text{final}}}{\text{mass in polymer at } t_{\text{intial}}} && (2.11) \\ &= \frac{\sum dm_{\text{tr}}}{c_{\text{intial}} \cdot V_{\text{polymer}}} && (2.12) \\ &= \frac{\sum (c \cdot dV_{\text{tr}})}{1 \cdot V_{\text{polymer}}} && (2.13) \\ &= \frac{dV_{\text{tr}}}{V_{\text{polymer}}} \sum c \times 100\% && (2.14) \end{aligned}$$

It is important to note that this simplification is only valid when volume elements in the therapeutic region are of equal size. Results for FMP typically fall between about 0.5% and 5% for simulations spanning a time interval of one week.

2.8.3 Area Contact Index

The ACI is an index introduced to measure the negative impact on tissue health following stent deployment. From a dose delivery perspective, having a hollow cylindrical, sheath-like stent would be optimal since it would deliver mass evenly over the entire surface of the intimal layer, however such a stent would prevent important mass transport between the blood and the intima, and would trigger a very pronounced inflammatory response. These negative consequences would far outweigh the benefits of optimal local drug delivery. The ACI is introduced in order to quantify these negative consequences, and is calculated according to the expression

$$\text{ACI} = \frac{\text{Length or area of stent contacting vascular wall}}{\text{Length or area of therapeutic region contacting vessel lumen}} \times 100\% \quad (2.15)$$

The ACI is defined as the ratio of the area of the stent in contact with the vascular wall to the total area of the vascular wall within the stented area immediately after deployment, since through healing and restenosis the ACI would be seen to increase over time. The total stented area is equivalent to the wall of the therapeutic region bordering the vessel lumen. In 2D this factor is a ratio of lengths, whereas in 3D it is a ratio of areas.

2.9 Model Validation

The most effective verification of numerical models is done using comparisons with corresponding experimental trials. This method of verification is not used in this work because the resources to carry out animal trials were not available, and if they were, current vascular wall concentration measurement techniques lack the necessary resolution for meaningful comparison with a numerical model. As a result, the verification of this model will be done through comparisons with existing experimental data, as well as traditional FEM verification methods ensuring grid and time-step independence, and agreement with analytical solutions in simplified geometries.

2.9.1 Comparison to Experimental Data

Two types of experimental data were used to set the diffusion characteristics used in the numerical simulations. First, diffusion coefficients for various compounds through vascular tissues, blood and polymers were compiled and compared (Table 2.3). Using these values, a general relationship between diffusivities in the lumen and vascular wall was set in the following manner:

$$D_{\text{lumen}} = 10D_{\text{vwall}} \tag{2.16}$$

Second, these relative values were fixed and simulations were run over a range of diffusion coefficients for the polymer medium (coated, half-embedded struts, inter-strut spacing of 1500 μm and Reynolds number 100). Equivalent FMP values were calculated from experimental results for drug-eluting stents, and ranges from 0.006% for the compound Sirolimus [56] to 2.36% for Paclitaxel [54] were reported three days after deployment. A less direct means of verifying the appropriateness of diffusivities is through comparison to other numerical models. Homogeneity comparison is possible with the work of Hwang and Edelman [78], in which values between 0.6 and 1.5 were reported for a parameter equilvalent to the DHI. These values span approximately the same range

Compound	Diffusive Medium	Diffusivity (cm^2/s)	Reference
Heparin	Water	1.45×10^{-6}	[46]
	Media	7.73×10^{-8}	[46]
	Adventitia	1.21×10^{-7}	[46]
Taxol	Vascular wall, lower limit	2.22×10^{-8}	[52]
	Vascular wall, upper limit	3.76×10^{-8}	[52]
Water	Plaque lipid core	2.60×10^{-6}	[83]
	Collagenous cap	2.60×10^{-6}	[83]
	Media	2.60×10^{-6}	[83]
	Media	4.50×10^{-6}	[43]
Albumin	Media	7.20×10^{-9}	[44]
	Bovine blood serum	3.50×10^{-7}	[84]

Table 2.3: Diffusion coefficients for various compounds through pertinent media from experimental trials.

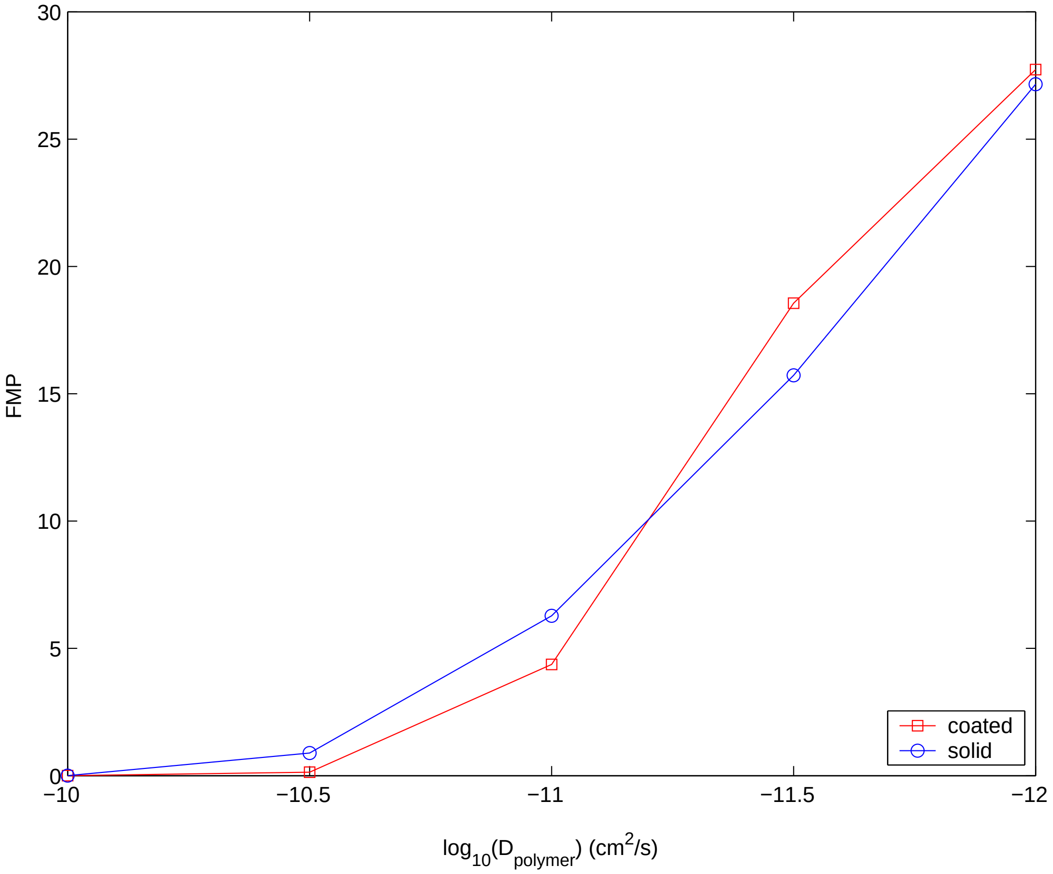

Figure 2.7: Final mass results after 3 days with varying polymer diffusivity.

as values in this work (0.5 to 1.7), showing relatively good agreement considering the inherent differences in the geometries and solution parameters between the two models. From Figures 2.7 and 2.8, it can be seen that a polymer diffusivity of 10^{-11} cm^2/s produces results which agree best with mass and homogeneity values appearing in these other works. As a result, the relative diffusion coefficients were fixed to the following values:

$$D_{\text{lumen}} = 10D_{\text{vwall}} = 1000D_{\text{polymer}} \tag{2.17}$$

and the following absolute diffusivities were applied for the remainder of the 2D simulations (before simplifications are applied):

$$D_{\text{lumen}} \;=\; 10^{-8}\ \text{cm}^2/\text{s} \tag{2.18}$$

$$D_{\text{vwall}} = 10^{-9}\ \text{cm}^2/\text{s} \tag{2.19}$$

$$D_{\text{polymer}} = 10^{-11}\ \text{cm}^2/\text{s} \tag{2.20}$$

Note that these diffusion coefficients are 10 to 100 times less than actual values seen in Table 2.3. This is due to the effective model of diffusion that is applied in the simulations, neglecting porosity, drug binding mechanics, transmural pressure gradients, directionally dependent diffusion and other bulk tissue anisotropy. This is the most important simplification of the model, but because the alignment of final mass results from numerical simulations to experimental trials is empirically corrected, the model is expected to produce acceptable final dose distribution results.

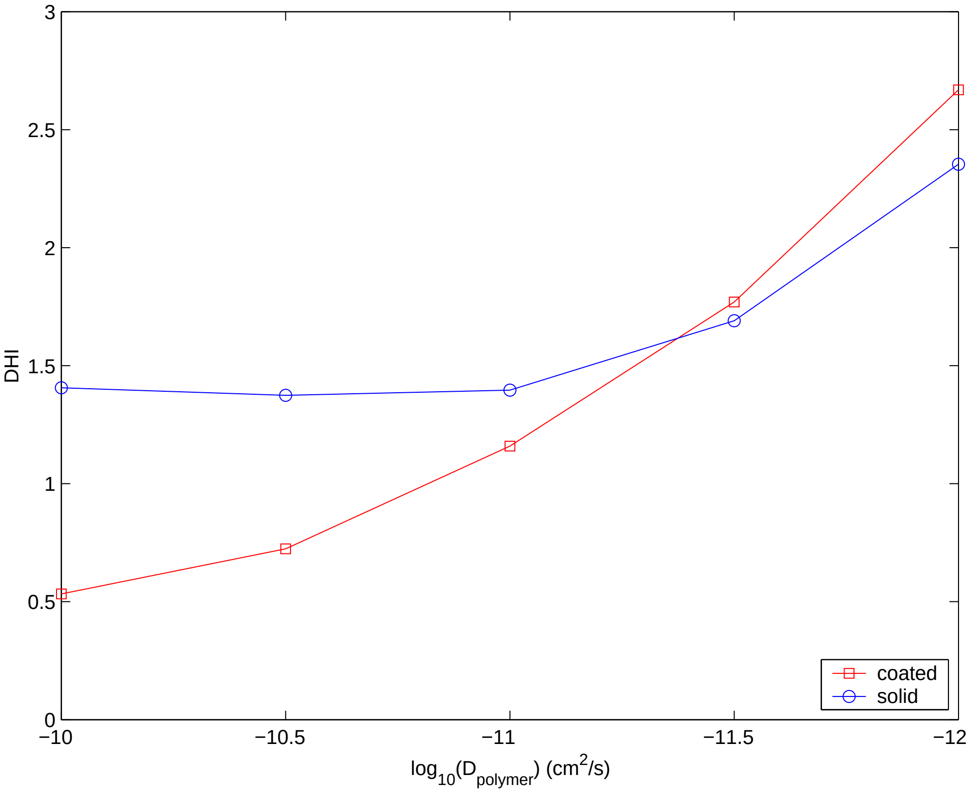

Figure 2.8: Dose homogeneity results after 3 days with varying polymer diffusivity.

2.9.2 Grid Independence

Having set the material properties in the simulation to produce results in agreement with experimental trials, the FEM components of the simulation were verified. Grid-independence was used to select a suitable small element size while limiting solution times. Table 2.4 shows results for DHI and FMP for decreasing polymer element side lengths for coated and solid struts. Grid independence was achieved for polymer element sizes of 5 to 40 μm (coated) and 20 to 50 μm (solid) because they represent the best compromise between solution times and agreement with the next smallest element sizes in the comparison.

	Coated				Solid			
Mesh	Size (μm)	t_{CPU} (s)	DHI	FMP	Size (μm)	t_{CPU} (s)	DHI	FMP
Coarse	10 to 80	57	0.848	0.790	40 to 100	52	1.193	2.218
Mid	5 to 40	465	0.844	0.725	20 to 50	234	1.344	2.312
Fine	2.5 to 20	7189	0.843	0.721	10 to 25	2237	1.370	2.329

Table 2.4: Grid independence results for coarse, mid and fine meshes (coated and solid struts).

2.9.3 Time-step Independence

In order to achieve time-step independence, DHI and FMP were compared for time-steps over a range from 0.5×10^5 s to 0.03125×10^5 s for solid and coated strut simulations. Table 2.5 shows the results for time-step independence. Time-steps of 0.125×10^5 s were selected for the remainder of the 2D simulations because they represented the best compromise between solution times and agreement with the next smaller time-step of 0.0625×10^5 s.

	Coated			Solid		
Time Step (s)	t_{CPU} (s)	DHI	FMP	t_{CPU} (s)	DHI	FMP
0.5×10^5	201	0.940	1.009	103	1.349	2.560
0.25×10^5	286	0.877	0.813	149	1.345	2.378
0.125×10^5	479	0.844	0.725	228	1.344	2.312
0.0625×10^5	796	0.843	0.719	416	1.344	2.309
0.03125×10^5	1511	0.843	0.718	771	1.344	2.308

Table 2.5: Time-step independence results for decreasing time-steps (coated and solid struts).

2.9.4 Analytical Solution Comparison

Tests were carried out in order to verify that FIDAP produces results in agreement with analytical findings for scale lengths and material parameters similar to those used in the drug-eluting stent model. Two comparisons were done: a flow simulation in a straight pipe of diameter 0.3 cm with fully developed inlet boundary conditions, and a 2D species mass transfer experiment with zero concentration at the outer wall and initial conditions of unit concentration at the inner wall. The results of these comparisons follow.

Poiseuille Flow

In order to verify the accuracy of FIDAP for flow simulations, results were compared for fully developed Poiseuille flow in a pipe. An axisymmetric pipe model was implemented with fully developed flow at the inlet, as in the drug-eluting stent simulations. The dimensions of the pipe matched those for the drug-eluting stent simulations, and a velocity profile for u_x was examined at the halfway point of the pipe (at $x = 0.4$ cm).

The analytical solution for this geometry is given by the equation

$$u_x = 22.20 - 986.72y^2 \tag{2.21}$$

for the velocity in cm/s^2. Comparison to the FEM results showed excellent agreement, shown in Figure 2.9.

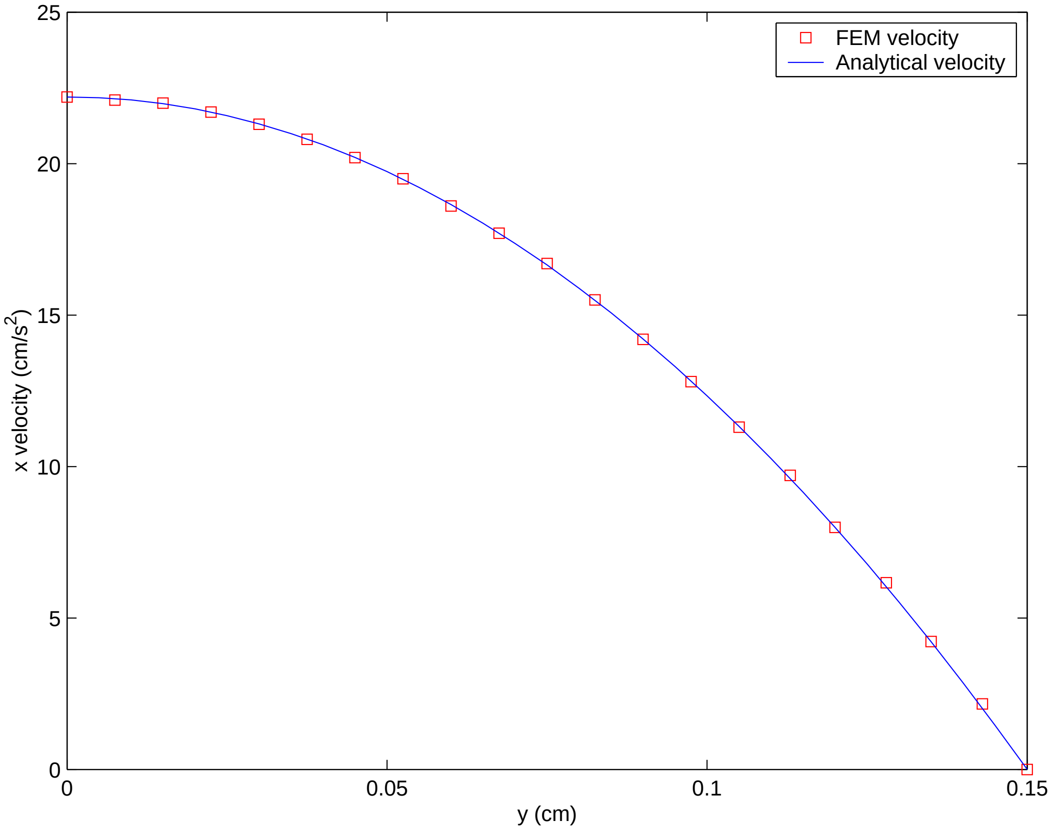

Figure 2.9: Analytical and FEM comparison for u_x velocity profiles in a straight pipe.

1D Mass Transfer

A transient one-dimensional mass transfer problem was solved analytically and compared to an analogous FEM solution. For the basic partial differential equation

$$\frac{\partial c}{\partial t} = D\frac{\partial^2 c}{\partial y^2} \tag{2.22}$$

a solution of the form

$$c_n(y,t) = c_0 \exp\left(-\left(\frac{n\pi}{L}\right)^2 D \cdot t\right) \sin\frac{n\pi y}{L} \tag{2.23}$$

represents the basis of an infinite family of product solutions with boundary conditions $c(0,t) = 0$ and $c(L,t) = 0$, and $n = 1, 2, 3 \ldots$. Setting $n = 1$ and imposing a constant multiple over a half-domain from $y = 0.04$ cm to $y = 0.08$ cm corresponding to $L = 0.04$ cm, the solution becomes:

$$c(y,t) = 0.208 \exp\left(-\left(\frac{\pi}{2L}\right)^2 D \cdot t\right) \sin\left(\frac{\pi}{2}\left(\frac{y}{L} + 1\right)\right) \tag{2.24}$$

For comparison with the FEM results, we examine the solution at $t = 6 \times 10^5$ s with diffusivity $D = 10^{-9}$ cm^2/s corresponding to vascular wall material properties. FEM results were seen to agree very well with analytical results, as shown in Figure 2.10.

These comparisons show that uncoupled analytical solutions with dimensions and material properties matching those implemented in FEM simulations produce near-identical results. Although Fluent has certainly performed rigorous verification of its code through comparisons to analytical solutions, these tests demonstrate the solver's accuracy for the specific geometry and material properties of the model developed in this work.

2.10 Conclusion

Based on key simplifications of vascular physiology, a 2D model has been developed for modelling mass transfer from drug-eluting stents in coronary arteries. Preliminary results from the numerical model were verified through comparison to experimental data, other numerical models and basic analytical solutions to analogous geometries. The model will now be applied to coated and solid struts while varying inter-strut spacing and strut apposition, followed by solid struts in a curved vessel. Data analysis will be carried out using three dimensionless parameters which give indications of dose homogeneity, final mass and strut contact area within the specified therapeutic region.

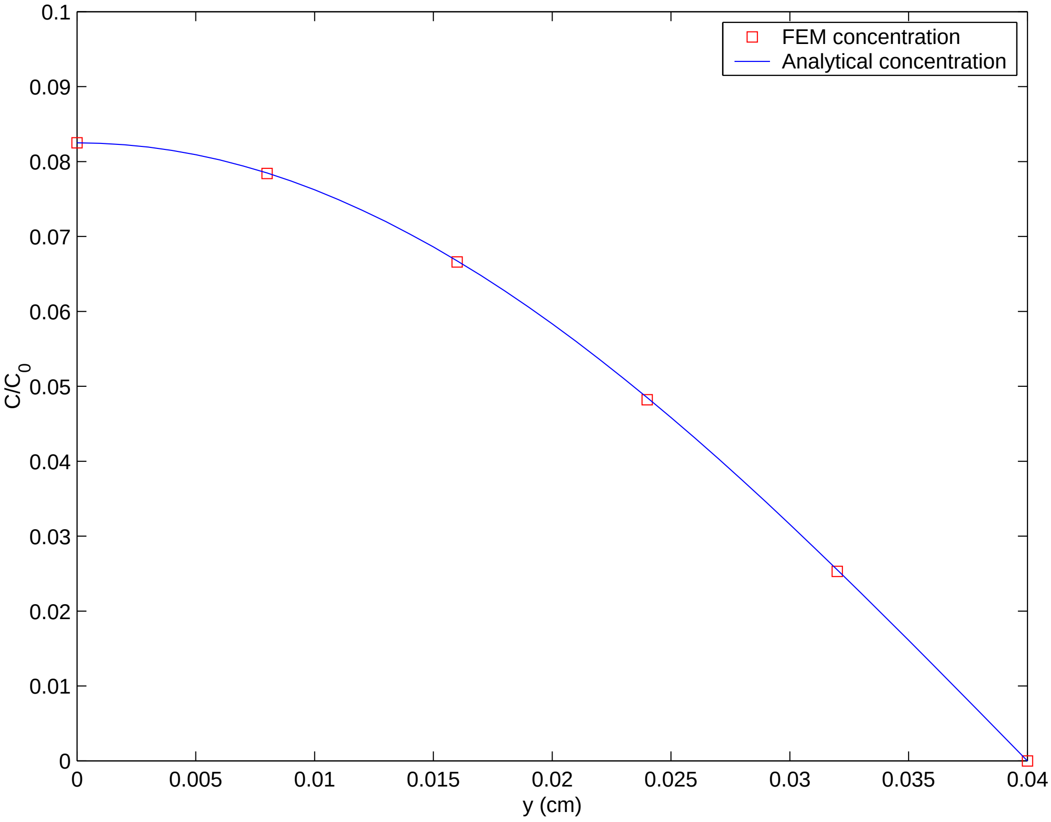

Figure 2.10: Analytical and FEM comparison for 1D concentration profiles in a vascular wall section.

Chapter 3

Results From 2D Models

3.1 Overview

Two-dimensional results are divided into two main experiments. The first experiment compares the drug delivery from coated metallic stents to that from solid polymeric stents while varying inter-strut spacing and the degree of strut embedment. The second experiment compares dose delivery results of the inside and outside walls of a curved vessel geometry.

3.2 Standards for Comparison

Benchmark results for basic coated and solid strut configurations are presented here in order to provide reference values for results from simulations where geometric parameters are varied. These results are for half-embedded struts spaced at 1500 μm, with a Reynolds number of 100. Figures 3.1 and 3.2 show concentration in the therapeutic region for solid and coated strut scenarios at time $t = 6 \times 10^5$ s (approximately one week). Note that the scales of concentrations are different in Figures 3.1 and 3.2. The value of $t = 6 \times 10^5$ s is used for the remainder of the simulations as the final dose measurement time. Stent struts can be seen regularly spaced, and are represented by regions of zero concentration, although there is mass present in struts. Table 3.1 shows DHI, FMP and ACI values for these two benchmark simulations.

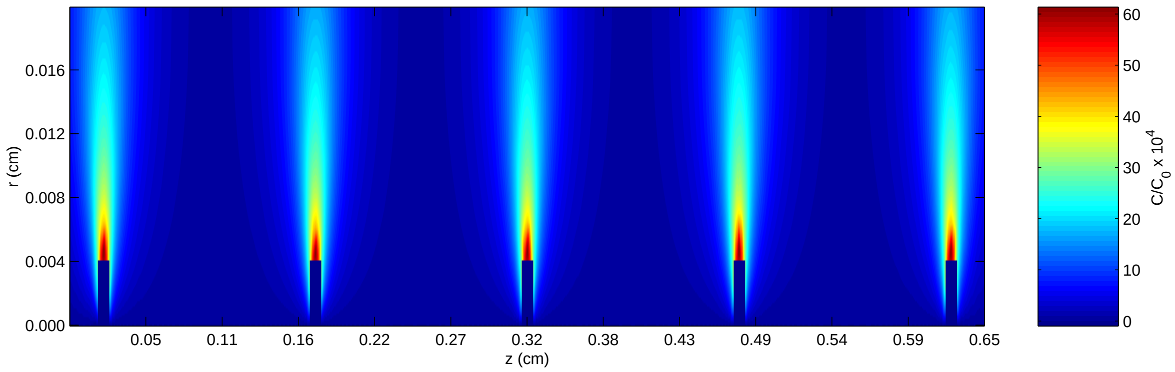

Figure 3.1: Concentration in the therapeutic region for solid stent struts. Struts are evenly spaced, and are represented by regions of zero concentration.

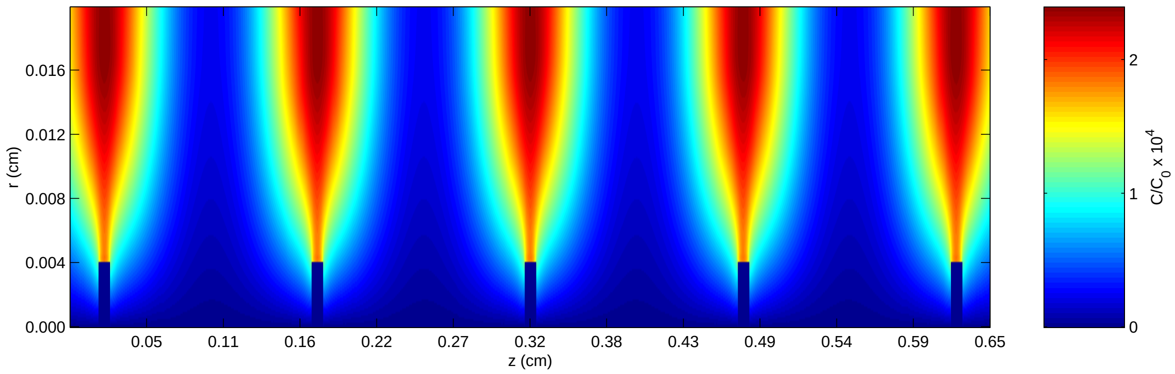

Figure 3.2: Concentration in the therapeutic region for coated stent struts. Struts are evenly spaced, and are represented by regions of zero concentration.

3.3 Transient Analysis Results

A transient analysis of FMP and DHI was performed for coated and solid strut models over a simulation period of two weeks (Figures 3.3 and 3.4). In these simulations, struts are half-embedded and spaced at 1500 μm, and have flow corresponding to a Reynolds

Strut Type	Time (s)	FMP	DHI	ACI
Solid	6×10^5	2.31	1.34	12.9
Coated	6×10^5	0.73	0.84	12.9

Table 3.1: Benchmark results for coated and solid struts.

number of 100. Data are shown for time-steps of 10^5 s (1.16 days), with the horizontal axis measured in days.

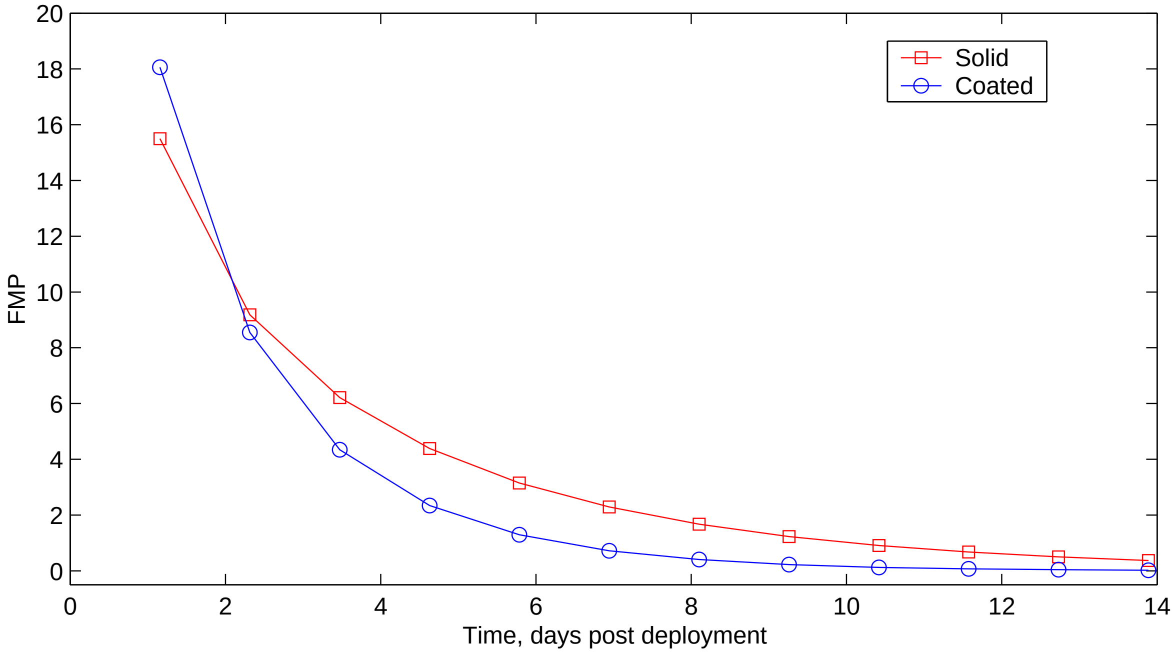

Figure 3.3: Mass percentage vs time in the therapeutic region over the course of two weeks for solid and coated struts.

3.4 Inter-strut Spacing Results

Results for FMP and DHI at $t = 6 \times 10^5$ s (approximately 7 days) with varying inter-strut spacing appear in Figures 3.5 and 3.6. Again, struts are half-embedded with a flow field corresponding to a Reynolds number of 100. Inter-strut spacing is increased from 500 μm to 2000 μm (see Figure 2.3). Therapeutic regions in these trials increase

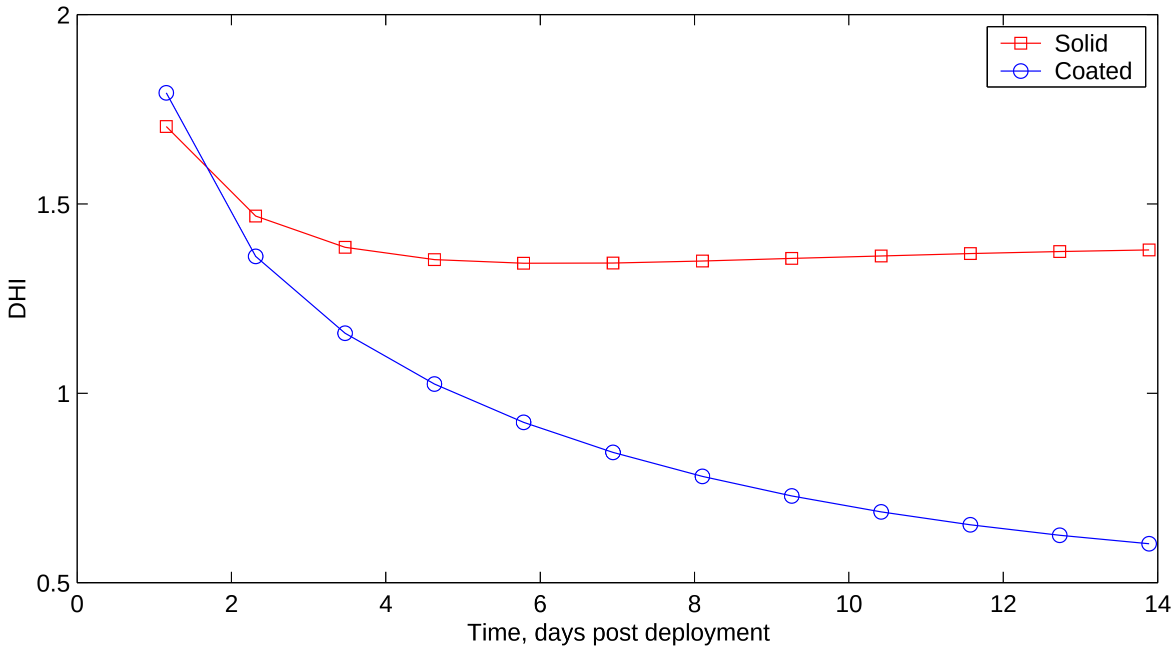

Figure 3.4: DHI vs time in the therapeutic region over the course of two weeks for solid and coated struts.

in area as inter-strut spacing increases, extending in the z-direction 200 μm beyond extreme struts in all cases. Table 3.2 shows ACI values for the four inter-strut spacings investigated.

Inter-Strut Spacing (μm)	ACI
500	32.3
1000	17.9
1500	12.9
2000	9.4

Table 3.2: Area contact indices for different inter-strut spacings (coated and solid struts).

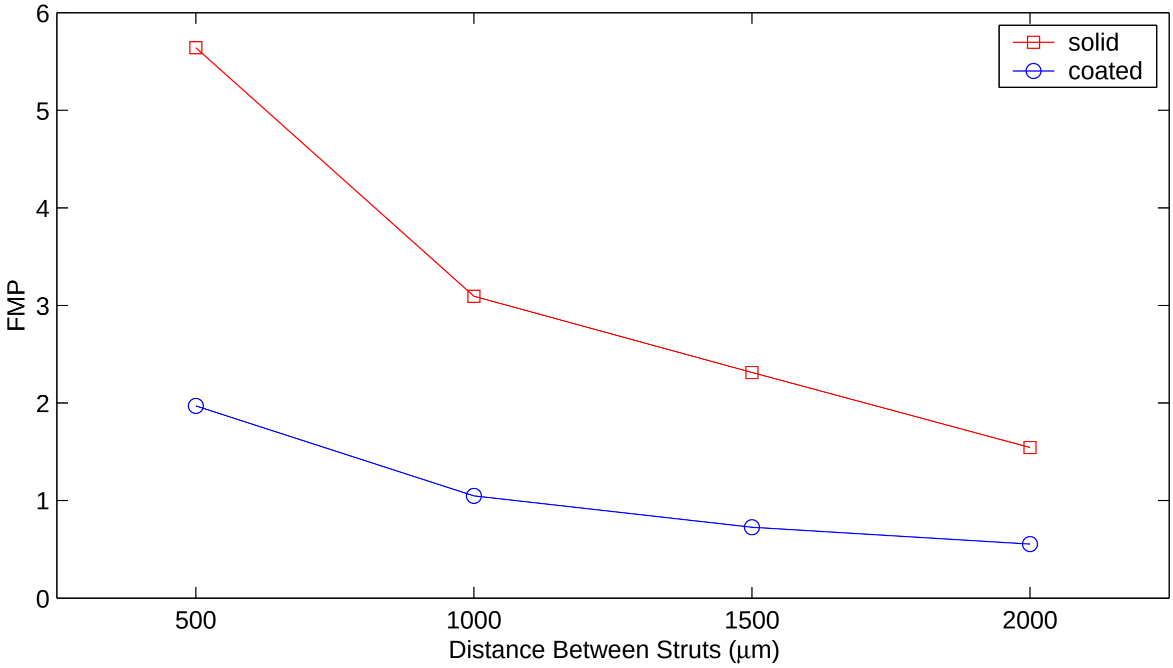

Figure 3.5: FMP vs inter-strut spacing for solid and coated stent struts.

3.5 Strut Apposition Results

Results for FMP and DHI for varying degrees of strut embedment (completely embedded, halfway embedded and contacting) appear in Figures 3.7 and 3.8. It should be noted that at some point after stent deployment, all struts are made fully-embedded through healing processes and restenosis. This effect is not considered in this study. Inter-strut spacing is held constant at 1500 μm and the Reynolds number is 100. Table 3.3 shows ACI values for different strut embedment scenarios.

Apposition scenario	ACI
Contacting	6.2
Halfway embedded	12.3
Fully embedded	18.5

Table 3.3: Area contact indices for different embedment scenarios (coated and solid struts).

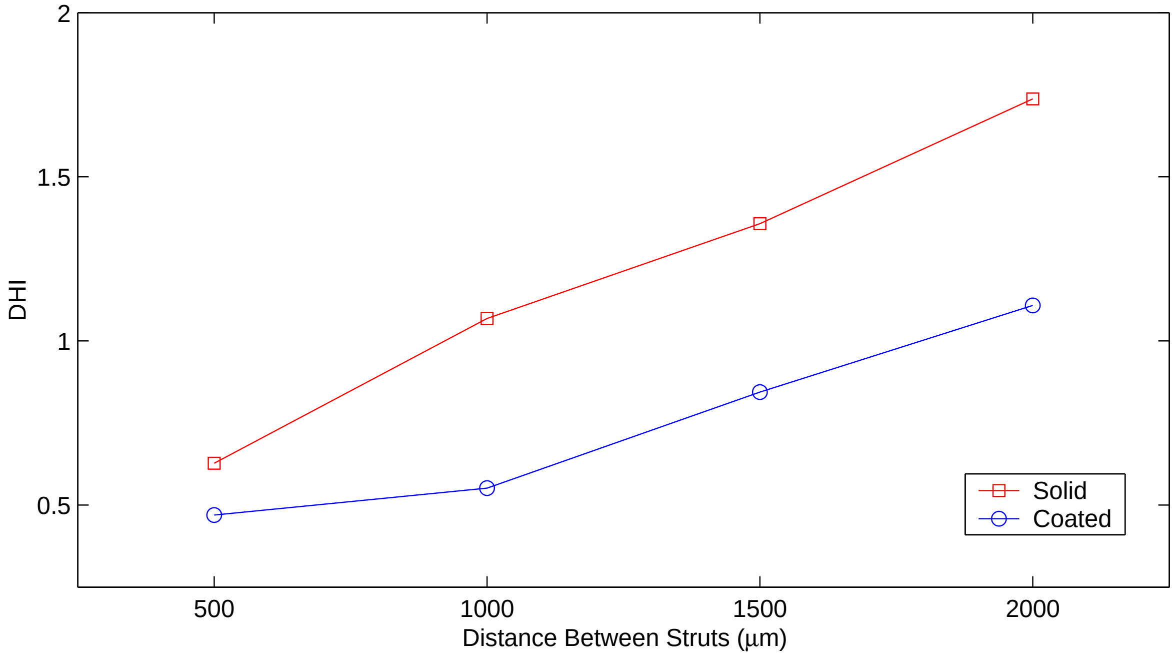

Figure 3.6: DHI vs inter-strut spacing for solid and coated stent struts.

3.6 Vessel Curvature Results

Curved artery simulations were conducted for solid stent struts only, and examine a section of the vessel in the plane of curvature. Other features of the simulation are carried over from previous axisymmetric trials, such as the halfway embedded strut scenario, and a Reynolds number of 100. Inter-strut spacing for struts on the inner and outer walls are based on angular intervals corresponding to a vessel midline inter-strut spacing, d_{ISS}, of 1.5 mm. So, for example, with an R/d value of 10, corresponding to $R = 3.0$ cm, the angular interval would be:

$$d_{\text{ISS}} = R\theta \tag{3.1}$$

$$\theta = \frac{d_{\text{ISS}}}{R} \tag{3.2}$$

$$\theta = \frac{0.15}{3.0} \tag{3.3}$$

$$\theta = 0.05 \text{ rad} \tag{3.4}$$

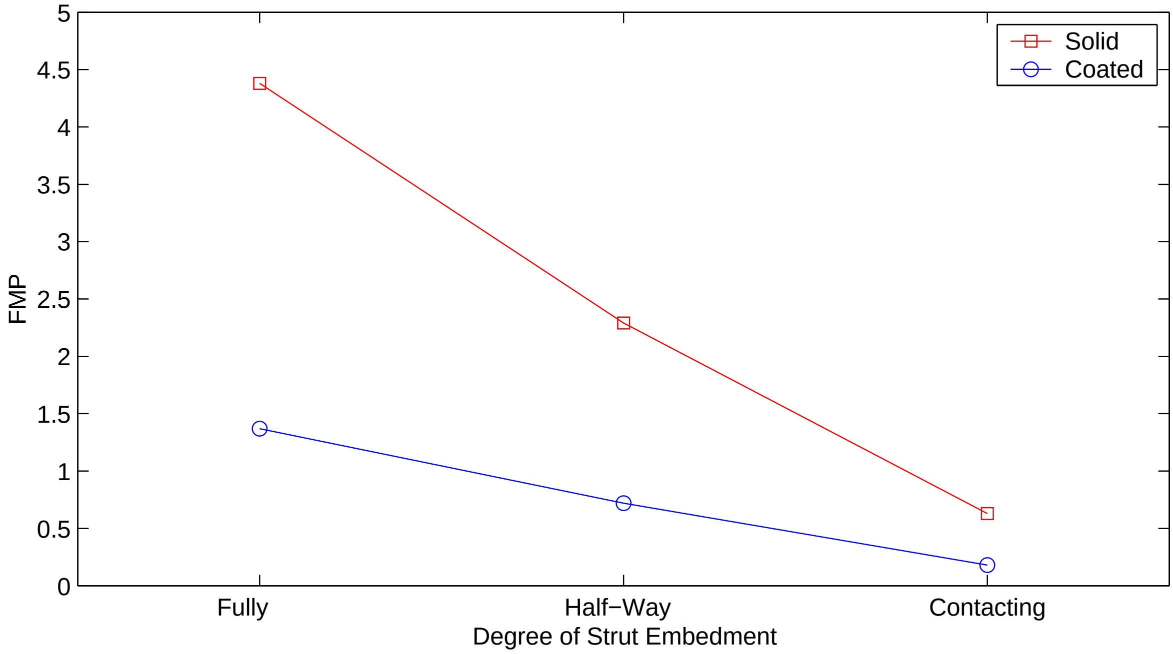

Figure 3.7: FMP values corresponding to different embedment scenarios for solid and coated stent struts.

This angular inter-strut spacing would result in inter-strut spacings measured as the arc length between struts of 1.575 mm on the outside wall and 1.425 mm on the inside wall. This difference in inter-strut spacing between the inner and outer walls leads to different ACI values, as shown in Table 3.4. Figures 3.9 and 3.10 compare FMP and DHI results in the inner- and outer-wall therapeutic regions. The horizontal dashed lines in these plots represent values for FMP and DHI in a straight vessel.

3.7 Discussion of 2D Results

3.7.1 Benchmark Results

Benchmark results for solid and coated stent struts in 2D are shown in Table 3.1. These results correspond to an inter-strut spacing of 1500 μm and Reynolds number of 100 (based on a vessel diameter of 3 mm), with halfway embedded struts. These results show that the solid strut model provides a greater degree of mass retention in the

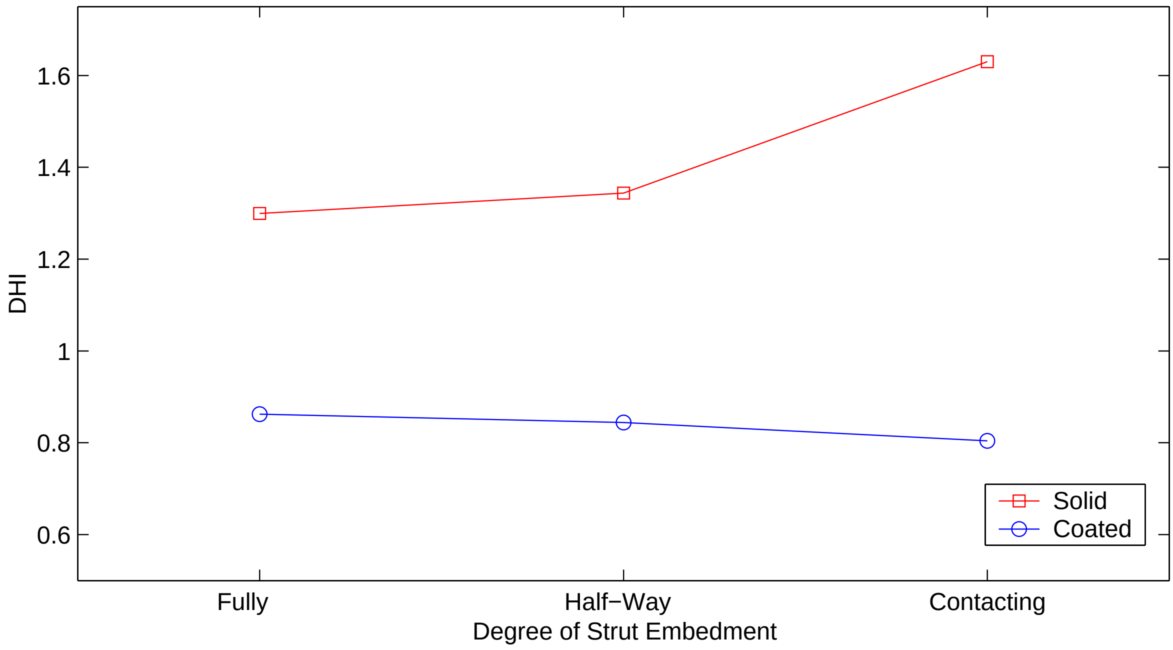

Figure 3.8: DHI values corresponding to different embedment scenarios for solid and coated stent struts.

vascular wall than the coated stent, with an FMP of 2.31 for the solid strut compared to 0.73 for the coated strut. The dose in the solid strut model is less homogeneous than that seen in the coated strut model, with a DHI of 1.34 for the solid strut and 0.84 for the coated strut. The ACI is the same in both cases owing to their identical surface contact characteristics. These results are discussed in the following section with reference to transient results for the solid and coated models just described.

3.7.2 Transient Analysis

Transient simulations for coated and solid polymeric struts show two things. Firstly, mass is retained to a higher degree for solid struts than for coated struts (Figure 3.3). Secondly, homogeneity is seen to improve over the entire two-week period for coated struts, but is seen to improve then worsen after one week for solid struts (Figure 3.4). Mass retention is higher in the solid strut case because there is no diffusive barrier preventing mass from the outer half of the strut (the wetted side of the strut in halfway

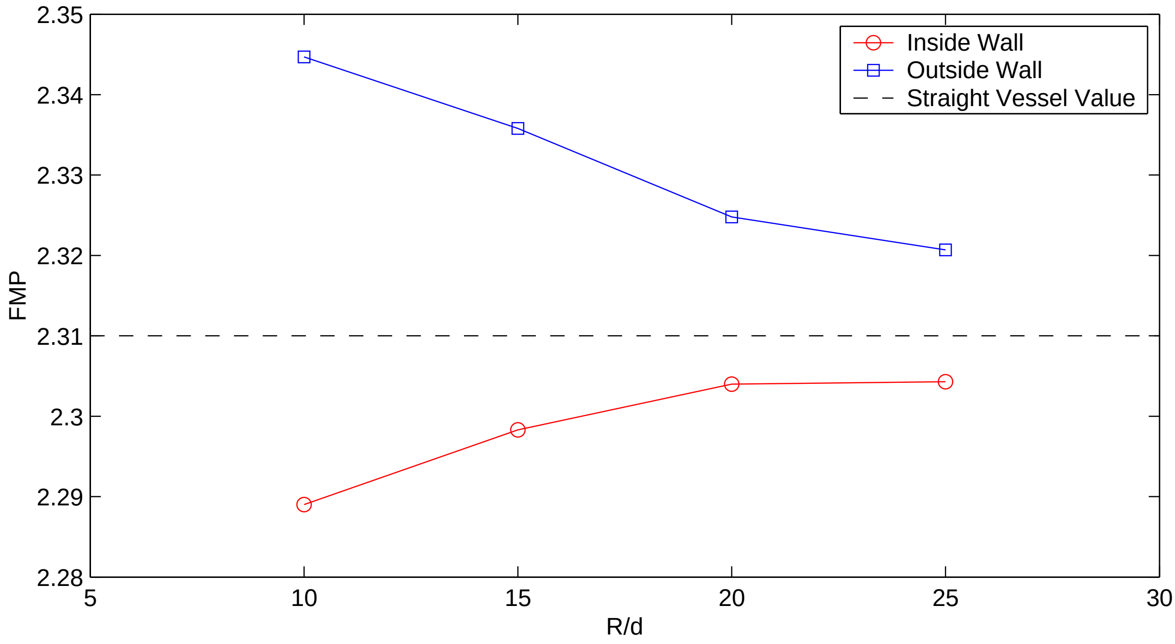

Figure 3.9: FMP values for increasing ratios R/d (see Figure 2.5) for inner and outer walls of a curved artery model.

embedded trials) from entering the vessel wall, and the drug is free to diffuse directly through the center of the stent strut. In the case of the coated strut, the metal core of the strut renders mass transport from the wetted half of the stent into the vascular wall through its centre impossible. The vast majority of this mass diffuses into the lumen, immediately precluding the transport of approximately half of the loaded drug from the coated strut into the vascular wall.

Explaining homogeneity results is somewhat more difficult. Coated struts produce a more homogeneous dose because the ratio of contact area to mass is larger for these struts, and because in their initial state the dose is not localized. The drug-loaded polymer coating can be considered a single wavefront from a source at the center of the strut that propagates through the vascular wall, whereas the dose in the solid strut is more akin to a cannonball moving into the vascular wall. This cannonball effect is caused by the draining of dose released through the sides of the strut into first the vascular wall, then the lumen. Dose released from the top of the strut does not

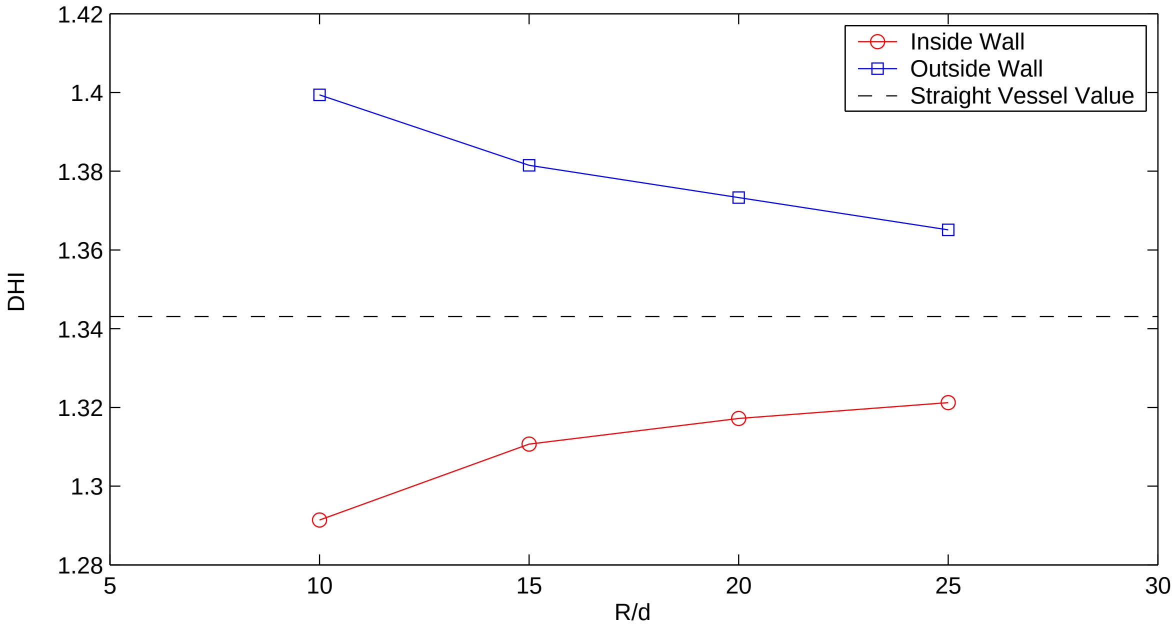

Figure 3.10: DHI values for increasing ratios R/d (see Figure 2.5) for inner and outer walls of a curved artery model.

experience as pronounced a draining effect, and appears as a localized mass propagating outward radially into the vascular wall.

The inversion of DHI for the solid struts at one week can also be explained using the cannonball/wavefront analogy; after the cannonball has left the solid strut, leaving the strut essentially empty, mass is drained from the vascular wall through the vasa vasorum and the inter-strut space in contact with the lumen. This draining acts to isolate these areas of localized dose in the vascular wall, decreasing dose homogeneity. In the case of the coated strut, as the wavefronts continue to propagate, their overlapping acts to increase homogeneity in the vascular wall.

3.7.3 Inter-strut Spacing Analysis

Three factors must be considered in determining an optimal inter-strut spacing: inflammatory response from strut contact, mechanical support characteristics, and dose delivery. At $t = 6.94$ days, these simulations show that as inter-strut spacing increases,

R/d	Inner Wall ACI	Outer Wall ACI
10	13.56	12.27
15	13.32	12.46
20	13.21	12.56
25	13.14	12.63
∞	12.88	12.88

Table 3.4: Area contact indices for varying R/d values in the curved vessel model.

mass retention decreases and the final dose is less homogeneous for both solid and coated stent struts (Figures 3.5 and 3.6). Both of these results are expected. As inter-strut spacing increases, the area of the therapeutic region also increases, but the mass of drug in the strut does not, leading to a lower FMP. Homogeneity worsens as inter-strut spacing increases because the dose delivered from each strut becomes more isolated. Despite differing initial values, the overall behavior of DHI and FMP with varying inter-strut spacing is similar for solid and coated struts. Table 3.2 shows that ACI decreases as inter-strut spacing increases, from 32.3% at 500 μm to 9.4% at 2000 μm, which is a strictly geometric result.

3.7.4 Strut Apposition Analysis

Strut embedment varies significantly following stent deployment due to irregular vessel geometry and wall anisotropy. Strut embedment also varies from patient to patient, and can be controlled to a certain extent through modulation of angioplasty balloon deployment pressures. Inflammatory response from strut contact, mechanical support characteristics and dose delivery are all sensitive to the degree of strut embedment.

Mass retention results show that as FMP decreases as strut embedment decreases for both solid and coated struts (Figure 3.7). This result is expected, since the contact area between the vascular wall and strut decreases. Since any drug reaching the vessel lumen is immediately washed away, the resulting higher contact area between strut and lumen also contributes to lower FMP values. Homogeneity results show an opposite effect for solid and coated struts (Figure 3.8). For solid struts, DHI increases as embedment (hence contact area) decreases, meaning the dose is less homogeneous. For coated struts, DHI decreases slightly with decreasing embedment, meaning the dose is slightly more homogeneous. This opposing homogeneity effect can be explained by considering the cannonball/wavefront analogy discussed in the comparison of transient results. Table 3.3 shows that ACI decreases as the degree of embedment decreases, from 18.5% for completely embedded struts to 6.2% for contacting struts.

3.7.5 Vessel Curvature Analysis

Homogeneity results for curved arteries can be explained by considering the geometry of the therapeutic region as curvature increases. Corresponding struts on the inner and outer vessel are placed on lines of constant angle from the center of curvature, with the inter-strut spacing at the midline of the lumen held constant at 1500 μm. As a result, smaller R/d values lead to an increase in therapeutic region area and inter-strut spacing distance on the outer wall, and a decrease of these quantities on the inner wall. Homogeneity results from the inter-strut spacing trials correctly predict that as the radius of curvature decreases, DHI decreases on the inner wall. The opposite occurs on the outer wall.

FMP results show that mass retention is greater on the outer wall, and decreases as R/d increases. The opposite is true on the inner wall. This is because the outer wall has a greater therapeutic region than the inner wall, and more mass is accounted for in the outer wall therapeutic region, especially in regions surrounding the extreme struts. Since this is a geometric effect resulting from area-weighting in the arbitrarily determined therapeutic region, it is also useful to examine the mean concentrations in the therapeutic regions. Mean concentration values appear in Table 3.5, and show that mean concentration levels on the inner wall are consistently higher than those on the outer wall. Mean concentration and FMP results are in general very similar on the inside and outside walls, and since the two indicators of mass retention lead to opposite conclusions with respect to dose delivery effectiveness, they are not considered meaningful in this analysis.

	$\frac{\bar{C}}{C_0} \times 10^{-4}$	
R/d	Inner Wall	Outer Wall
10	5.87	5.40
15	5.77	5.47
20	5.73	5.49
25	5.69	5.51
∞	5.62	5.62

Table 3.5: Mean concentrations at varying R/d values on inner and outer walls of the curved vessel model.

These homogeneity and mass results taken together indicate that a less homogeneous dose on the outer wall of curved coronaries may lead to a higher degree of in-stent restenosis in those areas. Flow considerations were not seen to have any effect on the parameters of interest in the curved vessel simulations for reasons explained in Chapter 4.

3.8 Conclusions

The comparison between coated and solid struts indicates that, in spite of superior mass retention for solid struts, coated struts produce more favourable dose delivery results. Low final mass percentages for coated struts can easily be corrected by increased initial mass loading. A similar correction for the homogeneity of solid struts does not exist. The stability of the homogeneity of coated struts with varying strut embedment is another important result. A lower degree of strut embedment calls for lower balloon deployment pressures, which may decrease the overall tissue damage and inflammation in the region. These conclusions indicate that the most favourable overall scenario might involve the coating of solid polymeric struts with a drug-loaded layer rather than loading the entire strut.

Inter-strut spacing and strut embedment results show that the most favourable results come with close, highly embedded struts. The negative effects on surrounding tissues that would result from a stent designed and deployed with this in mind must be carefully considered, and a compromise between tissue injury, mechanical support and dose delivery must be achieved. With these factors in mind, and considering the results of the simulations, half-embedded struts with 1000 to 1500 μm inter-strut spacing appear to be the best compromise.

Vessel curvature is seen to have a notable effect on homogeneity, but little effect on mass retention characteristics. Introducing a stent design with more struts, or a denser strut pattern on the outer wall of curved arteries is not practical from a manufacturing standpoint. As a result, changing dose homogeneity characteristics on the outer wall would be difficult. Differential mass loading on inner and outer struts is another option, but it is difficult to do. The most sensible solution to this problem is to overestimate the initial drug loading on stents destined for curved arteries. The difference between the inner and outer wall masses is not large enough that initial overloading would lead to toxicity on the inner wall, and overloading would not increase the expense or difficulty of stent design, construction and deployment.

Chapter 4

Analysis of Flow and Model Simplification

This chapter will analyze the impact of flow on dose delivery in the two-dimensional model, and discuss appropriate simplifications to the flow field that can be applied to the three-dimensional model. All of the results shown in the previous chapter correspond to flow with a Reynolds number of 100, corresponding to a mean vessel flow velocity of 11.1 cm/s, and flow rate of 0.05 L/min. In the first part of this chapter, Reynolds numbers are varied over the physiologic range for flow in coronary arteries (5 to 35 cm/s [85]) and beyond, and the effects are analyzed using FMP and DHI results. The second part of this chapter proves that flow can be neglected with appropriate changes to the lumen diffusion coefficient. This simplification to the model greatly reduces the size and computational expense of 3D simulations.

4.1 Flow Analysis

A solid, half-embedded strut model with inter-strut spacing of 1500 μm was used to evaluate flow effects in the therapeutic region. Reynolds numbers were varied from values well below the physiologic range to the upper physiologic range, and DHI and FMP values in the therapeutic region were calculated. Figure 4.1 shows the results for these simulations. It can be seen from this figure that within the physiologic flow range for coronary arteries, there is very little change in FMP and DHI, and as Reynolds numbers become very small, the values are noticeably affected. At low Reynolds numbers, the dose is more homogeneous, mass is retained to a high degree and the dose can be seen to collect in proximal regions of the vessel wall (Figure 4.2). The areas within the therapeutic region which would be most sensitive to the effects of flow in the lumen are those closest to the intima. In order to evaluate the near-wall effects of flow, a region lying in between successive struts is isolated (Figure 4.3), and FMP and DHI are measured in this region over the same range of Reynolds numbers used previously. Figure 4.4 shows these results. Again, within the physiologic range there is little variation in DHI and FMP. Reducing this area by 50% (Figure 4.5) and repeating the simulation shows a slight increase in FMP and DHI variability at low Reynolds numbers, but the plateau region is still within the physiologic range as seen in Figure 4.6. From these results it

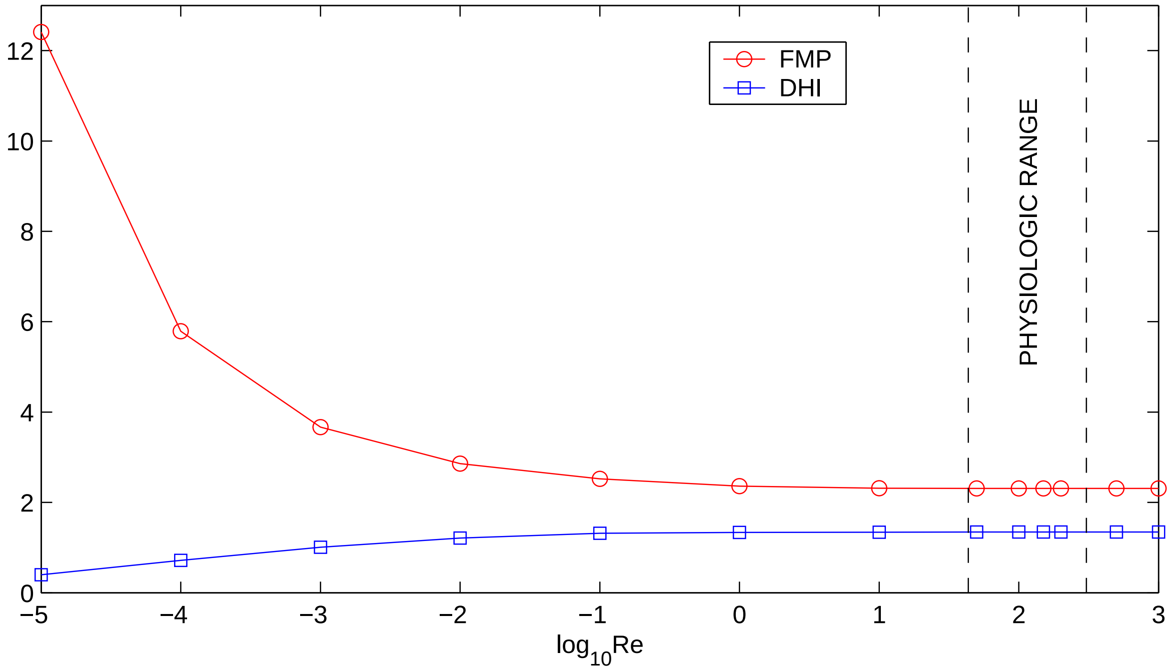

Figure 4.1: FMP and DHI vs Reynolds number in the therapeutic region, with the physiologic range of coronary flow shown.

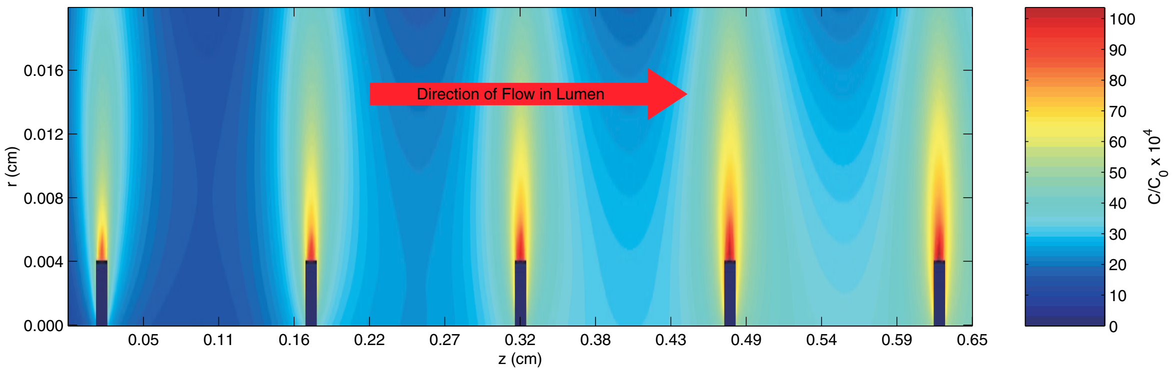

Figure 4.2: Dose distribution in the therapeutic region of the vessel wall for low Reynolds number 10^{-5}.

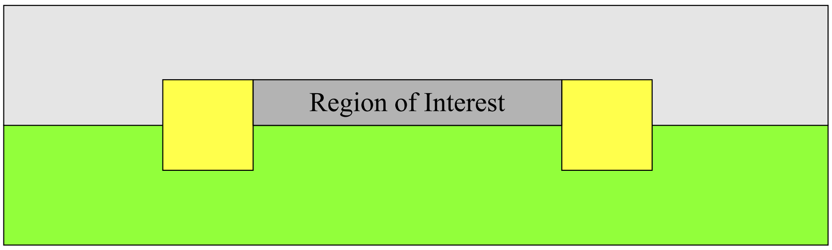

Figure 4.3: Reduced region of interest between successive half-embedded struts.

can be seen that over physiologic flow ranges for coronary arteries, there is a very small change in the parameters of interest in this study. At low flow rates there is an effect on these parameters, but such flow rates do not occur naturally in coronary arteries. The importance of convective and diffusive mass transport mechanisms in determining the stability of FMP and DHI is discussed in the following section.

4.2 Model Simplifications

This section examines possible simplifications to the previously discussed 2D simulations which would reduce the size and computational expense of the analogous 3D model. There are two considerations in making these simplifications. First, the parameters of interest (FMP and DHI) must be proven stable with the simplified model,

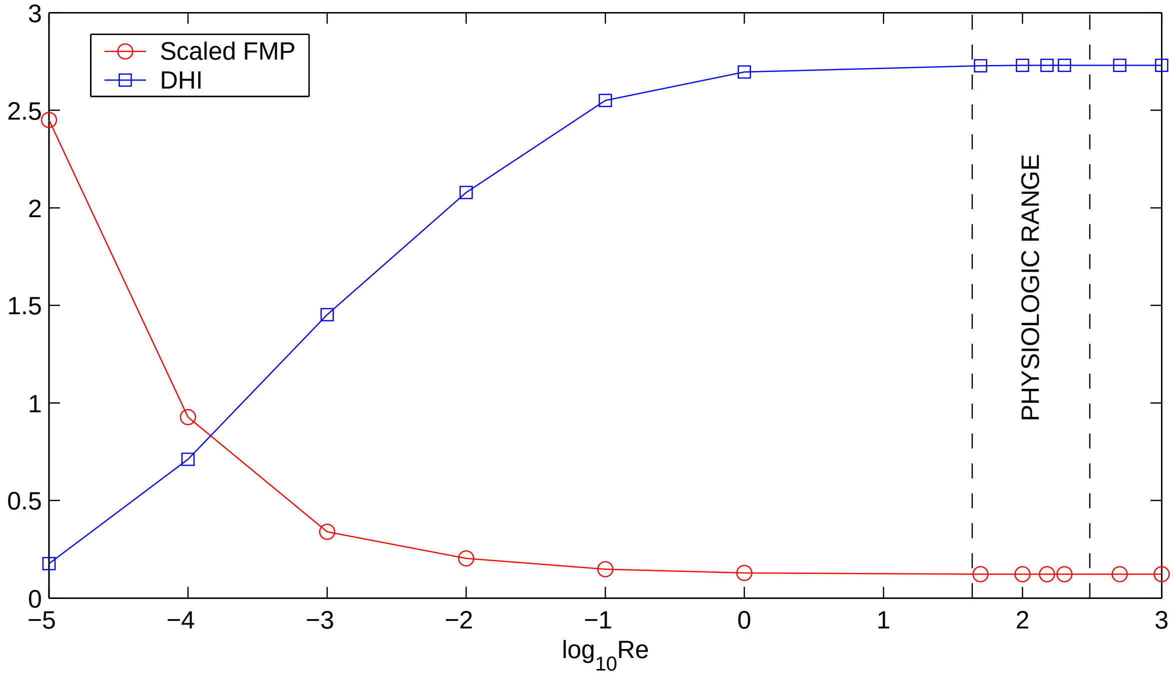

Figure 4.4: FMP and DHI vs Reynolds number in a reduced area of interest (see Figure 4.3), with the physiologic range of coronary flow shown.

and second, any fundamental changes to the underlying physics of the problem must be justified. Two dimensionless parameters are examined to show the appropriateness of the simplifications applied. They are the Peclet number, Pe, which is an indicator of the relative importance of convective and diffusive transport mechanisms in a given model, and a dimensionless mass transport number, M, which is an indication of the overall magnitude of mass transport in a given model. Both of these dimensionless numbers can be expressed in terms of the Reynolds number already defined in Equation 2.7 and the Schmidt number, Sc, defined below:

$$\mathrm{Sc} = \frac{\mu}{\rho D} \tag{4.1}$$

The Peclet number is then defined as

$$\mathrm{Pe} = \frac{u_0 L}{D} = \mathrm{Re} \cdot \mathrm{Sc} \tag{4.2}$$

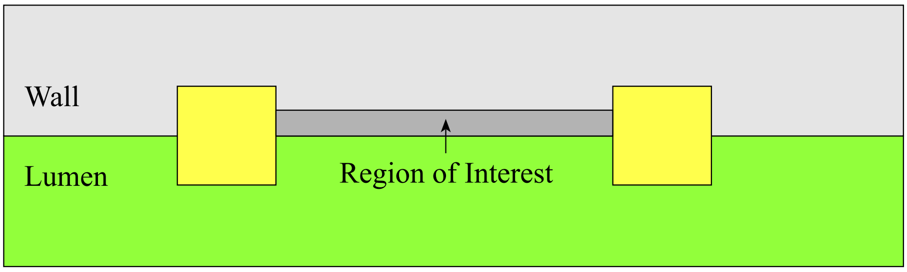

Figure 4.5: Further reduced region of interest between successive half-embedded struts.

and the mass transport number as

$$\mathrm{M} = u_0 L D \left(\frac{\rho}{\mu}\right)^2 = \frac{\mathrm{Re}}{\mathrm{Sc}} \tag{4.3}$$

A discussion of the stability of the FMP and DHI over a range of the dimensionless numbers Pe and M will be used to justify simplifications to the model in preparation for the extension to three dimensions.

4.2.1 FMP and DHI results with varying Pe

In this investigation, the Peclet number is varied in two ways. The first is to hold Re constant and vary Sc, and the second is to hold Sc constant and vary Re. Simulations were performed using an inter-strut spacing of 1500 μm, with half-embedded solid stent struts and the standard therapeutic region definition. The Reynolds number was fixed at 10^{-4} while Sc was varied, and the Schmidt number was fixed at 3.33×10^6 while Re was varied. The nominal Peclet number, Pe_n corresponding to a mean flow of 11.1 cm/s and lumen diffusivity of 10^{-8} cm^2/s is

$$\mathrm{Pe}_n = \frac{u_0 L}{D_{\mathrm{lumen}}} = 3.33 \times 10^8. \tag{4.4}$$

Figure 4.7 shows results for FMP and DHI holding one of the variables fixed and varying the other. This figure can be considered two planar sections of the schematic contour plot shown in Figure 4.8. It can be seen that along lines of constant Pe, FMP values

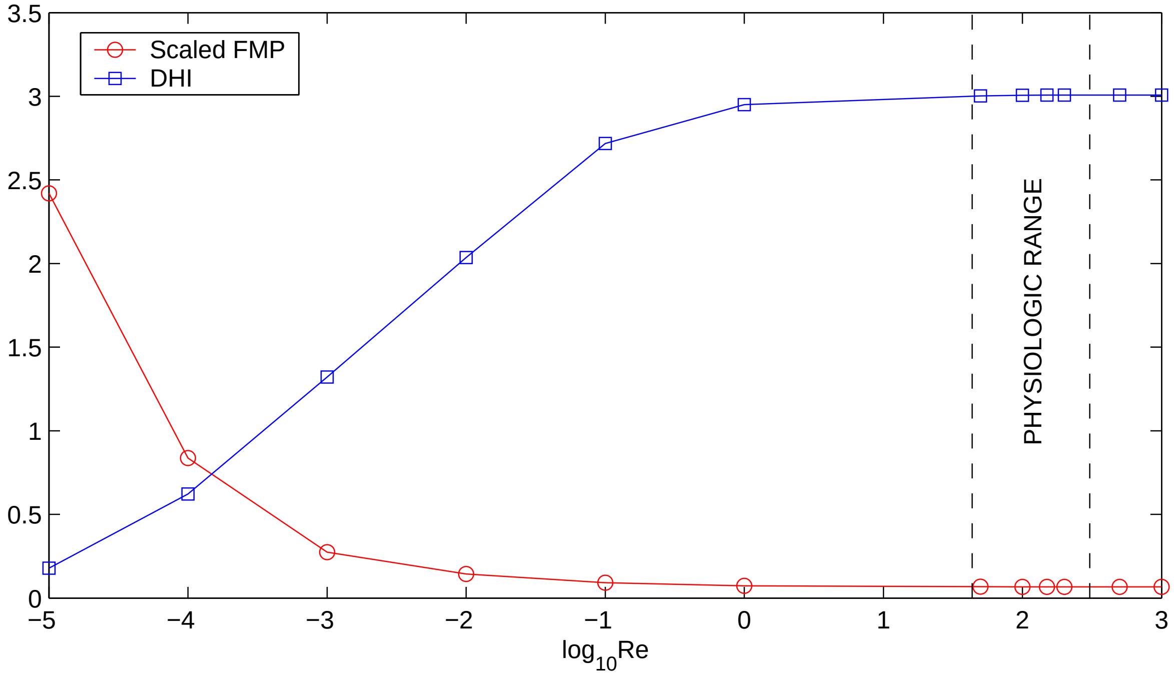

Figure 4.5: FMP and DHI vs Reynolds number in a further reduced area of interest (see Figure 4.5), with the physiologic range of coronary flow shown.

decrease significantly at low values of Re and 1/Sc, however along lines of constant M, FMP is comparatively stable.

4.2.2 FMP and DHI results with varying M

Previous results show that constant Pe-values do not ensure stability of homogeneity and mass values. This section shows that constant values of the parameter M, especially when M is large, can ensure the stability of FMP and DHI values. This effect can be clarified by rearranging Equation 2.3 in the following way:

$$\frac{\partial c}{\partial t} = D\nabla^2 c - (\mathbf{u} \cdot \nabla)c \tag{4.5}$$

It can be seen that if both D and $\mathbf{u}$ are small, then $\frac{\partial c}{\partial t}$ will be small (for $c_0 \approx 1$). In the case of this model's geometry, this effect can be interpreted as follows: If both $\mathbf{u}$ and D are small in the flow region, mass is present in the lumen for long enough to affect concentration levels in the vascular wall. If they are both large, the lumen

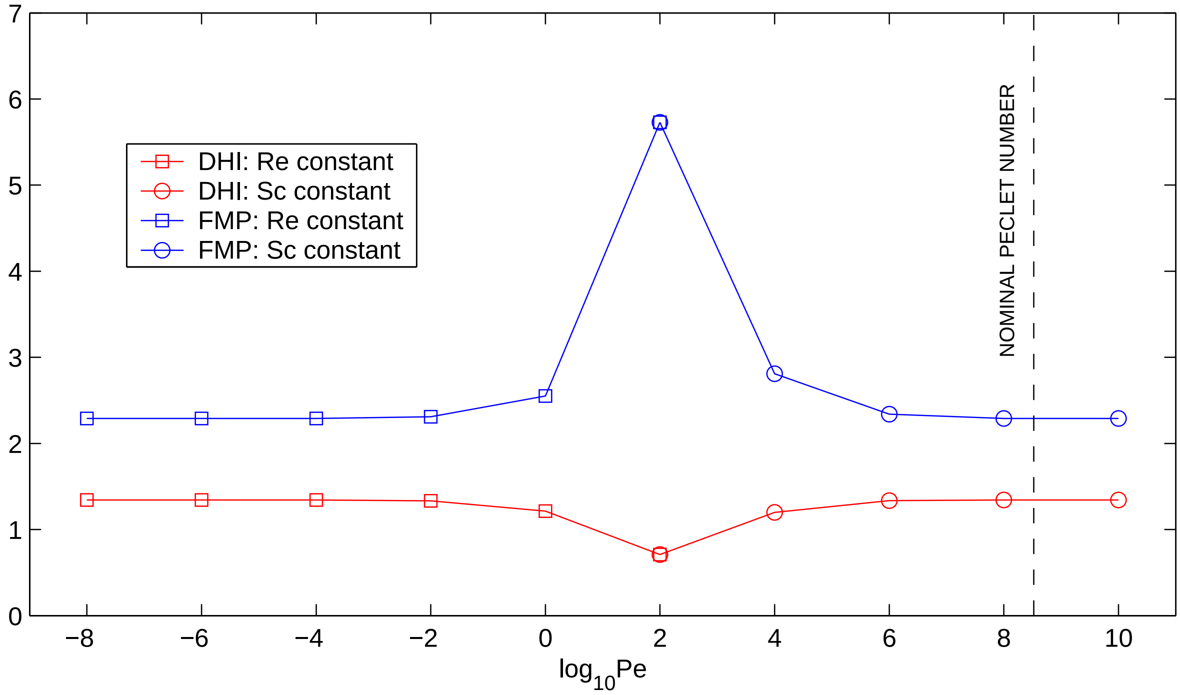

Figure 4.7: FMP and DHI vs Peclet number holding Re and Sc constant.

concentration will be maintained at a near-zero value. It can be shown that there is a threshold value of M above which concentration in the vascular wall is unaffected.

Figure 4.9 shows the behaviour of DHI and FMP with increasing M, with Re held constant at 10^{-4}, and the threshold value is indicated by a solid vertical line. This plot establishes the fact that FMP and DHI values are stable above the M-value threshold of 10^{-6}. This is a crucial step in making simplifications to the 2D model in preparation for the step to 3D simulations.

4.2.3 Simplifications based on these results

The proposed simplification to the 2D model involves reducing $\mathbf{u}$ to a near-zero value and increasing D in the lumen such that the parameter M is above the threshold value established in the previous section. The proposed simplification is outlined below.

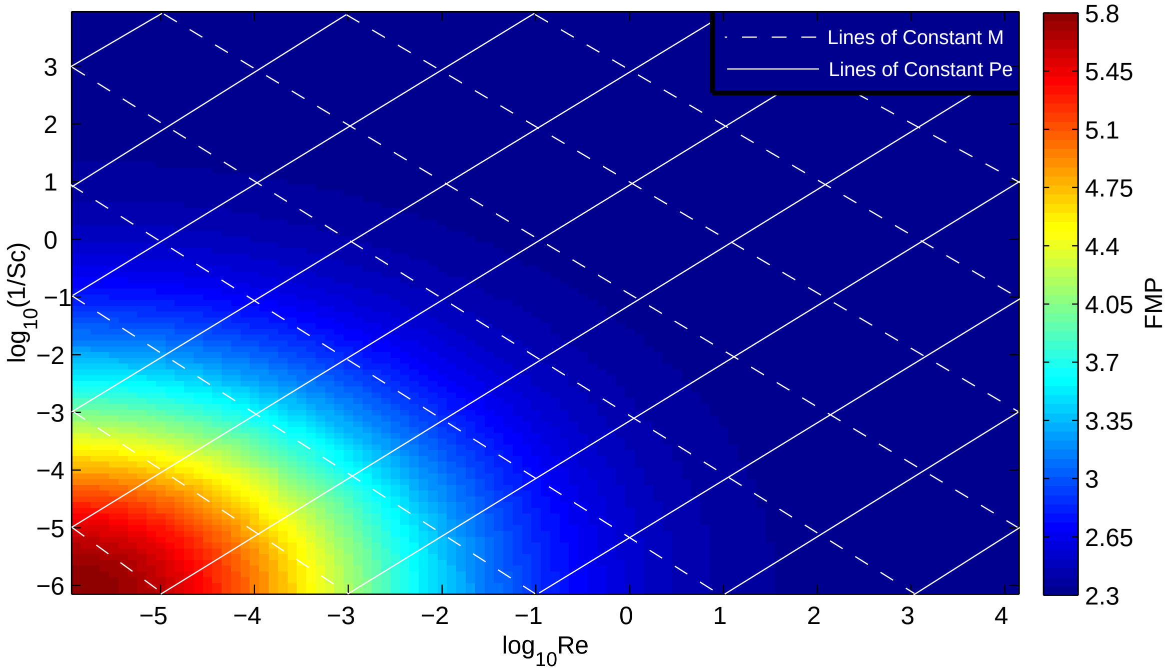

Figure 4.8: Schematic contour plot showing FMP as a function of Re and 1/Sc. Lines of constant Pe and M are shown.

Justifying a quasi-stationary flow hypothesis

For a sufficiently small value of Re, the net flow over the total solution time of one week can be considered negligible for the following reasons. For a flow of speed u_L over an arbitrary length L, the flow can always be reduced to the point where, after the time t_s, the following is true:

$$u_L \cdot t_s \ll L \tag{4.6}$$

If this is true, then mass transport due to convection after time t_s can be considered negligible. The first assumption in the simplification is that small flow rates such as these are equivalent to having no flow in the lumen. The next part of the simplification is to arrive at an M value above the threshold described in the previous section after selecting a sufficiently small value of Re to approximate quasi-stationary conditions.

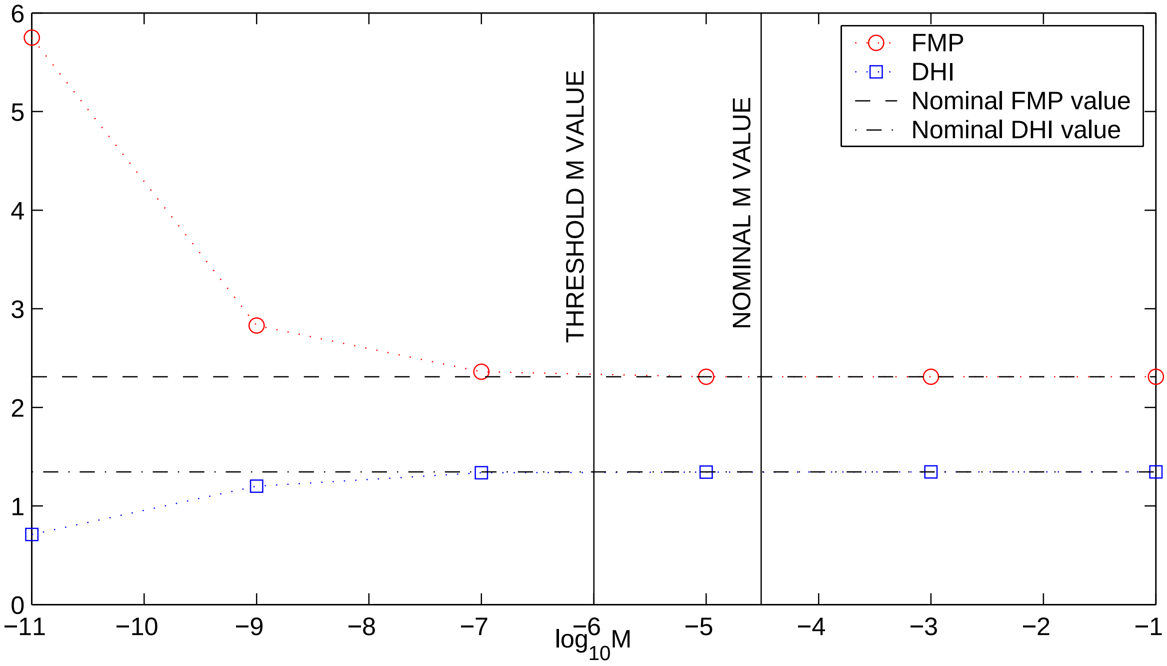

Figure 4.9: FMP and DHI with varying M values.

Selecting an appropriate value of Sc

To achieve an M value above the threshold M_t, an Sc value of between 1 and 10 is required based on a flow speed corresponding to $Re = 10^{-6}$. This value of Sc corresponds to a lumen diffusivity of $D_{\text{lumen}} = 100\ \text{cm}^2/\text{s}$.

In addition to setting these new values of Re and Sc as part of the implementation of the simplification, boundary conditions are modified in the lumen. Instead of imposing a zero-concentration condition at the vessel inlet which would introduce asymmetry, the lumen area is reduced and a zero boundary condition is imposed along the entire length of the inner wall of the lumen, as shown in Figure 4.10.

4.2.4 Summary and Results

In summary, the following steps are used to implement the quasi-stationary flow hypothesis:

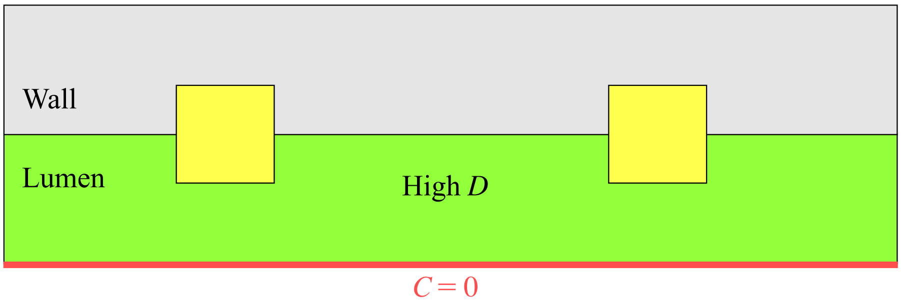

Figure 4.10: Reduced lumen area with zero-concentration boundary condition at the inner wall.

1. Show that for sufficiently small flow speeds, flow is negligible over a characteristic length.
2. Impose a quasi-stationary flow: $\mathrm{Re} = 10^{-6}$
3. Select Sc such that M is greater than M_t: $\mathrm{Sc} = 10$, $\mathrm{M} = 10^{-5}$
4. Modify boundary conditions: $c = 0$ on lumen inner surface

The resulting FMP and DHI values from simulations with this simplification imposed are identical to values from nominal flow simulations (FMP = 2.31, DHI = 1.34). It should be noted that this simplification has been proven appropriate based on these parameters of interest but may not be universally applicable to such models. It is made possible by the fact that, for physiologic flows and diffusion characteristics applied in the advection-diffusion simulations, the resulting M-value ($\mathrm{M} = 3 \times 10^{-5}$) is above the stability threshold ($\mathrm{M}_t = 10^{-6}$). With this simplification in place, the system of governing equations for mass transfer in the problem becomes

$$\frac{\partial c}{\partial t} = D_{\text{polymer}} \nabla^2 c \tag{4.7}$$

$$\frac{\partial c}{\partial t} = D_{\text{vwall}} \nabla^2 c \tag{4.8}$$

$$\frac{\partial c}{\partial t} = D_{\text{lumen}} \nabla^2 c \tag{4.9}$$

and the diffusion coefficients are modified to

$$D_{\text{polymer}} = 10^{-11}\ \text{cm}^2/\text{s} \tag{4.10}$$

$$D_{\text{vwall}} = 10^{-9}\ \text{cm}^2/\text{s} \tag{4.11}$$

$$D_{\text{lumen}} = 100\ \text{cm}^2/\text{s} \tag{4.12}$$

Simulations run with these quasi-stationary simplifications in place were seen to run in 65% of the time taken for full flow simulations.

4.3 Conclusions

This section has shown the behavior of FMP and DHI values with changes to dimensionless mass transport variables Pe and M. It has been shown that DHI and FMP are not stable for constant Pe-values, but are comparatively stable for constant M-values. By selecting a sufficiently high M-value, the removal of flow from the model can be justified. FMP and DHI values for the quasi-stationary flow hypothesis have been proven identical to those produced with the full-flow model. This simplification along with modifications to the lumen boundary conditions can then be extended to the 3D model, reducing its size and solution time.

Chapter 5

Extension to Three Dimensional Model

5.1 Overview

This chapter describes the adaptation of the simplified 2D model to three dimensions. The first part of the chapter is devoted to the geometry creation, meshing and solving of three-dimensional models, followed by a verification of the simplifications described in the 2D model. The final objective of the 3D simulations is to develop a computational tool for evaluating different stent designs on the basis of local drug delivery. The means of evaluating dose efficacy are adaptations of the parameters of interest in the 2D model, namely final mass percentage (FMP), dose homogeneity index (DHI) and area contact index (ACI). These three parameters are weighted and combined into a single dose effectiveness score.

5.2 Geometry Creation

Geometries were created using PTC's parametric CAD package Pro Engineer (Pro/E). Three main geometries were created, each with a slightly different method, in order to allow for comparison between different stent designs. Each geometry is represented by three volumes; stent, vascular wall and lumen. Stent struts are halfway embedded, and are considered solid diffusive entities in these trials owing to difficulties with meshing both thin polymer coatings and the outer regions of the vascular wall while maintaining a sufficiently small problem size. Overall dimensions of these volumes are similar in the three cases, with the primary difference being the stent design itself. The details of each geometry will now be discussed.

5.2.1 Symbiotech Geometry

The Symbiotech geometry is the design of primary interest, and is the subject of other parallel studies characterizing its material properties and other parameters. The design is made up of rows of hexagonal cells, inverted and everted, separated by rows of connecting struts (Figure 5.1). In Pro/E, the design is created by wrapping a sketch of the stent design onto a cylinder, cutting away voids and using a thin surface extrusion. A complete description of the construction of the stent design can be seen in the document *Guide to the 3D Representation and Numerical Structural Analysis of a Coronary Stent*, written by Emile Abou-Mansour in 2001 as a part of his Mechanical Engineering honours thesis at McGill University.

In order to simplify the meshing of the three volumes, the strut cross-section is kept square throughout the stent. A suitably small stent section comprising three rows of hexagonal cells, two everted, one inverted, and two rows of joining struts, is used. In addition to using a shortened stent section, the solution domain is reduced to one quarter of the total cylindrical geometry, a simplification made possible by the stent's symmetry.

The vascular wall and lumen region were generated by creating cuts with the quilt surface of the stent into hollow cylindrical sections. A Pro/E assembly containing the three volumes was created in preparation for meshing. The total length of the solution

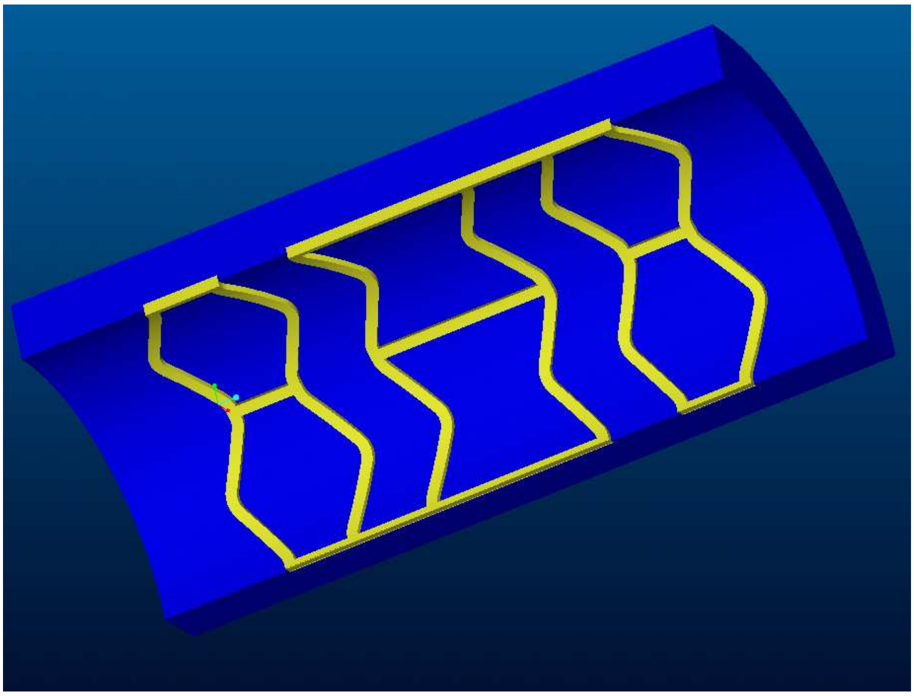

Figure 5.1: Symbiotech design with lumen volume removed.

domain is 8000 μm, with a 6000 μm stent section and 1000 μm on either end of extreme struts. Vascular wall, strut thickness and embedment dimensions are identical to those used in 2D simulations, with a wall thickness of 400 μm, strut height and thickness of 80 μm and halfway embedment. The core of the lumen is removed, and the radial thickness of the lumen volume is 200 μm.

5.2.2 CardioCoil Geometry

The helical CardioCoil geometry was generated by using a helical protrusion with a circular cross section (diameter 80 μm) over a length of 6000 μm (Figure 5.2). The reason for using a circular cross-section instead of a square cross-section as used in the other two designs of interest is that this is the design for the CardioCoil helicoid stent. Lumen and vascular wall dimensions are the same as those used in the Symbiotech design. The construction of the lumen and vascular wall are carried out in the same way as well, using the quilt surface cut option in Pro/E on cylindrical shell volumes.

Five struts are included in the quarter-cylinder solution domain. As in the Symbiotech design, the total length is 8000 μm, with a 6000 μm stent section and 1000 μm on either end of extreme struts.

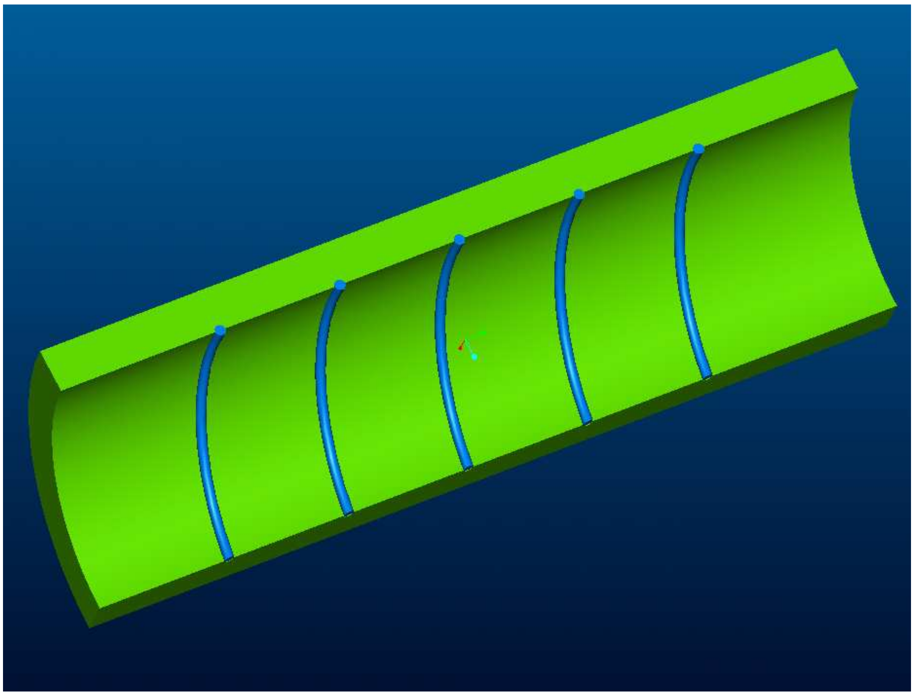

Figure 5.2: CardioCoil design with lumen volume removed.

5.2.3 Palmaz-Schatz Geometry

The geometry presented here is based on the original Palmaz-Schatz stent design of the early 1980s which involved a diagonal weave of struts over the length of the stent (Figure 5.3). The design has been simplified slightly in areas of strut intersection, but the main design features are preserved. The stent volume was generated in a similar fashion to the Symbiotech stent. A sketch of the planar section was created and wrapped on a cylinder. After making the appropriate cuts, a thin surface extrusion was made. A quilt surface of the stent was used to generate the vascular wall and lumen volumes, as in the previous geometries. Once again, the total length is 8000 μm, with a 6000 μm stent section and 1000 μm on either end of extreme struts. Struts are 100 μm wide and

60 μm thick, and other vascular wall and lumen dimensions are the same as those for the previous geometries.

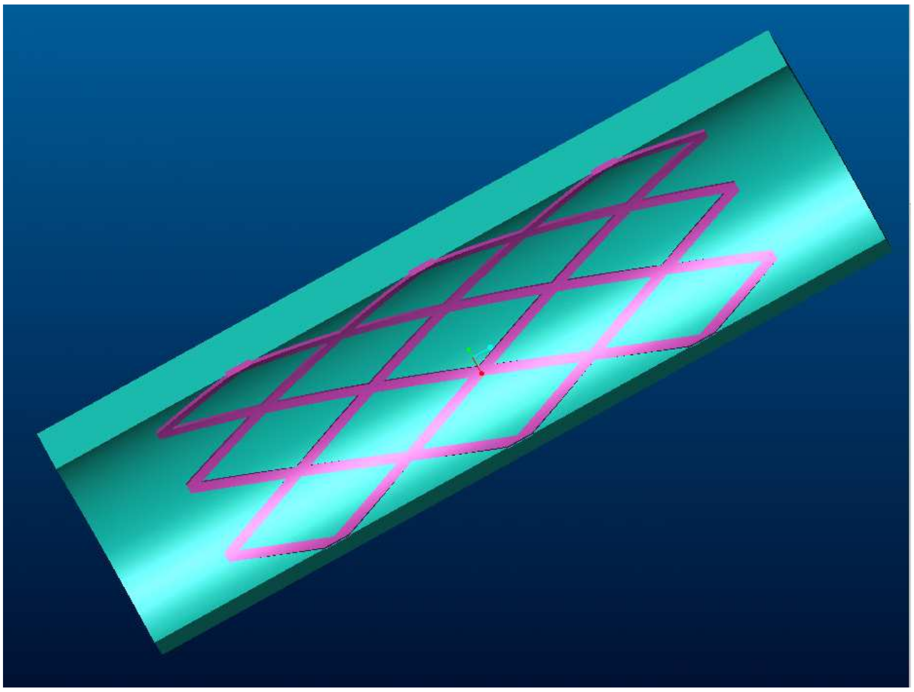

Figure 5.3: Palmaz-Schatz geometry with lumen volume removed.

5.3 FEM Implementation

This section describes the meshing and solving of the 3D mass transport problem with emphasis on the differences between 3D and 2D problem implementation. Many of the differences stem from the increased complexity of 3D geometries, and the difficulty in exporting suitable solid geometry files to Fluent's GAMBIT meshing package. A brief description of the computational differences between the solution methods in 2D and 3D is also given.

5.3.1 Meshing in 3D

The first critical step in carrying out 3D simulations is the exportation of geometry to the meshing package. ICEM/CFD was selected as the 3D meshing package because a direct Pro/E interface is available, and because there is the option of mesh optimization with this package. The use of ICEM/CFD eliminates the need to use standard file types in the geometry export process, a step which often leads to lengthy geometry clean-up and other problems. The three geometries described in the previous section are set up and exported using the Pro/E–ICEM/CFD interface. Within Pro/E, family assignments are made, and the geometry is exported in ICEM/CFD `.TIN` format.

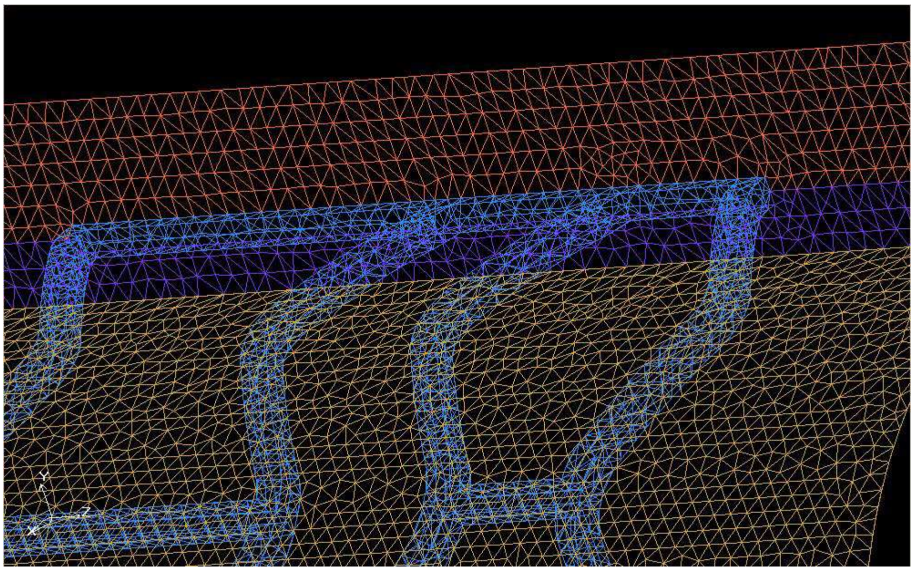

Figure 5.4: Symbiotech stent mesh with 60 μm mean element size in the three volumes.

Several different meshing philosophies were attempted. The first attempt involved using small element sizes in the stent with increasing element sized in the lumen and vascular wall. In terms of the solution of the problem this type of mesh was successful, however different element sizes in the therapeutic region necessitated the interpolation of data to a structured 3D grid in order to accurately determine the DHI. This is because the DHI, being a comparison of identical field points in a sample, demands that each data point have the same volume size associated with it in order to avoid a smoothing effect from larger elements. Casting the 3D data in this form was possible, but took on the order of 30 minutes to perform, and between 4 and 10 percent of the data points were returned as `NaN`s (“Not a Number”s) by Matlab. In order to eliminate the need for 3D interpolation in the post-processing stage, a mesh with equal element sizes in all three regions was adopted. Although total solution times were increased by 40% (from 43 to 60 minutes), the one-hour post-processing time was essentially reduced to zero and the overall accuracy of the output was increased. As a result, this “brute-force” approach was adopted for the remainder of 3D simulations. Figures 5.4, 5.5 and 5.6 show the meshes for the three geometries of interest.

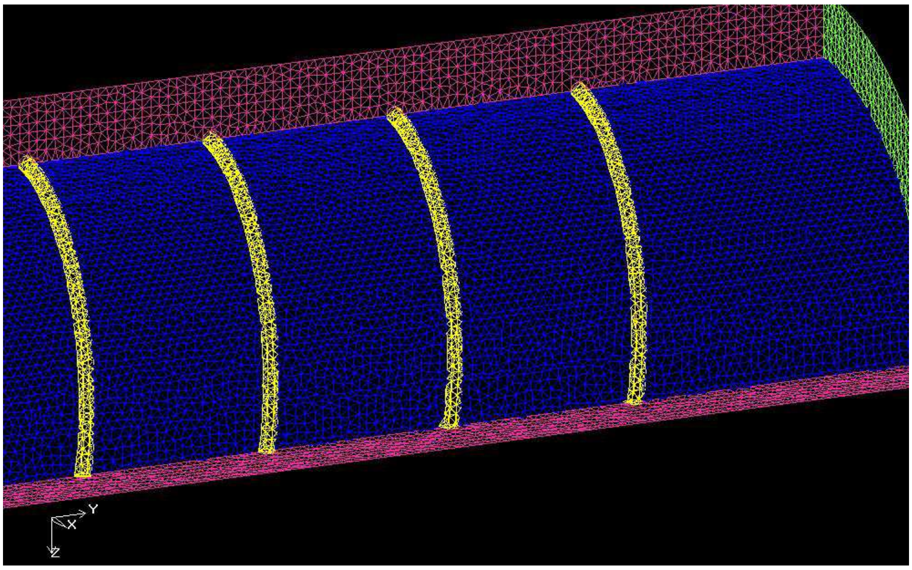

Figure 5.5: CardioCoil stent mesh with 60 μm mean element size in the three volumes.

Volume entities were named and specified using material points in ICEM/CFD. After specifying the curve and surface element sizes for all of the families in the geometry, the `.TIN` file was saved, and ICEM Tetra was used to begin meshing the solution domain. The three geometry meshes were approximately equal in size, having about 850 000 elements and 142 000 nodes each. Each mesh was smoothed up to a tetrahe-

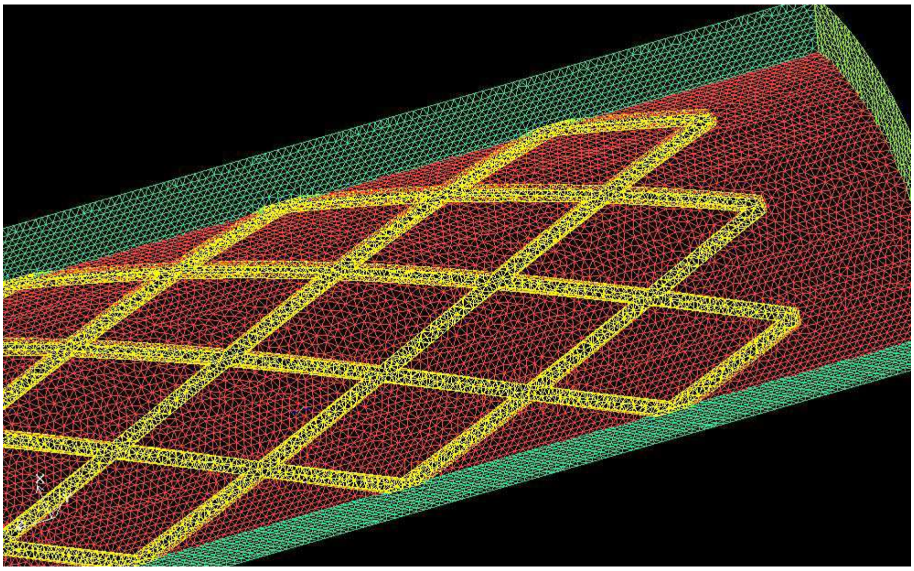

Figure 5.6: Palmaz-Schatz stent mesh with 60 μm mean element size in the three volumes.

dral aspect ratio quality factor of 0.3 with five iterations of Laplace smoothing. An empty boundary conditions file was created, and two FIDAP output files are created. These FIDAP files, an `.FDNEUT` mesh file and an `.FDREAD` file, were then ready to be interpreted by FIDAP.

5.3.2 FIDAP Implementation

Two main problem types are addressed in three dimensions. The first is an advection-diffusion type problem as described in the 2D section, developed in order to verify the appropriateness of the quasi-stationary flow hypothesis. The second is a purely diffusive problem with the quasi-stationary flow hypothesis applied. Appendix A-3 contains the `.FDREAD` files used in the formulation of the advection-diffusion problem. Key differences between the 3D problem and the 2D problem for flow simulations are outlined in Table 5.1. Most of the differences are clearly needed to make the transition from two to three dimensions, but several (time unit scaling, time steps, lumen entity definition) are elements unique to the 3D model. The zero-concentration vasa vasorum

Simulation Parameter	**2D**	**3D**
Lumen entity	Full radius (1500 μm)	Reduced (inner 200 μm)
Time steps	Constant, 1.25×10^4 s	Variable; initially 1 s
Time unit scaling	10^5 s per time unit	10^2 s per time unit
Solution method	Successive substitution	Segregated
Flow BCs	Parabolic at inlet, $u_r = 0$ at symmetry line	Parabolic at inlet, constant on inner lumen surface
Symmetry BCs	Not needed	Zero-flux

Table 5.1: Simulation setup differences between 2D and 3D advection-diffusion problems.

and inlet boundary conditions are applied in 3D as in 2D. Results from the 3D advection-diffusion simulations outlined here appear in Section 5.5.

The simplified quasi-stationary problem in 3D is essentially identical to the advection-diffusion problem with all flow variables removed. Flow is negligible, a zero-concentration inner lumen wall boundary condition is imposed (as in the simplified 2D case), and D_{lumen} is set to a value of 100 cm^2/s. Unlike the flow problem, a non zero relaxation factor is not needed to ensure convergence in purely diffusive simulations. A zero-concentration vasa vasorum boundary condition is applied, and initial strut concentrations are similar to those in 2D. The simplified `.FDREAD` file is shown in Appendix A-4 and outlines all of these details. These input files are essentially identical for the three geometries of interest.

5.4 Analysis Tools in 3D

The three parameters of interest, FMP, DHI and ACI, were adapted for application to 3D results. Based on these three parameters, a weighted value is constructed taking their relative importance into consideration. This factor, the local delivery effectiveness score (LDES), is meant to provide a simple means of comparing dose delivery effectiveness between 3D stent designs.

5.4.1 FMP in Three Dimensions

Both FMP and DHI calculations are simpler than those in 2D owing to elements of approximately equal size throughout the therapeutic region. In two dimensions, it is necessary to fit data from the unstructured mesh to a structured grid before calculating FMP and DHI. For the FMP this is done to remove the need to area-weight each field point, and for DHI this is necessary to ensure comparison between identical sample points. With approximately identical element sizes in 3D, FMP can be calculated by simply dividing the therapeutic region volume by the number of elements it contains to find an approximate mean element size. The total stent volume is determined using Pro/E measurement tools, and Equation 2.14 is used to calculate FMP. Table 5.2 shows volumes and embedded surface areas (for use in ACI calculations) for each of the three stent designs.

5.4.2 DHI in Three Dimensions

Owing to the equal volume sizes in 3D simulations, DHI calculations consist of simple analysis within the therapeutic region. The DHI for a sample c is calculated as follows:

$$\mathrm{DHI} = \frac{\sigma(c)}{\bar{c}} \tag{5.1}$$

The interpretation for DHI in three dimensions is the same as that for 2D analysis.

Stent	Volume ($\times 10^{-2}$ mm^3)	Embedded surface area (mm^2)
Symbiotech	14.16	1.17
CardioCoil	9.20	0.17
Palmaz-Schatz	21.25	3.54

Table 5.2: Volumes and embedded surface area values for three stent designs. Volumes correspond to quarter-cylinder geometries, and surface area values are used to calculate the ACI in three dimensions.

5.4.3 ACI in Three Dimensions

Extending ACI from 2D to 3D involves considering the ratio of area contact instead of linear contact. The embedded surface area is calculated using Pro/E (see Table 5.2), and this quantity is divided by the area of the therapeutic region in contact with the lumen:

$$\text{ACI} = \frac{A_{\text{embedded}}}{A_{\text{ther}}} \cdot 100\% \tag{5.2}$$

5.4.4 Development of the Local Delivery Effectiveness Score

The LDES is a score out of ten based on weighted FMP, DHI and ACI values. The weighting values are subjective, and those implemented here are briefly justified, however the important concept is the method of constructing the LDES and the arrival at a single number in evaluating different stent designs. The first step in constructing the LDES is to normalize FMP, DHI and ACI values using the most favourable value from among the designs being compared. In the case of DHI and ACI, the inverse is used since small values are more favourable. This produces scores out of 1 for each of the three parameters. Weighting parameters α, β and γ (where $\alpha + \beta + \gamma = 10$) are applied, and the generalized form of the LDES is given as:

$$\text{LDES} = \alpha \cdot \frac{\text{FMP}}{\text{FMP}_{\text{max}}} + \beta \cdot \frac{\text{DHI}_{\text{min}}}{\text{DHI}} + \gamma \cdot \frac{\text{ACI}_{\text{min}}}{\text{ACI}} \tag{5.3}$$

The weighting scheme shown in Table 5.3 is adopted for the remainder of this work. The LDES includes three important factors in determining dose delivery, but could be extended to include other parameters influencing dose delivery effectiveness and restenosis rates through the addition of terms and appropriate changes to the weighting scheme.

5.5 Model Verification

Verification of 3D simulations is divided into three parts. First, the simplification described for two-dimensional simulations is extended to three dimensions, and the results for 3D flow simulations and 3D simplified simulations are performed. Second, a comparison between 2D simulations and the analogous 3D geometry (resulting from the rotation about the axis of symmetry of the 2D geometry) is carried out. Finally, a brief grid independence investigation is shown.

Parameter	LDES Weight	Parameter value	Notes
FMP	20%	$\alpha = 2$	Initial mass loading can be adjusted to modulate final mass values.
DHI	50%	$\beta = 5$	Homogeneous dose is critical in successful treatment, and is strongly connected to stent design.
ACI	30%	$\gamma = 3$	High strut contact ratios lead to inflammation and increased restenosis rates.

Table 5.3: Weighting scheme for parameters of interest in constructing the dose effectiveness score.

5.5.1 Implementation and Verification of Model Simplification

Flow simulations were set up and performed for the Symbiotech design. It was observed that for nominal flow and diffusivity values, convergence could not be achieved over the total simulation time in spite of extensive scaling and relaxation attempts. The limiting factor was found to be lumen diffusivity for nominal Reynolds numbers of 100. This Reynolds number is based on a full lumen diameter of 1500 μm with an average flow speed of 11.1 cm/s, although here the lumen diameter is reduced and the average flow speed in the reduced volume is actually less than 11.1 cm/s. For this flow, the smallest lumen diffusivity resulting in a convergent solution was found to be $D_{\text{lumen}} = 10^{-2}$ cm^2/s. Larger diffusivities resulted in good convergence behaviour. As lumen diffusivity decreased, the solution was found to become increasingly unstable.

In order to work around this convergence problem, the flow speed was reduced and values of the mass transport parameter M (Equation 4.3) were matched to nominal values of $\mathrm{M} = 3 \times 10^{-5}$. Values of M were varied by fixing the Reynolds number at unity and varying lumen diffusion coefficients over the range of interest. The results for FMP and DHI with varying flow and diffusivity parameters are shown in Table 5.4. This table also includes the zero-flow values for FMP and DHI, which agree very well with the stable plateau region values for DHI, and to within 0.02% for FMP. As in 2D, the quasi-stationary flow hypothesis involves removing all flow variables from the problem, increasing the lumen diffusivity to $D_{\text{lumen}} = 100$ cm^2/s, and applying zero-concentration boundary conditions on the inner wall of the reduced lumen volume. Full advection-diffusion simulations were seen to take 108 minutes including the flow solution phase, while the simplified quasi-stationary flow simulations took 58 minutes. This result and the very good agreement between FMP and DHI values support the implementation of the simplifications described to the remainder of 3D simulations.

M	FMP	DHI	Pe	Re	Sc
3×10^{-7}	1.725	0.672	3×10^{-11}	10^{-2}	3×10^{-9}
3×10^{-5}	1.665	0.682	3×10^{-9}	10^{-2}	3×10^{-7}
3×10^{-3}	1.667	0.681	3×10^{-3}	10^{0}	3×10^{-3}
3×10^{-1}	1.658	0.683	3×10^{-1}	10^{0}	3×10^{-1}
3×10^{1}	1.660	0.682	3×10^{5}	10^{2}	3×10^{3}
No Flow	**1.643**	**0.682**	na	na	na

Table 5.4: FMP and DHI numbers with varying flow and diffusivity parameters for Symbiotech geometry, with quasi-stationary values included.

5.5.2 Comparison between 2D and 3D Annular Results

In order to compare results from two-dimensional simulations to an exactly analogous geometry in three dimensions, an annular strut geometry was constructed and meshed. The 3D geometry corresponds to a rotation of the standard 2D geometry, with inter-strut spacing of 1500 μm and strut height and width of 80 μm. A simulation was carried out for the 3D geometry with the quasi-stationary flow hypothesis in place. Table 5.5 compares these results to 2D values. Results from this comparison show that FMP is 1.42% lower and DHI is slightly lower in the 3D simulation. The lower mass retention value is a result of the fundamental differences between mass transport in a planar area and a volume. This difference can be seen by comparing the ratio of stent to therapeutic

Model	FMP	DHI
Standard 2D	2.31	1.34
Simplified 3D	0.89	1.20

Table 5.5: Comparison between FMP and DHI results for the standard 2D simulation and analogous 3D simulation.

areas in 2D (0.027) and stent to therapeutic volumes in 3D (0.024). In spite of these geometric differences, this value for FMP is smaller; better agreement between the two values was expected. DHI values vary for the same geometric reasons as FMP values. The overall conclusion that can be drawn from these results is that dose distribution properties are maintained from 2D to 3D, however mass retention characteristics are not. A further examination of this effect is needed in order to provide an explanation. Due to the more realistic geometry presented in the 3D simulations, these results are taken as being more accurate than 2D results. Also, the general characteristics of the results do not change from 2D to 3D, and so conclusions based on the LDES would be similar in 2D and 3D.

5.5.3 Grid Independence

Grid independence simulations were carried out in 3D using the Symbiotech design with three mesh sizes. Average tetrahedral element sizes of 40, 60 and 80 μm (base-to-vertex lengths) were used to mesh the geometry, and quasi-stationary simulations were carried out. Grid independence was seen for a mesh size of 60 μm. This mesh size was selected on the basis of a compromise between problem size and the similarity of values for 40 and 60 μm meshes. The 60 μm mesh size was applied to all other geometries based on these results, as shown in Table 5.6. Time-step independence studies were not carried out on 3D geometries because of the variable time-step algorithm used.

Element size (μm)	FMP	DHI	File size (MB)	Solution time (min.)
80	0.684	1.523	58	49
60	0.684	1.643	70	58
40	0.685	1.658	228	174

Table 5.6: Results from grid independence simulations in 3D with Symbiotech design and quasi-stationary flow hypothesis.

5.6 3D Results and Discussion

This section shows results from simplified, quasi-stationary flow simulations in three dimensions. These results are analyzed with the goal of developing a single numerical score out of ten to evaluate dose effectiveness called the LDES. Although the individual FMP, DHI and ACI scores have inherent importance in comparing stent designs on the basis of local drug delivery, the primary interest of this part of the study has been to develop the LDES and to prove its usefulness.

5.6.1 Transient Simulation Results

Transient results for the three stent geometries show similar overall behaviour in terms of FMP and DHI. It can be seen that the Symbiotech and Palmaz-Schatz stent designs produce very similar mass retention and homogeneity results owing to their general geometric similarities. The CardioCoil stent shows less favourable mass retention and homogeneity results over the one-week simulation period. Results are shown in Figures 5.7 and 5.8.

In spite of large disparities between days 0 and 5, the final FMP results are within 1% of one another. Although it is natural to assume that the higher dose exposures (the area under FMP vs time curves) of the Symbiotech and Palmaz-Schatz geometries are more desirable than that for the CardioCoil stent, the similarity of dose in time must also be considered. For example, in the case of a perfectly flat FMP vs time curve the same amount of drug would be present in the vascular wall at all times. In this idealized situation the drug concentration could be prescribed very accurately and would not threaten to exceed the toxic threshold. So there are advantages to the relatively flat FMP vs time curve seen for the CardioCoil geometry, but in this case any such benefits are outweighed by the geometry's very poor DHI results.

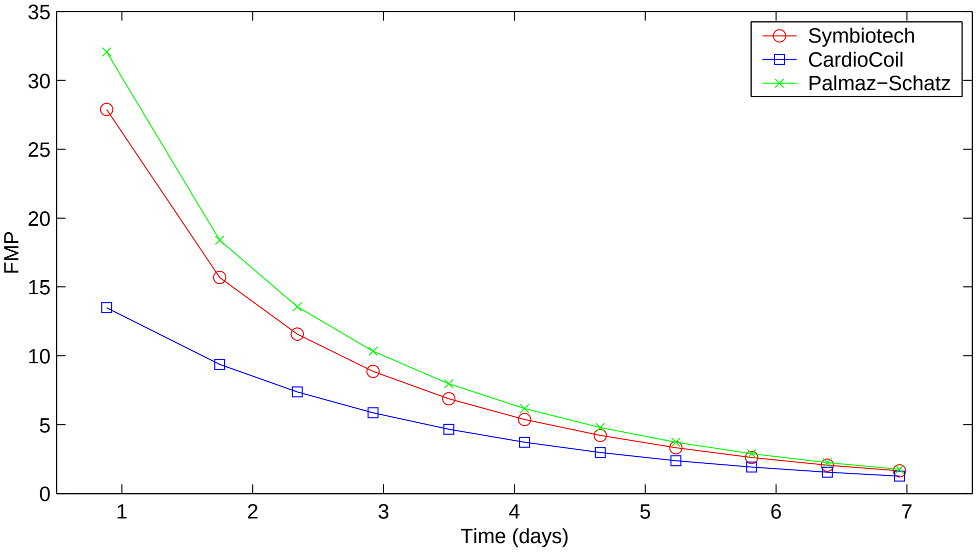

Figure 5.7: Transient FMP results for the three stent designs.

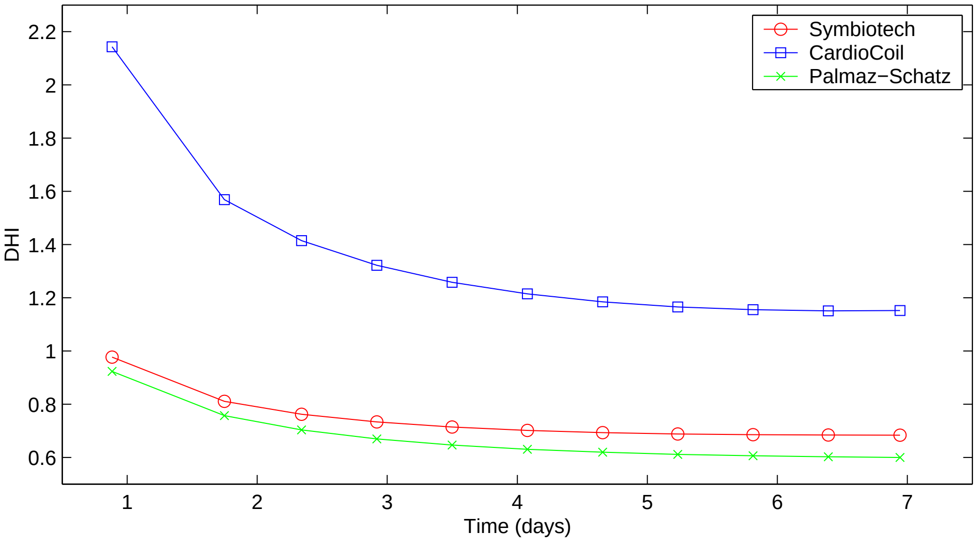

Figure 5.8: Transient DHI results for the three stent designs.

5.6.2 LDES Results for the Three Geometries

Figure 5.9 shows basic concentration results for a cylindrical cut (constant r) and transverse cut (constant θ) for the Symbiotech stent design. No scale or dimensions are

Stent design	FMP	DHI	ACI	LDES
Symbiotech	1.64	0.68	15.8	**7.9**
CardioCoil	1.26	1.15	8.9	**7.0**
Palmaz-Schatz	1.76	0.60	23.6	**8.1**

Table 5.7: LDES results based on FMP, DHI and ACI values for the three stent geometries.

given; this figure is meant to give only a qualitative description of 3D dose distribution. Based on the three designs of interest, simulations were run with the quasi-stationary flow hypothesis in place for 60 μm element meshes. The three parameters of interest (FMP, DHI and ACI) were recorded and used with Equation 5.3 to calculate the LDES. These results appear in Table 5.7. Based on the weighting scheme applied, LDES results show that the Palmaz-Schatz stent geometry is the most favourable of the three from a local delivery standpoint with an LDES of 8.1. The Symbiotech stent, which has a similar crossing strut geometry, shows a similar result of 7.9, and the CardioCoil stent is the least favourable of the three at 7.0.

It should be noted that the three parameters that make up the LDES are correlated, with the most pronounced correlation existing between the ACI and DHI, where one is inversely proportional to the other. To illustrate this point the following case can

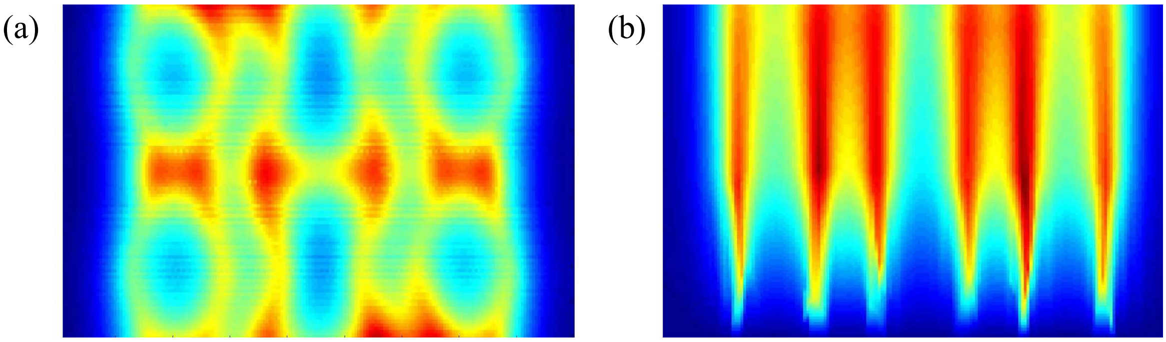

Figure 5.9: Dose distribution results for (a), a cylindrical cut (constant r), and (b), a transverse cut (constant θ).

be considered: An ACI of 100 corresponding to a solid sheath-like geometry would be very damaging to arterial tissues, but would lead to a very low DHI in the vessel wall. Conversely, with a very sparse stent geometry like the CardioCoil's, the ACI is very low and the DHI is very high as a result. These two opposite cases would produce similar results in the LDES. This effect is moderated somewhat by the weighting factors, but is still important to acknowledge.

So based on a sample of three stent designs, a tool for evaluating local delivery effectiveness from drug-eluting stents has been successfully developed. The LDES has the benefit of combining a number of elements into a single score out of 10, making interpretation and comparison between designs very straightforward. In future, different weighting schemes and choice of parameters can be investigated and added to the framework for the LDES presented here.

5.7 Summary

This chapter has developed the adaptation of two-dimensional drug-eluting stent simulations to three dimensions with the goal of developing a tool for the evaluation of local delivery effectiveness from real 3D stent designs. Geometries were generated using Pro/E and meshed with ICEM/CFD. The 3D model was verified through comparison to the equivalent 2D model and a grid independence study. The objective of constructing a single dose effectiveness parameter for 3D stents was achieved. Based on the quasi-stationary flow hypothesis verified in two dimensions, FMP, DHI and ACI values were obtained and normalized against extreme values in the sample of three designs. These normalized values were then assigned weights and summed to produce the LDES. As a single score out of 10, the LDES provides a straightforward and easy-to-interpret way of evaluating the local delivery effectiveness of real stent designs.

Chapter 6

Conclusions

6.1 Limitations and Recommendations

This investigation has the obvious limitation that no parallel animal trials or experiments were carried out as a means of verification. Such studies would be very expensive and time consuming, and are beyond the scope of this work. The numerical limitations encountered came in the development of the 3D model. Achieving convergence with the 3D advection-diffusion simulation could not be achieved for the nominal flow and diffusion parameters considered. The application of the quasi-stationary flow simplification effectively removed this problem, however until *in vitro* or animal studies are carried out it is difficult to establish the appropriateness of this simplification. If the flow and diffusion parameters in such experiments place FMP and DHI results above the stability threshold of the parameter M, then the quasi-stationary flow hypothesis will have been proven appropriate.

Another limitation is the gross simplification of biological tissue in the simulations. All of the diffusion in these simulations is perfectly isotropic. In reality, the layering of normal arterial tissue and the presence of a wide range of pathological tissues make accurate modelling of the embedded drug-eluting stent model very difficult.

In order to improve the models described here, several important elements must be addressed. It was shown that small changes to diffusion coefficient values had a large impact on dose characteristics. In order to improve the accuracy of the results, experiments to determine diffusion coefficients for drugs that are likely to be used in this context need to be carried out. Such experiments would need to have a relatively high spatial resolution in concentration measurements so that proper comparisons between experimental and numerical results could be done. Another improvement to the model would be the implementation of directionally dependent diffusivity characteristics. It has been shown that diffusion happens at a higher rate in the axial direction owing to the laminar nature of medial tissue.

The development of 3D reconstructions of pathological arteries using IVUS data is currently underway within our group. The development of an embedded stent CAD model using this geometry could provide very interesting results. As with the standard model, accurate diffusion coefficients for pathological tissues would need to be obtained in order to make the results credible. Another means of verifying flow results from this numerical model is through particle image velocimetry (PIV). Owing to the difficulties in conducting PIV in curved flow regions, simplifications to the 3D geometry could also be considered. By examining a flat stent section embedded in a planar vascular wall and comparing mass retention and dose homogeneity results to those from cylindrical results reported here, the appropriateness of such a simplification could be investigated.

6.2 Summary

The success of drug-eluting stents in treating restenosis depends on their ability to deliver doses with sufficient concentration levels and homogeneities while limiting their direct contact with intimal tissue. These factors can be controlled to a certain extent by stent design and stent deployment techniques. This study has developed a 2D model to investigate basic geometric considerations of local delivery from drug-eluting stents, and extended this model to 3D where a tool was developed for evaluating local delivery effectiveness based on mass retention, homogeneity and area contact parameters.

A two-dimensional numerical model for solid polymeric and coated metallic stent struts was developed and applied to variable inter-strut spacing and strut apposition geometries. It was found that for both solid and coated struts, mass retention and homogeneity results worsened as inter-strut spacing increased. In terms of stent design, these negative effects of increasing inter-strut spacing are moderated by a decrease in intimal strut contact, and hence inflammatory response in the stented region. For strut apposition trials it was found that mass retention decreased with decreasing embedment, as one would expect. Homogeneity results show that coated struts are insensitive to apposition, while solid struts show less homogeneous results as embedment decreases. Overall these findings suggest that coated struts would provide more favourable local delivery vehicles than solid struts. One recommendation based on these results would be to coat solid polymeric struts with a drug-loaded polymer rather than having the entire strut act as a dose carrier. The current development of biodegradable solid polymeric stents which may have the capacity to act as local delivery vehicles makes this information particularly useful.

Solid polymeric strut simulations comparing dose delivery on the inner and outer walls of a curved vessel geometry were also conducted. Final mass percentage, mean concentration, and dose homogeneity values were measured while varying the radius of curvature from the lower physiologic limit to an upper limit represented by a straight vessel. It was found that dose homogeneity results were more favourable on the inside wall of the curved vessel. Final mass percentage and mean concentration results showed relatively little change over different degrees of curvature. Differential mass loading on inner and outer struts is one possible way of addressing this problem, however the most plausible solution is to increase the initial drug loading on stents being deployed in curved arteries. The difference between the inner and outer wall masses is not large enough that initial overloading would lead to toxicity on the inner wall, and overloading would not increase the expense or difficulty of stent design, construction and deployment.

In preparation for the transition to the three-dimensional model, simplifications to the advection-diffusion problem were investigated. It was shown that imposing a quasi-stationary flow condition in the lumen is appropriate because the nominal flow and diffusion characteristics in the problem place results beyond a stability threshold for the dimensionless mass transport parameter M. By selecting appropriate velocities and diffusion coefficients, the implementation of a purely diffusive model is justified.

A three-dimensional model derived from the 2D model was developed with the objective of developing a tool for the evaluation of local delivery effectiveness from real 3D stent designs. Using three realistic stent designs, parameters measuring mass retention, homogeneity and area contact were normalized, weighted and summed. The results was a single local delivery effectiveness score. This first attempt at developing such a tool was successful, and leaves much room for the inclusion of new terms and refinement of weighting factors. Further developments to this tool will improve its usefulness to stent designers.

This study has successfully implemented a simple mass transport model in describing dose delivery from various stent designs in two dimensions, and was successfully adapted to three dimensions where a tool for evaluating stent designs on the basis of local drug delivery effectiveness was developed. The results are meant to provide useful information for stent designers and cardiologists as they continue to refine stent designs and deployment techniques. Until these results are validated using parallel animal studies, the results cannot be considered wholly accurate, however they provide a first-order estimate of dose delivery characteristics which could limit the size and expense of such a parallel animal study if and when it is carried out.

Bibliography

[1] K Detre R Holbukov *et al.* Percutaneous transluminal coronary angioplasty in 1985-1986 and 1977-1981. *New England Journal of Medicine*, 318:265–270, 1988.

[2] DR Holmes RE Vlietstra *et al.* Restenosis after percutaneous transluminal coronary angioplasty (PTCA): A report from the PTCA registry of the national heart, lung, and blood institute. *American Journal of Cardiology*, 53:77C–81C, 1984.

[3] GE Austin NB Ratliff. Intimal proliferation of smooth muscle cells as an explanation for recurrent coronary artery stenosis after percutaneous transluminal coronary angioplasty. *Journal of the American College of Cardiologists*, 6:369–375, 1985.

[4] AA Giraldo OM Esposo JM Meis. Intimal hyperplasia as a cause of restenosis after percutaneous transluminal coronary angioplasty. *Archives of Pathological Laboratory Medicine*, 109:173–175, 1985.

[5] M Nobuyoshi T Kimura *et al.* Restenosis after successful percutaneous transluminal coronary angioplasty: Serial angiographic follow-up of 229 patients. *Journal of the American College of Cardiologists*, 12:616–623, 1988.

[6] PW Serruys HE Luijten *et al.* Incidence of restenosis after successful coronary angioplasty: A time-related phenomenon. *Circulation*, 77:361–371, 1988.

[7] RM Califf DF Fortin *et al.* Restenosis after coronary angioplasty: An overview. *Journal of the American College of Cardiologists*, 17:2B–13B, 1991.

[8] GS Roubin KA Robinson *et al.* Early and late results of intracoronary arterial stenting after coronary angioplasty in dogs. *Circulation*, 76:891–897, 1987.

[9] RA Schatz JC Palmaz *et al.* Balloon-expandable intracoronary stents in the adult dog. *Circulation*, 76:450–457, 1987.

[10] H Mudra E Regar *et al.* Serial follow-up after optimized ultrasound-guided deployment of Palmaz-Schatz stents. *Circulation*, 65:363–370, 1997.

[11] MP Savage DL Fischman *et al.* Long-term angiographic and clinical outcome after implantation of a balloon-expandable stent in the native coronary circulation. *Journal of the American College of Cardiologists*, 24:1207–1212, 1994.

[12] DP Faxon DO Williams *et al.* Improved in-hospital outcome with expanded use of coronary stents: Results from the NHLBI dynamic registry. *Journal of the American College of Cardiologists*, 33 Supl.:91.

[13] DL Fischman MB Leon *et al.* A randomized comparison of coronary-stent placement and balloon angioplasty in the treatment of coronary artery disease. *New England Journal of Medecine*, 331:496–501, 1994.

[14] PW Serruys P de Jaegere *et al.* A comparison of balloon-expandable-stent implantation with balloon angioplasty in patients with coronary artery disease. *New England Journal of Medecine*, 331:489–495, 1994.

[15] PR Moreno IF Palacios *et al.* Histopathologic comparison of human coronary in-stent and post-balloon angioplasty restenotic tissue. *American Journal of Cardiology*, 84:462–466, 1999.

[16] LM Khachigian HC Lowe SN Oesterle. Coronary in-stent restenosis: Current status and future strategies. *Journal of the American College of Cardiologists*, 39:183–193, 2002.

[17] SL Goldberg A Loussararian *et al.* Predictors of diffuse and aggressive intra-stent restenosis. *Journal of the American College of Cardiologists*, 37:1019–1025, 2001.

[18] AJ Carter JR Laird *et al.* Coronary stenting with a novel stainless steel balloon-expandable stent: Determinants of neointimal formation and changes in arterial geometry after placement in an atherosclerotic model. *Journal of the American College of Cardiologists*, 27:1270–1277, 1996.

[19] R Hoffmann GS Mintz *et al.* Patterns and mechanisms of in-stent restenosis: A serial intravascular study. *Circulation*, 94:1247–1254, 1996.

[20] C Rogers ER Edelman. Endovascular stent design dictates experimental restenosis and thrombosis. *Circulation*, 91:2995–3001, 1995.

[21] A Schomig A Kastrati D Hall. Long-term outcome after coronary stenting. *Current Controlled Trials Cardiovascular Medicine*, 1:48–54, 2000.

[22] AH Gershlick. Treating atherosclerosis: Local drug delivery from laboratory studies to clinical trials. *Atherosclerosis*, 160:259–271, 2002.

[23] SK Sharma S Duvvuri *et al.* Rotational atherectomy for in-stent restenosis: Acute and long-term results of the first 100 cases. *Journal of the American College of Cardiologists*, 32:1358–1365, 1998.

[24] NA Mahdi AZ Pathan *et al.* Directional coronary atherectomy for the treatment of Palmaz-Schatz in-stent restenosis. *American Journal of Cardiology*, 82:1345–1351, 1998.

[25] J vom Dahl U Dietz *et al.* Rotational atherectomy does not reduce recurrent in-stent restenosis: Results of the angioplasty versus rotation atherectomy for treatment of diffuse in-stent restenosis trial (ARTIST). *Circulation*, 105:583–588, 2002.

[26] GS Mintz JJ Popma *et al.* Arterial remodeling after coronary angioplasty. *Circulation*, 94:35–43, 1996.

[27] R Mehran G Dangas *et al.* Treatment of in-stent restenosis with excimer laser coronary angioplasty versus rotational atherectomy. *Circulation*, 101:2484–2489, 2000.

[28] WJ van der Giessen AM Lincoff. Marked inflammatory sequelae to implantation of biodegradable and nonbiodegradable polymers in porcine coronary arteries. *Circulation*, 94:1690–1697, 1996.

[29] S Windecker I Mayer *et al.* Stent coating with titanium-nitride-oxide for reduction of neointimal hyperplasia. *Circulation*, 104:926–933, 2001.

[30] OF Bertrand R Sipehia *et al.* Biocompatibility aspects of new stent technology. *Journal of the American College of Cardiologists*, 32:562–571, 1998.

[31] R Sheppard MJ Eisenberg. Intracoronary radiotherapy for restenosis. *New England Journal of Medecine*, 334:295–297, 2001.

[32] JA Condado R Waksman *et al.* Long-term angiographic and clinical outcome after percutaneous transluminal coronary angioplasty and intracoronary radiation therapy in humans. *Circulation*, 96:727–732, 1997.

[33] AE Raizner SN Oesterle *et al.* Inhibition of restenosis with β-emitting radiotherapy: Report of the proliferation reduction with vascular energy trial (prevent). *Circulation*, 96:727–732, 1997.

[34] HS Kim R Waksman *et al.* Edge stenosis and geographical miss following intracoronary gamma radiation therapy for in-stent restenosis. *Journal of the American College of Cardiologists*, 37:1026–1030, 2001.

[35] IP Kay AJ Wardeh *et al.* Radioactive stents delay but do not prevent in-stent neointimal hyperplasia. *Circulation*, 103:14–17, 2001.

[36] R Waksman AE Ajani HS Kim. Clinical trials of vascular brachytherapy for in-stent restenosis: update. *Cardiovascular Radiation Medicine*, 2:107–113, 2001.

[37] MB DeYoung DA Dichek. Gene therapy for restenosis: Are we ready? *Circulation Research*, 82:306–313, 1998.

[38] DB Schneider AB Sassani *et al.* Adventitial delivery minimizes the proinflammatory effects of adenoviral vectors. *Journal of Vascular Surgery*, 29:543–550, 1999.

[39] A Frimerman PJ Welch *et al.* Chimeric DNA-RNA hammerhead ribozyme to proliferating cell nuclear antigen reduces stent-induced stenosis in a porcine coronary model. *Circulation*, 99:697–703, 1999.

[40] J Gunn CM Holt *et al.* The effect of oligonucleotides to C-*myb* on vascular smooth muscle cell proliferation and neointima formation after porcine coronary angioplasty. *Circulation Research*, 80:520–531, 1997.

[41] JM Wilson. Adenoviruses as gene-delivery vehicles. *New England Journal of Medicine*, 334:1185–1187, 1996.

[42] P Libby. Gene therapy of restenosis: Promise and perils. *Circulation Research*, 82:404–406, 1998.

[43] CE Glatz TA Massaro. Influence of glycosaminoglycan content on mass transfer behaviour of porcine artery wall. *Atherosclerosis*, 25:153–163, 1976.

[44] A Tedgui MJ Lever. Filtration through damaged and undamaged rabbit thoracic aorta. *American Journal of Physiology*, 247:H784–H791, 1984.

[45] TL Lambert V Dev E Rechavia *et al.* Localized arterial wall drug delivery from a polymer-coated removable metallic stent. *Circulation*, 90:1003–1011, 1994.

[46] MA Lovich ER Edelman. Mechanisms of transmural heparin transport in the rat abdominal aorta after local vascular delivery. *Circulation Research*, 77:1143–1150, 1995.

[47] I de Scheerder K Wang *et al.* Local methylprednisolone inhibition of foreign body response to coated intracoronary stents. *Coronary Artery Disease*, 7:161–166, 1996.

[48] AM Lincoff JG Furst *et al.* Sustained local delivery of dexamethasone by a novel intravascular eluting stent to prevent restenosis in the porcine coronary injury model. *Journal of the American College of Cardiologists*, 29:808–816, 1997.

[49] MA Lovich ER Edelman. Tissue concentration of heparin, not administered dose, correlates with the biological response of injured arteries *in vivo*. *Proceedings of the National Academy of Science USA*, 96:11111–11116, 1999.

[50] A Baumbach C Herdeg *et al.* Local drug delivery: Impact of pressure, substance characteristics, and stenting on drug transfer into the arterial wall. *Catheterization and Cardiovascular Intervention*, 47:102–106, 1999.

[51] MA Lovich C Creel K Hong *et al.* Carrier proteins determine local pharmacokinetics and arterial distribution of paclitaxel. *Journal of Pharmaceutical Sciences*, 90:1324–1335, 2001.

[52] CJ Creel MA Lovich ER Edelman. Arterial paclitaxel distribution and deposition. *Circulation Research*, 86:879–884, 2000.

[53] DE Drachman ER Edelman *et al.* Neointimal thickening after stent delivery of paclitaxel: Change in composition and arrest of growth over six months. *Journal of the American College of Cardiologists*, 36:2325–2332, 2000.

[54] A Farb PF Heller *et al.* Pathological analysis of local delivery of paclitaxel via a polymer-coated stent. *Circulation*, 104:473–479, 2001.

[55] E Alt I Haehnel *et al.* Inhibition of neointima formation after experimental coronary artery stenting: A new biodegradable stent coating releasing hirudin and the prostacyclin analogue iloprost. *Circulation*, 101:1453–1458, 2000.

[56] T Suzuki G Kopia *et al.* Stent-based delivery of sirolimus reduces neointimal formation in a porcine coronary model. *Circulation*, 104:1188–1193, 2001.

[57] MN Babapulle MJ Eisenberg. Coated stents for the prevention of restenosis: Part I. *Circulation*, 106:2734–2740, 2002.

[58] J Wöhrle E Al-Khayer *et al.* Comparison of the heparin coated vs the uncoated Jostent–no influence on restenosis or clinical outcome. *European Heart Journal*, 22:1808–1816, 2001.

[59] PW Serruys B van Hout *et al.* Randomised comparison of implantation of heparin-coated stents with balloon angioplasty in selected patients with coronary artery disease (Benestent II). *Lancet*, 352:673–681, 1998.

[60] JE Sousa MA Costa A Abizaid *et al.* Lack on neointimal proliferation after implantation of sirolimus-coated stents in human coronary arteries. *Circulation*, 102:R54–R57, 2000.

[61] F Feres A Abizaid. Sirolimus coated stent versus bare stent: Angiographic and IVUS analysis at four-month and one-year follow-up. *Journal of the American College of Cardiologists*, Supplements:59, 2002.

[62] M-K Hong GS Mintz *et al.* Paclitaxel coating reduces in-stent restenosis: A serial volumetric intravascular ultrasound analysis. *Journal of the American College of Cardiologists*, Supplement:38A, 2002.

[63] B Chevalier I De Scheerder *et al.* Effect on restenosis with a paclitaxel eluting stent: Factors associated with inhibition in the Elutes clinical study. *Journal of the American College of Cardiologists*, Supplement:59A, 2002.

[64] I De Scheerder Y Wang *et al.* Treatment of in-stent restenosis using paclitaxel eluting stents: Results from the Leuven pilot trial. *Journal of the American College of Cardiologists*, Supplements:59A, 2002.

[65] MN Babapulle MJ Eisenberg. Coated stents for the prevention of restenosis: Part II. *Circulation*, 106:2859–2866, 2002.

[66] AJ Fischman NM Alpert RH Rubin. Pharmacokinetic imaging: A noninvasive method for determining drug distribution and action. *Clinical Pharmacokinetics*, 41:581–602, 2002.

[67] RL Bratzler CK Colton KA Smith. Theoretical models for transport of low-density lipoproteins in the arterial wall. *Advances in Experimental and Medical Biology*, 82:943–951, 1977.

[68] GM Saidel ED Morris GM Chisolm. Transport of macromolecules in arterial wall *in vivo*: A mathematical model and analytical solutions. *Bulletin of Mathematical Biology*, 49:153–169, 1987.

[69] F Yuan S Chien S Weinbaum. A new view of convective-diffusive transport processes in the arterial intima. *Journal of Biomechanical Engineering*, 133:314–328, 1991.

[70] G Rappitsch K Perktold. Computer simulation of convective diffusion processes in large arteries. *Journal of Biomechanics*, 29:207–215, 1996.

[71] G Karner K Perktold. Effect of endothelial injury and increased blood pressure on albumin accumulation in the arterial wall: A numerical study. *Journal of Biomechanics*, 33:709–715, 2000.

[72] XY Wu Y Zhou. Finite element analysis of diffusional drug release from complex matrix systems. *Journal of Controlled Release*, 51:57–71, 1998.

[73] XY Wu Y Zhou. Finite element analysis of diffusional drug release from complex matrix systems. *Journal of Controlled Release*, 49:277–288, 1997.

[74] WS Kim JM Tarbell. Macromolecular transport through the deformable porous media of an artery wall. *Journal of Biomechanical Engineering*, 116:156–163, 1994.

[75] ZJ Huang JM Tarbell. Numerical simulation of mass transfer in porous media of blood vessel walls. *American Journal of Physiology*, 273:H464–H477, 1997.

[76] MA Lovich ER Edelman. Computational simulations of local vascular heparin deposition and distribution. *American Journal of Physiology*, 271:H2014–H2024, 1996.

[77] CW Hwang ER Edelman. Arterial ultrastructure influences transport of locally delivered drugs. *Circulation Research*, 90:826–832, 2002.

[78] CW Hwang D Wu ER Edelman. Physiological transport forces govern drug distribution for stent-based delivery. *Circulation*, 104:600–605, 2001.

[79] HF Younis AG Isasi *et al.* Three dimensional finite element analysis of the atherosclerotic human carotid bifurcation based on *in vivo* magnetic resonance images. *ASME Bioengineering Conference*, 50:759–760, 2001.

[80] CA Taylor TJR Hughes *et al.* Finite element modeling of three-dimensional pulsatile flow in the abdominal aorta: Relevance to atherosclerosis. *Annals of Biomedical Engineering*, 26:975–987, 1998.

[81] AO Frank PW Walsh *et al.* Computational fluid dynamics and stent design. *Artificial Organs*, 26:614–621, 2002.

[82] S Julien. Étude numérique de la diffusion et la convection du ^{45}Ca-DTPA émis par un stent pour le contrôle de la resténose. *Masters Thesis*, Université de Montréal: École Polytechnique, 2000.

[83] J-F Toussaint JF Southern V Fuster HL Kantor. Water diffusion properties of human atherosclerosis and thrombosis measured by pulse field gradient nuclear magnetic resonace. *Arteriosclerosis, Thrombosis, and Vascular Biology*, 17:542–546, 1997.

[84] WA Wakeham NH Salpadoru CG Caro. Diffusion coefficents for protein molecules in blood serum. *Atherosclerosis*, 25:225–235, 1976.

[85] T Akasaka A Yamamuro N Kamiyama *et al.* Assessment of coronary flow reserve by coronary pressure measurement. *Journal of the American College of Cardiologists*, 41:1554–1560, 2003.

Appendices

A-1 Example 2D Fidap Input File

```
/          CONVERSION OF NEUTRAL FILE TO FIDAP Database
/
FICONV( NEUTRAL )
INPUT( FILE="nc.FDNEUT" )
OUTPUT( DELETE )
END
/
TITLE
nc_r4
/
FIPREP
/
/          PROBLEM SETUP
/
EXECUTION( NEWJOB )
PRINTOUT( NONE )
DATAPRINT( CONTROL )
/
/          CONTINUUM ENTITIES
/
ENTITY ( NAME = "lumen", FLUID, PROPERTY = "lumen" )
ENTITY ( NAME = "art", SOLID, PROPERTY = "art" )
ENTITY ( NAME = "tr", SOLID, PROPERTY = "tr" )
ENTITY ( NAME = "stent", SOLID, PROPERTY = "stent" )
/
/          BOUNDARY ENTITIES
/
ENTITY ( NAME = "inlet", PLOT )
ENTITY ( NAME = "outlet", PLOT )
ENTITY ( NAME = "sym", PLOT )
ENTITY ( NAME = "vwall", PLOT )
ENTITY ( NAME = "vv", PLOT )
ENTITY ( NAME = "wall", WALL )
/
SOLUTION( S.S. = 500, VELC = 0.001, RESC = 0.001, ACCF = 0 )
PROBLEM( 2-D, TRAN, LAMI, NONL, ISOT, SPEC = 1 )
TIMEINTEGRATION( BACK, NSTE = 48, TSTA = 0, DT = 0.125, FIXE )
DENSITY( SET = "lumen", CONS = 1.051 )
VISCOSITY( SET = "lumen", CONS = 3500 )
DIFFUSIVITY( SET = "lumen", CONS = 0.001 )
DIFFUSIVITY( SET = "art", CONS = 0.0001 )
DIFFUSIVITY( SET = "tr", CONS = 0.0001 )
DIFFUSIVITY( SET = "stent", CONS = 1e-006 )
BCNODE( UX, ENTI = "inlet", POLY = 1, SYST = 1, CART )
2220107.834, -98671459.28, 0, 2, 0
BCNODE( UY, ENTI = "sym", ZERO )
BCNODE( VELO, ENTI = "vwall", ZERO )
BCNODE( SPEC = 1, ENTI = "vv", ZERO )
BCNODE( SPEC = 1, ENTI = "inlet", ZERO )
ICNODE( SPEC = 1, CONS = 1, ENTI = "stent" )
CLIPPING(MINIMUM)
0 0 0 0 0 0 0 0 1e-19
END(  )
/  *** of FIPREP Commands
CREATE(FIPREP,DELE)
CREATE(FISOLV)
PARAMETER(LIST)
```

A-2 Matlab DHI Function

```
function DHI(fname,xres,yres)
L=load(strcat(fname,'.txt'));
if size(L,2)==3
    N=sortrows(L,[1 2]);
    x=N(:,1);
    y=N(:,2);
    z=N(:,3);
else
    N=sortrows(L,[2 3]);
    x=N(:,2);
    y=N(:,3);
    z=N(:,5);
end

xlin=linspace(min(x),max(x),xres);
ylin=linspace(min(y),max(y),yres);

[X,Y]=meshgrid(xlin,ylin);
Z=griddata(x,y,z,X,Y,'cubic');
%   FIGURE
for i=1:yres
    Zflip(i,:)=Z(yres+1-i,:);
end

zoom on;
sp1=figure;
colormap(jet);
imagesc(Zflip);
ha=colorbar;
p = get(ha,'Ylabel');
set(p,'String','C/C_{0} {x} 10^{4}');
q=get(ha,'Ytick');
set(ha,'Yticklabel',q*1e4);

label_x=[0:(max(x)-min(x))/12:max(x)-min(x)];
label_y_pre=[min(y):(max(y)-min(y))/5:max(y)]-min(y);
for j=1:length(label_y_pre)
    label_y(j)=label_y_pre(length(label_y_pre)+1-j);
end
lx=num2str(transpose(label_x),'%6.2f');
ly=num2str(transpose(label_y),'%6.3f');
label_tick_x=[0:xres/12:xres];
label_tick_y=[0:yres/5:yres];
set(gca,'Xtick',label_tick_x);
set(gca,'Ytick',label_tick_y);
set(gca,'Xticklabel',lx);
set(gca,'Yticklabel',ly);
 xlabel('z (cm)');
 ylabel('r (cm)');
%   END FIGURE
C=reshape(Z,prod(size(Z)),1);
%imagesc(Z);
clear Z r t x y z N L
cnans=sum(isnan(C))
j=1;
D=zeros(length(C)-cnans,1);
for i=1:length(C)
    if ~isnan(C(i))
        D(j)=C(i);
        j=j+1;
    end
end
cmean=sum(D)/(length(D));
cstd=std(D);
DHI=cstd/cmean
sum(D)
```

A-3 Example 3D Fidap Flow Input File

```
ficon(neut)
input(file="nr_nc.FDNEUT")
end
title
nr_nc
/
CONFIG( FIDAPMEM=200000000, FISOLVMEM=0, COMPRESS, SHOW )
/
FIPREP
 PROB (3-D, INCO, STEA, LAMI, NONL, NEWT, MOME)
 EXEC (NEWJ)
 SOLU (SEGR = 100, VELC = 0.100000000000E-02, RESC = 0.100000000000E-02,
       CGS = 2000, CR = 1000, ACCF = 0.000000000000E+00)
 DATA (CONT)
 PRIN (NONE, BOUN)
 SCAL (VALU = 0.100000000000E-03)
/ THESE COMMANDS ARE FOR CONTINUUM ENTITIES
entity (name="LUMEN_PT",fluid          )
entity (name="VWALL_PT",solid          )
entity (name="STENT_PT",solid          )
/ THESE COMMANDS ARE FOR BOUNDARY ENTITIES
entity (name="STENT",plot          )
entity (name="VWALL",plot          )
entity (name="LUM_SYM2",plot          )
entity (name="VW_SYM2",plot          )
entity (name="VV",plot          )
entity (name="LUM_IN",plot          )
entity (name="INLET",plot          )
entity (name="VW_IN",plot          )
entity (name="VW_OUT",plot          )
entity (name="OUTLET",plot          )
entity (name="VW_SYM1",plot          )
entity (name="LUM_SYM1",plot          )
entity (name="VWALL_C",plot          )
entity (name="INLET_C",plot          )
entity (name="LUM_SYM1_C",plot          )
entity (name="LUM_SYM2_C",plot          )
entity (name="STENT_C",plot          )
entity (name="OUTLET_C",plot          )
entity (name="VV_C",plot          )
entity (name="LUM_IN_C",plot          )
entity (name="VW_IN_C",plot          )
entity (name="VW_OUT_C",plot          )
/
DENSITY( SET = "LUMEN_PT", CONS = 1.051 )
VISCOSITY( SET = "LUMEN_PT", CONS = 3500 )
/
BCNODE(UZ, ENTI = "INLET", POLY = 1, SYST = 1, CYLIN )
2.0e6, -0.898435, 2, 0, 0
BCNODE( UZ, ENTI = "LUM_IN", CONST = 4.81645320e05 )
/
/  Reynolds Number:  90
/  based on lumen diameter of 0.3~cm
/
BCNODE( VELO, ENTI = "VWALL", ZERO )
BCNODE( VELO, ENTI = "STENT", ZERO )
BCNODE( UX, ENTI = "LUM_SYM1", ZERO )
BCNODE( UY, ENTI = "LUM_SYM1", ZERO )
BCNODE( UX, ENTI = "LUM_SYM2", ZERO )
BCNODE( UY, ENTI = "LUM_SYM2", ZERO )
BCNODE( UX, ENTI = "LUM_IN", ZERO )
BCNODE( UY, ENTI = "LUM_IN", ZERO )
/
END
/
create(fisolv)
```

A-4 Example 3D Fidap Diffusion Input File

```
ficon(neut)
input(file="nr_nc.FDNEUT")
end
title
nr_nc
/
CONFIG( FIDAPMEM=200000000, FISOLVMEM=0, COMPRESS, SHOW )
/
FIPREP
 PROB (3-D, INCO, TRANS, LAMI, NONL, NEWT, NOMO, SPEC = 1.0 )
 EXEC (NEWJ)
 SOLU (SEGR = 100, VELC = 0.100000000000E-02, RESC = 0.100000000000E-02,
       CGS = 2000, CR = 1000, ACCF = 0.000000000000E+00)
 TIME (BACK, NSTE = 6000, TEND = 6.0e15, DT = 1.0e9, FIXED)
 DATA (CONT)
 PRIN (NONE, BOUN)
 SCAL (VALU = 0.1e-3)
/ THESE COMMANDS ARE FOR CONTINUUM ENTITIES
entity (name="LUMEN_PT",fluid, SPEC = 1, MDIFF = "LUMEN_PT" )
entity (name="VWALL_PT",solid, SPEC = 1, MDIFF = "VWALL_PT" )
entity (name="STENT_PT",solid, SPEC = 1, MDIFF = "STENT_PT" )
/ THESE COMMANDS ARE FOR BOUNDARY ENTITIES
entity (name="STENT",plot          )
entity (name="VWALL",plot          )
entity (name="LUM_SYM2",plot          )
entity (name="VW_SYM2",plot          )
entity (name="VV",plot          )
entity (name="LUM_IN",plot          )
entity (name="INLET",plot          )
entity (name="VW_IN",plot          )
entity (name="VW_OUT",plot          )
entity (name="OUTLET",plot          )
entity (name="VW_SYM1",plot          )
entity (name="LUM_SYM1",plot          )
entity (name="VWALL_C",plot          )
entity (name="INLET_C",plot          )
entity (name="LUM_SYM1_C",plot          )
entity (name="LUM_SYM2_C",plot          )
entity (name="STENT_C",plot          )
entity (name="OUTLET_C",plot          )
entity (name="VV_C",plot          )
entity (name="LUM_IN_C",plot          )
entity (name="VW_IN_C",plot          )
entity (name="VW_OUT_C",plot          )
/
 CLIP (MINI)
   0.0000000000E+00,  0.0000000000E+00,  0.0000000000E+00,  0.0000000000E+00,
   0.0000000000E+00,  0.0000000000E+00,  0.0000000000E+00,  0.0000000000E+00,
   0.1000000000E-19
/
DIFFUSIVITY( SET = "LUMEN_PT", CONS = 1.0E+00 )
DIFFUSIVITY( SET = "VWALL_PT", CONS = 1.0E-01 )
DIFFUSIVITY( SET = "STENT_PT", CONS = 1.0E-03 )
ICNODE( READ, VELOCITY, ALL)
/
BCNODE( SPEC = 1, ENTI = "VV", ZERO )
BCNODE( SPEC = 1, ENTI = "LUM_IN", ZERO )
ICNODE( SPEC = 1, ENTI = "STENT_PT", CONS = 1.0 )
END
/
create(fisolv)
```